

**ACTIVATION ENERGY FOR UTILIZING PEROXY-ACID FOR
TREATING POLYCYCLIC AROMATIC HYDROCARBONS (PAHS)**

By

Egidio F. Tentori

A Thesis Submitted to the Graduate
Faculty of Rensselaer Polytechnic Institute
in Partial Fulfillment of the
Requirements for the degree of
MASTER OF SCIENCE
Major Subject: ENVIRONMENTAL ENGINEERING

Approved by the
Examining Committee:

Dr. Marianne C. Nyman, Thesis Advisor

Dr. James (Chip) Kilduff, Member

Dr. Thomas F. Zimmie, Member

Rensselaer Polytechnic Institute
Troy, New York

April, 2013
(For Graduation May 2013)

© Copyright 2013
By
Egidio F. Tentori
All Rights Reserved

TABLE OF CONTENTS

LIST OF TABLES.....	vii
LIST OF FIGURES	x
ACKNOWLEDGMENTS	xii
ABSTRACT	xiii
1. INTRODUCTION.....	1
1.1 Research Objectives.....	4
2. LITERATURE REVIEW	5
2.1 Polycyclic Aromatic Hydrocarbons	5
2.1.1 Sources, Fate and Transport.....	5
2.1.2 Physico-Chemical Characteristics.....	7
2.1.2.1 Anthracene Characteristics	10
2.1.2.2 Benzo[a]pyrene Characteristics	11
2.1.2.3 Phenanthrene Characteristics	12
2.1.2.4 Pyrene Characteristics.....	13
2.1.3 Environmental and Human Health Effects	14
2.2 Advanced Oxidation Processes (AOPs).....	15
2.2.1 Physical Methods	16
2.2.1.1 Ultrasonic Methods	16
2.2.1.1.1 Mechanism.....	17
2.2.1.1.2 Advantages/Disadvantages	19
2.2.1.2 Ultraviolet Light Process	20
2.2.1.2.1 Mechanism.....	20
2.2.1.2.2 Advantages/Disadvantages	25
2.2.2 Chemical Methods	26
2.2.2.1 Fenton's Reagent Process	26

2.2.2.1.1	Mechanism.....	26
2.2.2.1.2	Advantages/Disadvantages	27
2.2.2.2	Ozone Chemical Oxidation Process.....	27
2.2.2.2.1	Mechanism.....	28
2.2.2.2.2	Advantages/Disadvantages	29
2.2.2.3	Potassium Permanganate	30
2.2.2.3.1	Mechanism.....	31
2.2.2.3.2	Advantages/Disadvantages	32
2.2.2.4	Peroxy-Acid Process	32
2.2.2.4.1	Mechanism.....	33
2.2.2.4.2	Advantages/Disadvantages	36
3.	MATERIALS AND METHODS	39
3.1	Materials.....	39
3.2	Methods.....	39
3.2.1	Peracetic Acid (PAA) Generation Study.....	39
3.2.1.1	Experimental Methods	39
3.2.1.2	Controls.....	41
3.2.1.3	Titrations	42
3.2.1.3.1	Potassium Permanganate Standardization	42
3.2.1.4	Hydrogen Peroxide and Peracetic Acid Determination	42
3.2.1.5	pH Measurements	43
3.2.2	PAH Degradation and Activation Energy.....	44
3.2.2.1	Experimental Methods	44
3.2.2.2	Controls.....	45
3.2.2.3	Extraction Methods	46
3.2.2.4	Sample Analysis.....	46

3.2.2.5	Rate Constants and Activation Energy	47
4.	RESULTS AND DISCUSSION.....	48
4.1	Hydrogen Peroxide and Peracetic Acid Study Results	48
4.1.1	Initial H ₂ O ₂ and PAA Study Results	48
4.1.1.1	pH Results	49
4.1.2	Behavior of H ₂ O ₂ and PAA in PAH Degradation Set-up	50
4.2	PAH Degradation and Activation Energy Experimental Results	52
4.2.1	Anthracene Degradation Results.....	53
4.2.1.1	Degradation and Reaction Rate at T = 25 °C.....	53
4.2.1.2	Degradation and Reaction Rate at T = 32 °C.....	55
4.2.1.3	Degradation and Reaction Rate at T = 40 °C.....	57
4.2.1.4	Reaction Rates and Activation Energy	59
4.2.2	Benzo[a]pyrene Degradation Results.....	60
4.2.2.1	Degradation and Reaction Rate at T = 25 °C.....	60
4.2.2.2	Degradation and Reaction Rate at T = 32 °C.....	62
4.2.2.3	Degradation and Reaction Rate at T = 40 °C.....	64
4.2.2.4	Reaction Rates and Activation Energy	66
4.2.3	Phenanthrene Degradation Results	67
4.2.3.1	Degradation and Reaction Rate at T = 25 °C.....	67
4.2.3.2	Degradation and Reaction Rate at T = 32 °C.....	69
4.2.3.3	Degradation and Reaction Rate at T = 40 °C.....	71
4.2.3.4	Reaction Rates and Activation Energy	73
4.2.4	Pyrene Degradation Results	74
4.2.4.1	Degradation and Reaction Rate at T = 25 °C.....	74
4.2.4.2	Degradation and Reaction Rate at T = 32 °C.....	76
4.2.4.3	Degradation and Reaction Rate at T = 40 °C.....	78
4.2.4.4	Reaction Rates and Activation Energy	80

4.2.5 Summary of Results	81
5. CONCLUSIONS	84
6. FUTURE WORK.....	86
REFERENCES	87
APPENDICES	100
Appendix A: ABBREVIATIONS	101
Appendix B: PAH CALIBRATION INFORMATION	106
Appendix C: GAS CHROMATOGRAPHY OVEN METHODS.....	115
Appendix D: PAH DEGRADATION STUDIES	120
Appendix E: PERACETIC ACID GENERATION STUDY	146
Appendix F: REACTION RATES & ACTIVATION ENERGIES.....	150

LIST OF TABLES

Table 2.1. Physico-chemical characteristics of the selected PAHs at T = 25 °C.	8
Table 2.2. Physico-chemical properties of anthracene.	10
Table 2.3. Physico-chemical properties of benzo[a]pyrene.....	11
Table 2.4. Physico-chemical properties of phenanthrene.....	12
Table 2.5. Physico-chemical properties of pyrene.....	13
Table 3.1. Experimental conditions for initial PAA study.	40
Table 3.2. Experimental conditions for initial PAA study, with anthracene.....	41
Table 3.3. Experimental and control set-up.....	45
Table 3.4. Example gas chromatograph oven program.....	47
Table 4.1. Results of the initial H ₂ O ₂ and PAA study.....	48
Table 4.2. Solution pH values of experimental set-up.....	49
Table 4.3. Anthracene reaction rates for the selected temperatures.....	59
Table 4.4. Benzo[a]pyrene reaction rates for the selected temperatures.....	66
Table 4.5. Phenanthrene reaction rates for the selected temperatures.....	73
Table 4.6. Pyrene reaction rates for the selected temperatures.....	80
Table 4.7. Summary of activation energies for the four selected PAHs.....	83
Table B.1. Anthracene standard concentrations and standard curve area count.....	107
Table B.2. Benzo[a]pyrene standard concentrations and standard curve area count. ...	108
Table B.3. Phenanthrene standard concentrations and standard curve area count.....	109
Table B.4. Pyrene standard concentrations and standard curve area count.....	110
Table B.5. Pipet calibration for anthracene experiments, T = 25 °C.....	111
Table B.6. Pipet calibration for anthracene experiments, T = 32 °C.....	111
Table B.7. Pipet calibration for anthracene experiments, T = 40 °C.....	111
Table B.8. Pipet calibration for benzo[a]pyrene experiments, T = 25 °C.....	112
Table B.9. Pipet calibration for benzo[a]pyrene experiments, T = 32 °C.....	112
Table B.10. Pipet calibration for benzo[a]pyrene experiments, T = 40 °C.....	112
Table B.11. Pipet calibration for phenanthrene experiments, T = 25 °C.....	113
Table B.12. Pipet calibration for phenanthrene experiments, T = 32 °C.....	113
Table B.13. Pipet calibration for phenanthrene experiments, T = 40 °C.....	113

Table B.14. Pipet calibration for pyrene experiments, T = 25 °C.	114
Table B.15. Pipet calibration for pyrene experiments, T = 32 °C.	114
Table B.16. Pipet calibration for pyrene experiments, T = 40 °C.	114
Table D.1. Anthracene degradation at T = 25 °C, experimental set-up.....	121
Table D.2. Anthracene degradation at T = 25 °C, all control set-ups.	122
Table D.3. Anthracene degradation at T = 32 °C, experimental set-up.....	123
Table D.4. Anthracene degradation at T = 32 °C, all control set-ups.	124
Table D.5. Anthracene degradation at T = 40 °C, experimental set-up.....	125
Table D.6. Anthracene degradation at T = 40 °C, all control set-ups.	126
Table D.7. Benzo[a]pyrene degradation at T = 25 °C, experimental set-up.	127
Table D.8. Benzo[a]pyrene degradation at T = 25 °C, all control set-ups.	128
Table D.9. Benzo[a]pyrene degradation at T = 32 °C, experimental set-up.	129
Table D.10. Benzo[a]pyrene degradation at T = 32 °C, all control set-ups.	130
Table D.11. Benzo[a]pyrene degradation at T = 40 °C, experimental set-up.	131
Table D.12. Benzo[a]pyrene degradation at T = 40 °C, all control set-ups.	132
Table D.13. Phenanthrene degradation at T = 25 °C, experimental set-up.	133
Table D.14. Phenanthrene degradation at T = 25 °C, all control set-ups.	134
Table D.15. Phenanthrene degradation at T = 32 °C, experiment set-up.	135
Table D.16. Phenanthrene degradation at T = 32 °C, all control set-ups.	136
Table D.17. Phenanthrene degradation at T = 40 °C, experimental set-up.	137
Table D.18. Phenanthrene degradation at T = 40 °C, all control set-ups.	138
Table D.19. Pyrene degradation at T = 25 °C, experimental set-up.....	139
Table D.20. Pyrene degradation at T = 25 °C, all control set-ups.....	140
Table D.21. Pyrene degradation at T = 32 °C, experimental set-up.....	141
Table D.22. Pyrene degradation at T = 32 °C, all control set-ups.....	142
Table D.23. Pyrene degradation at T = 40 °C, experimental set-up.....	143
Table D.24. Pyrene degradation at T = 40 °C, all control set-ups.....	144
Table D.25. Mass % of PAH after 24 hours, T = 25, 32, and 40 °C.	145
Table E.1. Initial H ₂ O ₂ and PAA determination study set-up.	147
Table E.2. Values of used titrant solutions.	147
Table E.3. Initial H ₂ O ₂ and PAA determination study titration results.	147

Table E.4. 100 μL pipet calibration for H_2O_2 and PAA study.....	148
Table E.5. Solution pH values for all set-ups, $T = 25$ and 40°C , time = 0 and 24 hrs.	148
Table E.6. Values of % H_2O_2 and % PAA for the PAH degradation study.....	149
Table F.1. Peroxy-acid process reaction rates and E_a of anthracene.	151
Table F.2. Peroxy-acid process reaction rates and E_a of benzo[a]pyrene.....	151
Table F.3. Peroxy-acid process reaction rates and E_a of phenanthrene.	151
Table F.4. Peroxy-acid process reaction rates and E_a of pyrene.....	151

LIST OF FIGURES

Figure 2.1. The four selected PAH compounds in this study.	5
Figure 2.2. Ranges at 25 °C in saturation vapor pressure (atm) for organic compounds..	9
Figure 2.3. Ranges in water solubility (mol L ⁻¹) for organic compounds.	9
Figure 2.4. Structure of anthracene.....	10
Figure 2.5. Structure of benzo[a]pyrene.	11
Figure 2.6. Structure of phenanthrene.	12
Figure 2.7. Structure of pyrene.	13
Figure 2.8. Concept of integrating AOPs to pre-treatment.....	16
Figure 2.9. Cavitation bubbles, possible sites of chemical reactions.	17
Figure 2.10. Diagram of possible degradation pathways using sonication and ozone.	19
Figure 2.11. Reaction system in the H ₂ O ₂ /UV system.	21
Figure 2.12. Reaction pathways in the O ₃ /UV system.	22
Figure 2.13. Direct photolysis possible reaction pathways.	24
Figure 2.14. Ozonation reaction pathways.	29
Figure 2.15. Permanganate reaction scheme of ethylene.	31
Figure 2.16. Peracetic acid chemical structure.	32
Figure 2.17. Hypothesized peroxy-acid degradation mechanism of a PAH.....	34
Figure 2.18. PAA epoxidation reaction of a C=C bond.	35
Figure 4.1. Values of H ₂ O ₂ (%), vs. time (hrs) for PAH degradation.	50
Figure 4.2. Values of PAA (%) vs. time (hrs) for PAH degradation.....	51
Figure 4.3. Anthracene degradation plotted as mass (m/m ₀) vs. time (hrs), 25 °C.	54
Figure 4.4. Anthracene reaction rate plotted as ln(m/m ₀) vs. time (hrs) at 25 °C.	54
Figure 4.5. Anthracene degradation plotted as mass (m/m ₀) vs. time (hrs), 32 °C.	56
Figure 4.6. Anthracene reaction rate plotted as ln(m/m ₀) vs. time (hrs) at 32 °C.	56
Figure 4.7. Anthracene degradation plotted as mass (m/m ₀) vs. time (hrs), 40 °C.	58
Figure 4.8. Anthracene reaction rate plotted as ln(m/m ₀) vs. time (hrs) at 40 °C.	58
Figure 4.9. Reaction rates (s ⁻¹) and activation energy of anthracene, ln(k) vs. 1/T.....	59
Figure 4.10. Benzo[a]pyrene degradation plotted as mass (m/m ₀) vs. time (hrs), 25 °C. 61	
Figure 4.11. Benzo[a]pyrene reaction rate plotted as ln(m/m ₀) vs. time (hrs) at 25 °C. .	61

Figure 4.12. Benzo[a]pyrene degradation plotted as mass (m/m_0) vs. time (hrs), 32 °C.	63
Figure 4.13. Benzo[a]pyrene reaction rate plotted as $\ln(m/m_0)$ vs. time (hrs) at 32 °C.	63
Figure 4.14. Benzo[a]pyrene degradation plotted as mass (m/m_0) vs. time (hrs), 40 °C.	65
Figure 4.15. Benzo[a]pyrene reaction rate plotted as $\ln(m/m_0)$ vs. time (hrs) at 40 °C.	65
Figure 4.16. Reaction rates and activation energy of benzo[a]pyrene, $\ln(k)$ vs. $1/T$.	66
Figure 4.17. Phenanthrene degradation plotted as mass (m/m_0) vs. time (hrs), 25 °C.	68
Figure 4.18. Phenanthrene reaction rate plotted as $\ln(m/m_0)$ vs. time (hrs) at 25 °C.	68
Figure 4.19. Phenanthrene degradation plotted as mass (m/m_0) vs. time (hrs), 32 °C.	70
Figure 4.20. Phenanthrene reaction rate plotted as $\ln(m/m_0)$ vs. time (hrs) at 32 °C.	70
Figure 4.21. Phenanthrene degradation plotted as mass (m/m_0) vs. time (hrs), 40 °C.	72
Figure 4.22. Phenanthrene reaction rate plotted as $\ln(m/m_0)$ vs. time (hrs) at 40 °C.	72
Figure 4.23. Reaction rates and activation energy of phenanthrene, $\ln(k)$ vs. $1/T$.	73
Figure 4.24. Pyrene degradation plotted as mass (m/m_0) vs. time (hrs), 25 °C.	75
Figure 4.25. Pyrene reaction rate plotted as $\ln(m/m_0)$ vs. time (hrs) at 25 °C.	75
Figure 4.26. Pyrene degradation plotted as mass (m/m_0) vs. time (hrs), 32 °C.	77
Figure 4.27. Pyrene reaction rate plotted as $\ln(m/m_0)$ vs. time (hrs) at 32 °C.	77
Figure 4.28. Pyrene degradation plotted as mass (m/m_0) vs. time (hrs), 40 °C.	79
Figure 4.29. Pyrene reaction rate plotted as $\ln(m/m_0)$ vs. time (hrs) at 40 °C.	79
Figure 4.30. Reaction rates and activation energy of pyrene, $\ln(k)$ vs. $1/T$.	80
Figure 4.31. Mass % values all four PAHs, degradation after 24 hours vs. T (°C).	81
Figure 4.32. Natural log of all rate constants for all four PAH compounds.	82
Figure B.1. Sample anthracene calibration curve.	107
Figure B.2. Sample benzo[a]pyrene calibration curve.	108
Figure B.3. Sample phenanthrene calibration curve.	109
Figure B.4. Sample pyrene calibration curve.	110
Figure C.1. Sample anthracene gas chromatography oven method.	116
Figure C.2. Sample benzo[a]pyrene gas chromatography oven method.	117
Figure C.3. Sample phenanthrene gas chromatography oven method.	118
Figure C.4. Sample pyrene gas chromatography oven method.	119
Figure F.1. All reaction rates (hr^{-1}) for all PAHs vs. T (K).	152

ACKNOWLEDGMENTS

I would like to thank my committee members, Dr. Marianne Nyman, Dr. James (Chip) Kilduff and Dr. Thomas Zimmie, for sharing their time and guidance. Your classes and knowledge were an instrumental part of my time here at Rensselaer. I am especially grateful to Dr. Nyman for being patient and understanding and for her support as my undergraduate and graduate advisor. I would like to thank Dr. E. Bruce Watson for finding space for me to work in his lab, providing me with a great learning opportunity and sparking my interest in research.

I would also like to thank Mr. Arto Nyman for his assistance with the gas chromatograph. I would like to express my gratitude to Jeanne Shoulder for helping in the lab with much of the methods and instrumentation as I was getting started and to Meredith Mayes and Su San Yap for their help, conversation and company which made the suffering much easier. I would also like to thank Mecaila Smith for her work in the Office of Graduate Education and organizing the NSF Louis Stokes Alliances for Minority Participation (LSAMP) Program in the summer of 2011 which helped me get started on my thesis research.

Most importantly, I would like to thank my friends and my family, especially my parents for their support. This would not have been possible without them.

ABSTRACT

Polycyclic aromatic hydrocarbons (PAHs) are a group of hydrophobic organic contaminants (HOCs) of importance due their environmental and human health effects, their widespread occurrence and persistence in the environment. Advanced oxidation processes (AOPs) are a set of treatment methods that have been proven to be successful in degrading organic contaminants in water, soils and sediments. AOPs usually rely on the oxidative potential of the hydroxyl radical (HO^\bullet) to degrade organic contaminants, like PAHs. The peroxy-acid process, an advanced oxidation process (AOP) proven to degrade PAHs, which utilizes a mixture of organic acids, like acetic acid, and hydrogen peroxide to oxidize organic compounds. Peracetic acid (PAA) is produced from the combination of acetic acid and hydrogen peroxide. The peroxy-acid process was used to investigate the degradation process of four PAHs: anthracene, benzo[a]pyrene, phenanthrene and pyrene.

Previous work done on PAHs found a correlation between the presence of PAA in solution and the degradation of PAHs undergoing the peroxy-acid process. A study was conducted to investigate the effects of varying amounts of hydrogen peroxide, acetic acid and an acid catalyst, sulfuric acid, would have on PAA concentrations in solution. Titrations were performed to determine the % amounts of hydrogen peroxide and PAA in solution. It was found that amount of hydrogen peroxide decreased over time while the amount of PAA in solution increased over time. In addition, the addition of the acid catalyst, sulfuric acid, increased significantly the amount of PAA present while decreasing the amount of hydrogen peroxide present in solution.

Peroxy-acid PAH degradation experiments were conducted to determine the peroxy-acid process reaction rate constants (k) of the four selected compounds: anthracene, benzo[a]pyrene, phenanthrene and pyrene. Three different temperatures (*e.g.*, 25, 32, and 40 °C) were investigated over a 24-hour time period. Reactions took place in 35 mL centrifuge tubes with volume ratios of 3:3:9 (v/v/v) acetic acid : 50% hydrogen peroxide : DI water with a total volume of 15 mL in each reaction vessel. Controls were also implemented for each of the reagents separately.

Once the reaction rate constants were obtained from the degradation for each of the four selected PAHs at the three selected temperatures, the activation energy (E_a) was calculated for anthracene, benzo[a]pyrene, phenanthrene and pyrene using the *Arrhenius* equation. The findings of the peroxy-acid degradation process at temperatures of 25, 32, and 40 °C after 24 hours were as follows: [i] anthracene mass % amount reductions of 30.5 %, 44.6 %, and 98.1 %, with reaction rate constants of 0.0107, 0.0182 and 0.1536 hr^{-1} , respectively; [ii] benzo[a]pyrene mass % amount reductions of 20.1 %, 38.1 %, and 92.4 %, with reaction rate constants of 0.0080, 0.0133 and 0.1027 hr^{-1} , respectively; [iii] phenanthrene mass % amount reductions of 17.9 %, 27.7 %, and 61.3 %, with reaction rate constants of 0.0068, 0.0112 and 0.0336 hr^{-1} , respectively; and [iv] pyrene mass % amount reductions of 19.8 %, 39.7 % and 89.6 %, with reaction rate constants of 0.0074, 0.0194 and 0.0852 hr^{-1} , respectively. The E_a s calculated from these reaction rates were found to be: 138.96 kJ mol^{-1} for anthracene, 133.13 kJ mol^{-1} for benzo[a]pyrene, 83.07 kJ mol^{-1} for phenanthrene and 126.76 kJ mol^{-1} for pyrene. These obtained reaction rate and E_a findings could prove to be a valuable asset in helping determine the exact reaction mechanism of the peroxy-acid process with PAHs and be potentially useful in the treatment of PAHs and other organic contaminants in the environment.

1. INTRODUCTION

Polycyclic aromatic hydrocarbons (PAHs) are organic compounds that are made up of two or more benzene rings or five carbon containing rings fused together, with no heteroatoms or substituents. Environmentally significant PAHs can range from two-ring structures (naphthalene) up to ten or more (ovalene). PAHs can be from both anthropogenic sources and natural sources. The major source of PAH inputs is the incomplete combustion of fossil fuels, and other sources of PAHs into the environment are numerous. PAH contamination is strongly associated with the waste produced by the gasification of fossil fuels in Manufactured Gas Plants (MGPs), an energy source used in the U.S. up to the 1950's. PAHs are of interest because of their toxicity and many PAHs have been found to be potential or known carcinogens (ATSDR, 1995). The chemical properties of PAHs allow them to be present in many phases in the environment including soils, and sediments; this is in part due to their wide range of chemical structures. PAHs are categorized as hydrophobic organic compounds (HOCs) as they are not very miscible in water, and have an affinity for soils, sediments and organic matter (OM) due to high octanol-water partition coefficients (K_{ow} s). The mentioned health effects, presence in the environment and potential for exposure drives PAH research today.

PAHs have been studied for many years and research on this topic is still ongoing. Strategies of PAH remediation are dependent on the extent and source of contamination, available technology and economic viability. Techniques of PAH remediation include containment, thermal techniques, physical-chemical techniques, bioremediation and phytoremediation (Henner *et al.*, 1997; Gan *et al.*, 2009). When using containment techniques; the contamination is enclosed in a barrier, to prevent the migration of the pollutant and further contamination of the environment. More complex containment techniques, like the use of geosorbents to prevent the mobilization of contamination, have been explored. However, since this method would be used in heterogeneous systems, a better understanding of the underlying physicochemical processes involved is needed (Luthy *et al.*, 1997). This containment technique is usually used as a temporary solution or when economic factors and location dictate the best mitigation strategy

(Swords and Strange, 2006). Thermal techniques use high temperatures in order to destroy or volatilize PAHs in contaminated soils. Examples of these techniques like soil venting-thermal-desorption (SVTD), which includes a soil venting component for collecting the volatilized contaminants from the soil, have been found to be effective in treating PAH-contaminated MGP soils (Harmon *et al.*, 2001). This process does have challenges, as moisture present in the contaminated soil has to be removed to ensure complete combustion and air pollution control devices are necessary to treat soil-emitted gases (Gan *et al.*, 2009). Physical-chemical techniques consist of removing the contaminant and transferring to another phase, which is then subsequently treated. Solvent extraction technology uses a solvent or mixtures of solvents to remove PAHs from contaminated soil. This solvent extraction process is used by excavating the contaminated soil, transporting it for treatment and extracting the PAHs with a solvent mixture (Silva *et al.*, 2005). The added cost of excavating and transporting soil often detracts from using this method. However, the use of both *in-situ* and *ex-situ* surfactants greatly aids the solvent extraction process and negates the need of excavating large amounts of contaminated soil (Deshpande *et al.*, 1999; Mulligan *et al.*, 2001). Bioremediation involves the use of microorganisms and capacity to naturally degrade PAHs. This technique is dependent on the bioavailability of the contaminants. Examples of varieties of bioremediation include land-farming and composting, aerobic remediation, anaerobic remediation, biosparging and use of fungi to degrade PAHs (Bossert *et al.*, 1984; Chang *et al.*, 2002; Lau *et al.*, 2003). Phytoremediation techniques, commonly used in remediation of metals, have also shown promise in remediation of non-volatile organics like PAHs. The plants are used in order to sequester the contaminants along with aided degradation of microorganisms in the soil and roots. These plants can then be harvested and disposed of along with the contaminants. Work done by Cunningham and colleagues (1993; 1995) has shown that *in-situ* phytoremediation techniques can be cheaper than *in-situ* soil remediation techniques, but more work is needed before this technology can be considered viable.

This study will focus on a type of chemical remediation technique, using an AOP (Xie *et al.*, 2010). AOPs use strong oxidizing agents like the hydroxyl radical (HO[•]) to degrade contaminants. AOPs have been widely used to treat numerous organic pollutants

effectively including compound classes such as PAHs, pesticides, substituted naphthalenes (Watts and Teel, 2005; Ferrarese *et al.*, 2008; Levitt *et al.*, 2003; N'Guessan *et al.*, 2004a; Shoulder, 2012).

As an AOP, the peroxy-acid process has been found to be effective for the degradation of multiple PAH compounds (N'Guessan *et al.*, 2004a; Alderman *et al.*, 2007; N'Guessan *et al.*, 2004b). The peroxy-acid process uses peracetic acid (PAA), formed by the combination of hydrogen peroxide (H_2O_2) and acetic acid (CH_3COOH). Using this AOP, a correlation between benzo[a]pyrene degradation rates and concentration of PAA has been observed (Alderman and Nyman, 2009; Shoulder, 2012; N'Guessan *et al.*, 2004b). Expanding on previous work done using the peroxy-acid treatment method, degradation efficiencies were determined at three different temperatures: 25, 32 and 40 °C, pseudo-first order rate constants were determined for four PAHs (*e.g.*, anthracene, benzo[a]pyrene, phenanthrene and pyrene) and the E_a of the peroxy-acid process for these four selected PAHs was calculated to help determine the mechanism of this peroxy-acid process in the future.

1.1 Research Objectives

This study examined the rate of degradation of four selected PAHs, specifically anthracene, benzo[a]pyrene, phenanthrene, and pyrene, using an AOP employing peroxy-acids as oxidizing agents. A peroxy-acid treatment method has been widely studied by Nyman group (Alderman, 2009; Alderman *et al.*, 2007; N'Guessan *et al.*, 2004a). The peroxy-acid process utilizes an organic acid, like acetic acid, and hydrogen peroxide to degrade the PAH structures. It is hypothesized that this reaction mechanism involves the hydroxyl radical (HO^\bullet), and/or peracetic acid (PAA). Therefore, the purpose of this study was to help determine part of the mechanism of the oxidative degradation of four selected PAHs and compute the E_a of this process for the four PAHs.

2. LITERATURE REVIEW

2.1 Polycyclic Aromatic Hydrocarbons

PAHs are organic compounds that are made up of two or more benzene rings or five carbon-containing rings fused together, with no heteroatoms or substituents. Environmentally significant PAHs can range from two-ring structures (naphthalene) up to ten or more (ovalene). The four PAH compounds that will be part of this study are [i] anthracene, [ii] benzo[a]pyrene, [iii] phenanthrene and [iv] pyrene. These four selected PAHs are all shown in Figure 2.1 below.

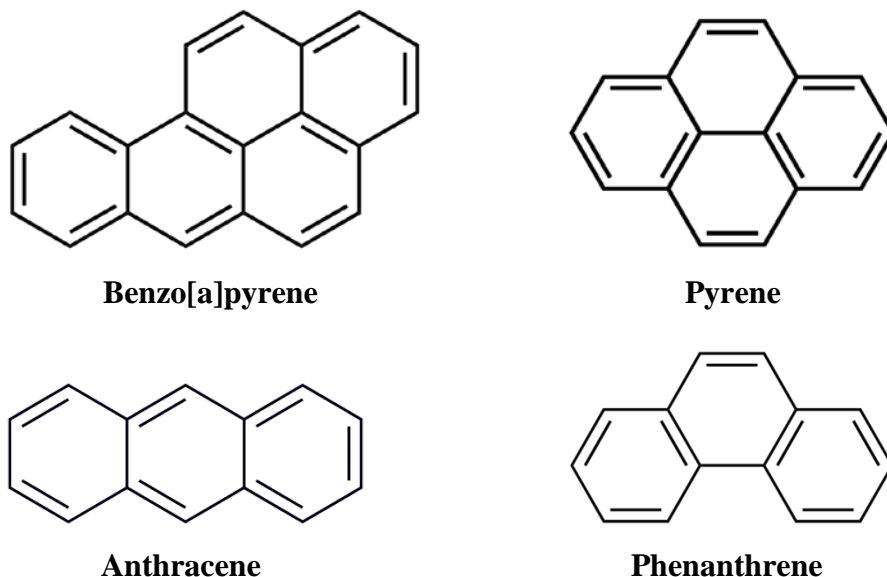


Figure 2.1. The four selected PAH compounds in this study.

2.1.1 Sources, Fate and Transport

PAH compounds are found in all media, including soil, air, vegetation, sediments, surface and drinking water. They can be present in the environment in many forms: adsorbed onto atmospheric particles, sediments, and OM; as a liquid film, dissolved in water or as a liquid or solid phase in pore water (Ghosal and Luthy, 1996).

Their ubiquitous nature, combined with the high potential for exposure and toxicity are why they are considered of the most important groups of environmental pollutants (Flowers *et al.*, 2002; Ma *et al.*, 2010). Sources of PAHs are both natural and anthropogenic. Natural sources include fossil fuels, like coal, and natural incomplete combustion of OM (Costa and Sauer, 2005; Achten and Hofmann, 2009; Ma *et al.*, 2010). Anthropogenic sources represent the largest contributions of PAHs into the environment. These sources include human combustion of organic material such as fossil fuels, natural gas and wood (Zhang and Tao, 2009). Of the anthropogenic sources, fossil fuel combustion for heat and power generation are the primary source of PAHs, nonetheless other industrial sources also contribute to anthropogenic sources (U.S. EPA, 2001). Other sources of PAHs to the environment include waste combustion, iron foundries, smelters, asphalt roofing, coke ovens, pulp mills and rayon-based carbon fiber manufacturing (U.S. EPA, 2001). PAHs are also the main component of creosote, commonly called coal tar creosote; a tar used in the wood industry because of its preservative properties. (Speight, 1994; Emsbo-Mattingly *et al.*, 2001; Emsbo-Mattingly, 2003). In turn, a large portion of the PAH contamination related to fossil fuel heat and power anthropogenic sources is due to Manufactured Gas Plants (MGPs) and their by-product; commonly referred to as coal tar.

MGPs were widely used to produce energy in the U.S. up to the 1950's when natural gas was adopted, the process involved heating up coal with water to produce a combustible gas mixture (NYS DEC, 2013). MGP contamination often mobilizes to other areas, polluting bodies of water such as streams, rivers and lakes. Coal tar is associated with groundwater contamination at many former MGP sites. Coal tar is a highly viscous dense non-aqueous phase liquid (DNAPL) consisting of PAHs and of many other organic compounds (Sauer and Costa, 2003). There is considerable information on PAH concentrations and their behavior globally. In soils their behavior is dependent on the climate of the region, soil temperature, moisture content, and organic carbon (OC) content as these factors would influence PAH decomposition rates, volatilization, bioavailability and partitioning in a given environment (Wilcke, 2000). Soil organic matter (SOM) is often the determining factor of PAH partitioning in soils and the most important part of the sorbent of PAHs in soils (Dzombak and Luthy, 1984).

The presence of “soot” or “black carbon” in soils resulting from forest fires and atmospheric deposition is also capable of strong PAH adsorption (Gustafsson *et al.*, 1997; Gerard and Gustafsson, 2006). Plant uptake of PAHs in contaminated soils is strongly correlated to soil concentrations, increasing concentrations of PAHs in soils lead to increasing concentrations of PAHs in plants (Wilcke, 2000). However, another significant source of PAHs in plants is from atmospheric inputs, where PAHs may enter the plant via gaseous phase or particle deposition on plants (Sims and Overcash, 1983). Elevated PAH concentrations have also been observed in marine sediments and seawater. Proximity to major urban areas is an indicator of these elevated PAH levels, where inputs have been related to combustion-related sources and the industry of the areas (Law *et al.*, 1997; Woodhead *et al.*, 1999).

2.1.2 Physico-Chemical Characteristics

If PAHs exist as pure, isolated chemicals they are generally colorless, white, yellowish or green-yellowish solid crystals. More than 100 different PAHs have been identified, generally existing as a mixture of these compounds (ATSDR, 1995). Of these, up to 28 PAH compounds have been identified as hazardous contaminants by the US Environmental Protection Agency (US EPA). To illustrate the variability PAHs have, the structure of several compounds and their properties are shown on Table 2.1. Seven of these PAHs (*e.g.*, acenaphthene, acenaphthylene, anthracene, benzo[g,h,i]perylene, fluorene, phenanthrene and pyrene) are listed on the US EPA Priority Chemical List (U.S. EPA, 2008). Compounds are listed as priority pollutants based on toxicity, persistence in the environment, ability to degrade and the nature and extent of the pollution.

These compounds are grouped together because they share similar physical and chemical characteristics. PAHs are highly hydrophobic and strongly adsorb onto particulate OM, and are present as persistent environmental contaminants in air, soil and water (Gan *et al.*, 2009). PAHs are classified as non-polar HOCs. As with other organic compounds, chemical properties of PAHs follow a trend relating to their structure and molecular weight (MW). Figure 2.2 and Figure 2.3 show this variation trend for some

important classes of organic compounds for vapor pressure (v_p) and aqueous solubility (S_w), respectively.

Table 2.1. Physico-chemical characteristics of the selected PAHs at $T = 25\text{ }^\circ\text{C}$.

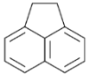
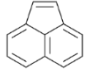
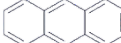
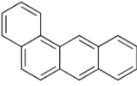
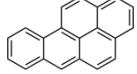
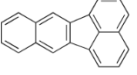
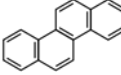
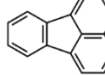
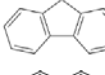

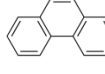
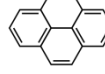
Name	Structure	Formula	MW (g mol^{-1})	T_m ($^\circ\text{C}$)	T_b ($^\circ\text{C}$)	v_p (mm Hg)	S_w (mg L^{-1})	$\log K_{ow}$
Acenaphthene		$\text{C}_{12}\text{H}_{10}$	154.21	93.4	279	2.15×10^{-3}	3.9	3.92
Acenaphthylene		$\text{C}_{12}\text{H}_{10}$	152.19	92.5	270	6.68×10^{-3}	3.91	4.00
Anthracene		$\text{C}_{14}\text{H}_{10}$	178.24	215	340	6.53×10^{-6}	0.0434	4.45
Benz[a]anthracene		$\text{C}_{18}\text{H}_{12}$	228.28	255	448	1.88×10^{-7}	0.0109	5.91
Benzo[a]pyrene		$\text{C}_{20}\text{H}_{12}$	252.32	176.5	495	5.49×10^{-9}	0.00162	6.13
Benzo[k]fluoranthene		$\text{C}_{20}\text{H}_{12}$	252.32	217	480	9.65×10^{-10}	0.0008	6.11
Chrysene		$\text{C}_{18}\text{H}_{12}$	228.28	255	448	4.52×10^{-9}	0.00203	5.81
Fluoranthene		$\text{C}_{16}\text{H}_{10}$	202.26	107.8	384	9.22×10^{-6}	0.026	5.16
Fluorene		$\text{C}_{13}\text{H}_{10}$	166.2	114.8	295	6.0×10^{-4}	1.69	4.18
Naphthalene		C_{10}H_8	128.18	80.2	218	0.085	31	3.3
Phenanthrene		$\text{C}_{14}\text{H}_{10}$	178.24	99.2	340	0.000121	1.15	4.46
Pyrene		$\text{C}_{16}\text{H}_{10}$	202.26	151.2	404	4.5×10^{-6}	0.135	4.88

Table adapted from (Shoulder, 2012) and (N'Guessan, 2005).

In the case of PAHs, this trend can be easily explained by the number of rings these chemicals have in their structure. The v_p and S_w are inversely proportional to the number of rings in the PAH structure, while the opposite trend exists between the K_{ow} and number of rings in the PAH structure. This is reflected in the ability of PAHs with

less than four rings to be dissolved in water at low levels, while PAHs with more than three rings are bound to particulate matter.

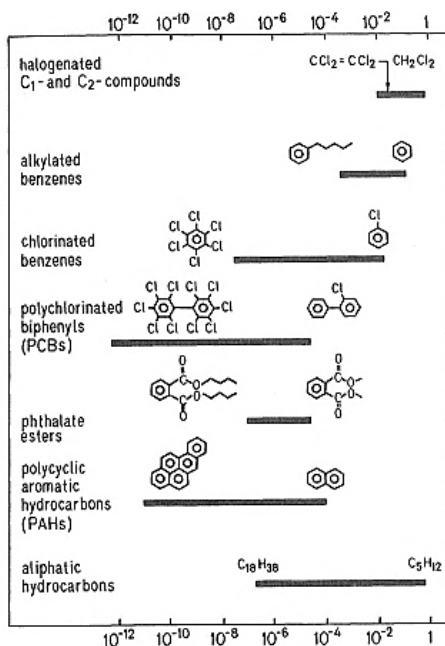


Figure 2.2. Ranges at 25 °C in saturation vapor pressure (atm) for organic compounds.

Figure adapted from (Schwarzenbach *et al.*, 1993).

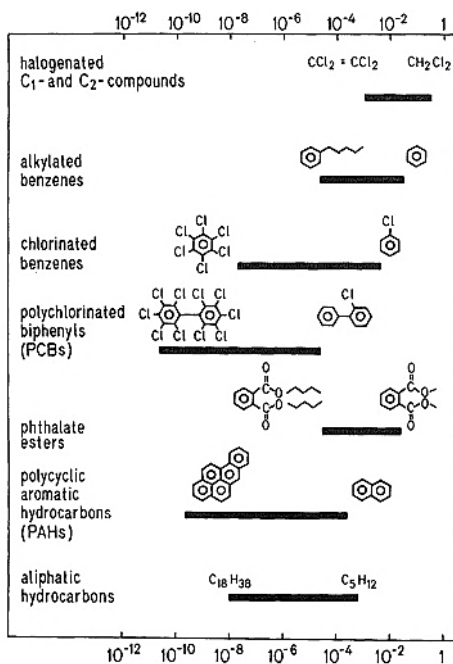


Figure 2.3. Ranges in water solubility (mol L^{-1}) for organic compounds.

Figure adapted from (Schwarzenbach *et al.*, 1993).

2.1.2.1 Anthracene Characteristics

Anthracene is a white crystalline organic compound that is non-volatile. It was first observed in coal tar. It is a three-membered PAH and it consists of the three benzene rings fused in a linear fashion. The chemical structure of anthracene is shown in Figure 2.4. Anthracene is produced by the burning of fossil fuels, coke ovens, and combustion of OM (Khalili *et al.*, 1995). Anthracene is also used in the production of dyes as a precursor of anthraquinone (Collin *et al.*, 2000). In addition, this compound is also used in plastics and has uses as an organic semiconductor. Anthracene is also one of the main components of coal tar.

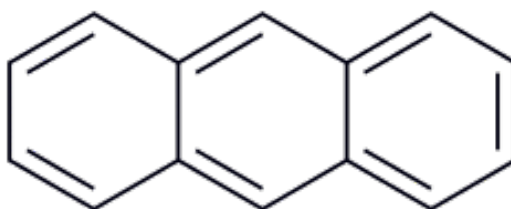


Figure 2.4. Structure of anthracene.

Selected physico-chemical properties of anthracene are shown below on Table 2.2. It is not very soluble in water with an S_w of 0.0434 mg/L. Anthracene has a $\log K_{ow}$ value of 4.45, suggesting that it will be more likely to be present in the solid phase than in the aqueous phase (see Table 2.2).

Table 2.2. Physico-chemical properties of anthracene.

Name	Formula	MW (g mol ⁻¹)	T _m (°C)	T _b (°C)	v _p (mm Hg)	S _w (mg L ⁻¹)	log K _{ow}
Anthracene	C ₁₄ H ₁₀	178.24	215	340	6.53 x 10 ⁻⁶	0.0434	4.45

2.1.2.2 Benzo[a]pyrene Characteristics

Benzo[a]pyrene is a PAH that consists of five fused benzene rings as illustrated in Figure 2.5. This compound is classified in the benzopyrene class of PAHs, which is formed by the fusion of a benzene ring to pyrene, due to incomplete combustion. The chemical structure of benzo[a]pyrene is shown in Figure 2.5. Sources of benzo[a]pyrene include combustion of organic material, like wood, fossil fuel combustion, and car exhaust from mainly diesel engines. In addition, benzo[a]pyrene is also found in cigarette smoke and charbroiled food.

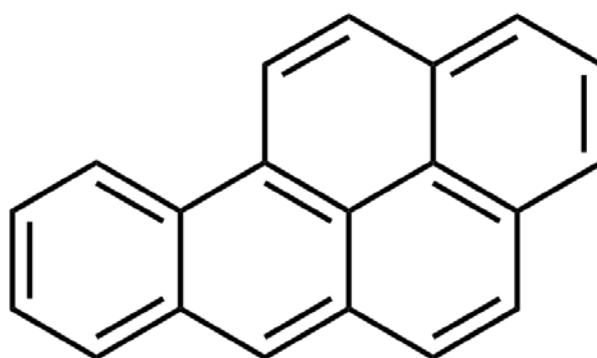


Figure 2.5. Structure of benzo[a]pyrene.

Benzo[a]pyrene has the lowest v_p out of all four selected PAHs being examined, meaning that this compound has the lowest tendency to transfer to the gaseous phase. It has the most number of rings with five aromatic rings and has the highest MW of all four compounds investigated. A $\log K_{ow}$ value of 6.13 indicates that benzo[a]pyrene is most likely to be present in the solid phase like anthracene. Other physico-chemical properties of benzo[a]pyrene are shown below on Table 2.3.

Table 2.3. Physico-chemical properties of benzo[a]pyrene.

Name	Formula	MW (g mol ⁻¹)	T _m (°C)	T _b (°C)	v_p (mm Hg)	S _w (mg L ⁻¹)	log K _{ow}
Benzo[a]pyrene	C ₂₀ H ₁₂	252.32	176.5	495	5.49 x 10 ⁻⁹	0.00162	6.13

2.1.2.3 Phenanthrene Characteristics

Phenanthrene is also a three-ring PAH like anthracene, but the orientation of the rings are different from the anthracene molecule (see Figure 2.4 and Figure 2.6). This molecule is a white crystalline-solid in appearance at room temperature. It also so produced by the combustion of fossil fuels, OM, coke ovens, metal foundries and wood processing. In addition, phenanthrene is also found in coal tar (Khalili *et al.*, 1995). The molecular structure of phenanthrene is illustrated below in Figure 2.6.

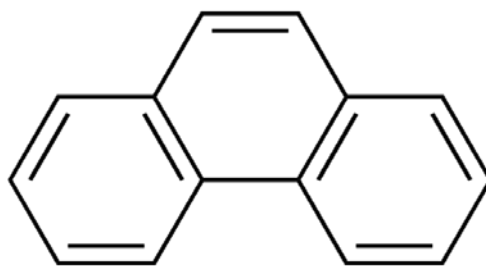


Figure 2.6. Structure of phenanthrene.

Phenanthrene has the same molecular formula (and weight) as anthracene since they both consist of the same amount of benzene rings, only in a different arrangement (see Figure 2.4 and Figure 2.6). Out of all the PAHs being examined in this study, phenanthrene has the highest S_w of 1.15 mg/L, and the highest v_p of 0.000121 mm Hg implying phenanthrene as the most volatile of the four selected PAH compounds. Some selected physico-chemical properties of phenanthrene are shown in Table 2.4.

Table 2.4. Physico-chemical properties of phenanthrene.

Name	Formula	MW (g mol ⁻¹)	T _m (°C)	T _b (°C)	v _p (mm Hg)	S _w (mg L ⁻¹)	log K _{ow}
Phenanthrene	C ₁₄ H ₁₀	178.24	99.2	340	0.000121	1.15	4.46

2.1.2.4 Pyrene Characteristics

Pyrene is a four-ringed PAH (see Figure 2.7). It is a clear-yellowish crystal-like solid at room temperature. It is the smallest PAH investigated where the rings are fused together on more than one face. It is formed during the incomplete combustion of OM. Pyrene was originally first isolated from coal tar. Sources of pyrene include smelting, fossil fuel combustion, and automobile emissions (Khalili *et al.*, 1995). Pyrene is also used in the production of dyes. The molecular structure of pyrene is shown below in Figure 2.7.

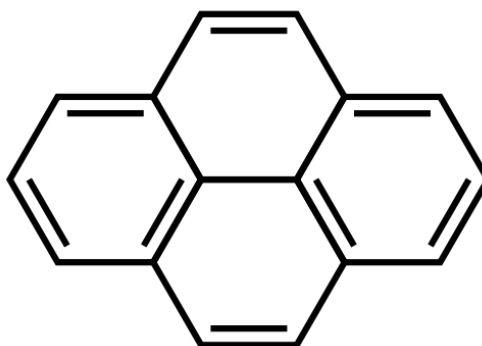


Figure 2.7. Structure of pyrene.

Pyrene has the second S_w of the four PAHs investigated, with an aqueous solubility 0.135 mg/L. The chemical structure of pyrene is related to benzo[a]pyrene; as it serves as base for the chemical structure of benzo[a]pyrene. Out of the four PAH compounds being examined, pyrene is second to benzo[a]pyrene having most rings with four as illustrated in Figure 2.7. Properties of pyrene are shown below on Table 2.1 below. The $\log K_{ow}$ has been found to be 4.88 indicating also the hydrophobicity of pyrene (see Table 2.5).

Table 2.5. Physico-chemical properties of pyrene.

Name	Formula	MW (g mol ⁻¹)	T _m (°C)	T _b (°C)	v _p (mm Hg)	S _w (mg L ⁻¹)	log K _{ow}
Pyrene	C ₁₆ H ₁₀	202.26	151.2	404	4.5 x 10 ⁻⁶	0.135	4.88

2.1.3 Environmental and Human Health Effects

PAHs are present in at least 600 sites of the sites that make up the National Priorities List (NPL). The NPL is a database of 1,408 hazardous waste sites identified by the U.S. EPA (ATSDR, 1995). PAHs are detrimental to the environment and may cause harmful health effects and even death to humans (U.S. EPA, 2008). Exposure to PAHs is typically due to a mixture of PAHs, not an individual PAH compound. Therefore, individual studies of PAH health effects are not common. The Department of Health and Human Services (DHHS) determined that benz[a]anthracene, benzo[b]fluoranthene, benzo[j]fluoranthene, benzo[k]fluoranthene, benzo[a]pyrene, dibenz[a,h]anthracene, and indeno[1,2,3-c,d]pyrene are known animal carcinogens. (ATSDR, 1995). The International Agency for Research on Cancer (IARC) has determined that benz[a]anthracene and benzo[a]pyrene are probably carcinogenic to humans; benzo[b]fluoranthene, benzo[j]fluoranthene, benzo[k]fluoranthene, and indeno[1,2,3-c,d]pyrene are possible human carcinogens; while anthracene, benzo[g,h,i]perylene, benzo[e]pyrene, chrysene, fluoranthene, fluorene, phenanthrene, and pyrene are not classifiable as to their carcinogenicity to humans (IARC, 2010). According to the EPA, benz[a]anthracene, benzo[a]pyrene, benzo[b]fluoranthene, benzo[k]fluoranthene, chrysene, dibenz[a,h]anthracene, and indeno[1,2,3-c,d]pyrene are probable human carcinogens and that acenaphthylene, anthracene, benzo[g,h,i]perylene, fluoranthene, fluorene, phenanthrene, and pyrene are not classifiable as human carcinogens (U.S. EPA, 2001).

Due to the sources of PAHs, these compounds may enter the body through inhalation, skin contact, or ingestion. Exposures to high concentrations of PAHs that lead to adverse health effects are often related to occupational exposure. Transport industry, carbon electrode production, road paving, roofing, metal foundry, coke production, wood impregnation and oil extraction related occupations have been related to higher exposures of PAHs and elevated risk of cancer in humans (Boffetta *et al.*, 1997; Marczynski *et al.*, 2009). The major organ target of PAH carcinogenicity seemed to be the lung, due to the PAHs present in particulate matter (PM), an increased risk of lung cancer was observed for domestic or workplace related high indoor levels of PAHs (Boffetta *et al.*, 1997; Gustafson *et al.*, 2008). An increased risk of skin cancer was also

observed following dermal exposure, and an increase in bladder cancer risk found in industries with high exposure to PAHs from coal tar sources. (Boffetta *et al.*, 1997). The presence of PAHs in tobacco smoke from cigarettes is also well known. PAHs in tobacco smoke play a significant role in smoking-related lung cancer cases (Hecht, 1999).

PAH-related adverse health effects observed in animals include decreased growth and birth weight and respiratory and reproductive problems (ATSDR, 1995; Straif *et al.*, 2005). Work performed on benzo[a]pyrene has shown that it can cause a significant increase in all lung tumors and a dose-dependent increase in malignant lung tumors for mice exposed to PAH-enriched exhausts (Schulte *et al.*, 1994). Similarly, benzo[a]pyrene has been found to cause tumors in rats, guinea pigs, rabbits, newts, monkeys, ducks and hamsters (Straif *et al.*, 2005). PAH concentrations in marine sediments have also been linked with abnormalities in bottom-feeding fish (Woodhead *et al.*, 1999). Due to its chemical characteristics and persistence, PAHs have been found to have the potential to bio-accumulate in organisms exposed to them (Flowers *et al.*, 2002).

2.2 Advanced Oxidation Processes (AOPs)

AOPs have been found to be an effective chemical remediation method and recent advances in technology have improved these methods. Concepts of further integration of AOPs into traditional treatment applications exist. An example of the concept of integration is shown in Figure 2.8. AOPs are oxidation methods that typically use a highly reactive species, like a hydroxyl radical (HO^\bullet), as part of the reaction mechanism that destroys a contaminant of interest. (Xie *et al.*, 2010; Comminellis *et al.*, 2008; Gogate and Pandit, 2004a; Gogate and Pandit, 2004b). A key aspect of AOPs is that they can break down large molecules into smaller components. Efficiency of AOPs has been linked to the contact the HO^\bullet , or respective degrading mechanism, has with the contaminant (Gogate and Pandit, 2004a). AOPs have shown to be able to treat chemical contamination, including PAHs, in a variety of situations, including water, groundwater, and soil contamination (Ferrarese *et al.*, 2008; Gan *et al.*, 2009; Watts and Teel, 2005;

Comninellis *et al.*, 2008; Xie *et al.*, 2010). A review of two different types of AOPs will be presented: [i] physical, and [ii] chemical. Physical methods examined will be ultrasonic and ultraviolet (UV) light and chemical methods will include Fenton's reagent, ozone, potassium permanganate and the peroxy-acid process. Combinations of these methods do exist but they will be discussed separately (Gogate and Pandit, 2004b). For each method a small review of their mechanisms of degradation and advantages/disadvantages will be presented.

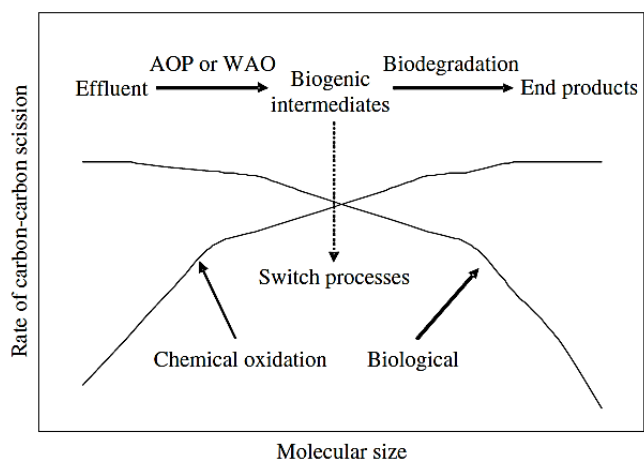


Figure 2.8. Concept of integrating AOPs to pre-treatment.

Figure adapted from (Comninellis *et al.*, 2008).

2.2.1 Physical Methods

2.2.1.1 Ultrasonic Methods

Ultrasonic methods use sound or frequency to induce cavitation, which lead to the formation of small bubbles that release energy and implode in liquids. This technique has been found to be an effective way of treating aromatic organic contaminants. (Rababah and Matsuzawa, 2002; Gogate and Pandit, 2004a; Weavers *et al.*, 1998). The cavitation process causes small bursts of high temperature and pressure surrounding the collapsing bubbles. These bursts can break molecules present creating highly reactive species, like the HO[•] radicals (Ince *et al.*, 2001; Weavers *et al.*, 1998). Cavitation can be induced using high-frequency sound waves in the range of 16-100 kHz, usually using

ultrasonic methods employing sonicators (Gogate and Pandit, 2004a). However, frequencies up to 500 kHz have also been used (Weavers *et al.*, 1998; Pétrier *et al.*, 1994).

2.2.1.1.1 Mechanism

Work done by Ince and colleagues (2001), proposes that the HO[•] radicals created in these cavitation bubbles may react in the gas phase, or recombine at gas-liquid interface surrounding the bubble and/or in the bulk solution to produce H₂O₂ and H₂O. A diagram of the possible radical producing sites of this process is shown (see Figure 2.9) and the process mentioned above involving HO[•] radicals is shown as Equations 2.1 through 2.5 (Ince *et al.*, 2001).

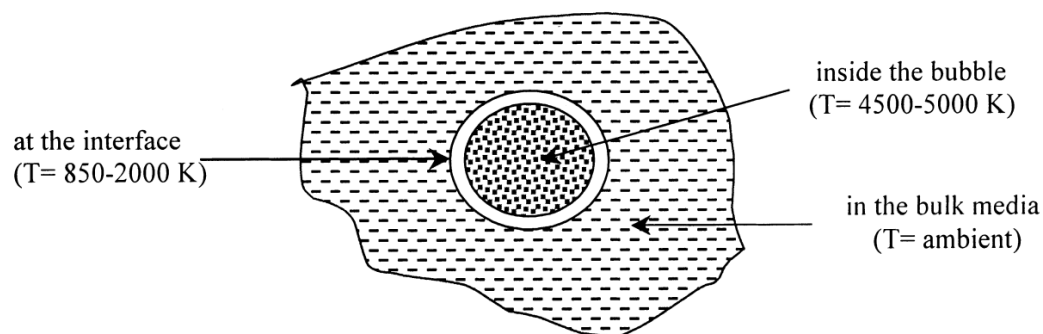
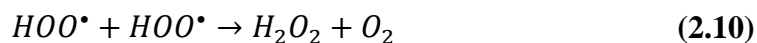


Figure 2.9. Cavitation bubbles, possible sites of chemical reactions.

Figure adapted from (Ince *et al.*, 2001).



If oxygen (O₂) is saturated in solution, more HO[•] and hydroperoxy radical (HOO[•]) can be formed in the gas phase due to the decomposition of O₂ into molecular oxygen and reaction with H₂O. They can also produce additional H₂O₂ which could perpetuate further production of HO[•]. These reactions are shown on Equations 2.6 through 2.10 (Pétrier *et al.*, 1994).



Using sonication, the destruction of the organic compounds can occur in three sites: [i] the cavitation bubble itself, [ii] the interfacial sheath between the bubble and the bulk liquid, [iii] the bulk aqueous solution. These three sites are illustrated in Figure 2.9 (Weavers *et al.*, 1998). The use of ozone (O₃) has also been reported to be effective in producing radicals in solution using ultrasonic techniques (Weavers *et al.*, 1998). While other radicals (*i.e.*, HOO[•]) are produced in these reactions, the primary oxidant present in solution and responsible for the majority of the destruction of organic compounds is thought to be the HO[•] (Ince *et al.*, 2001). A diagram showing the potential pathways of organic compound degradation using ultrasonic methods and ozone is shown on Figure 2.10. Volatile compounds have a tendency to be destroyed in the gas phase, due to their hydrophobicity; while non-volatile compounds tend to be destroyed in the bulk solution (Pétrier *et al.*, 1994). Higher frequencies have been found to correlate with larger amounts of radicals and H₂O₂ in solution and more effective organic compound degradation (Weavers *et al.*, 1998; Pétrier *et al.*, 1994).

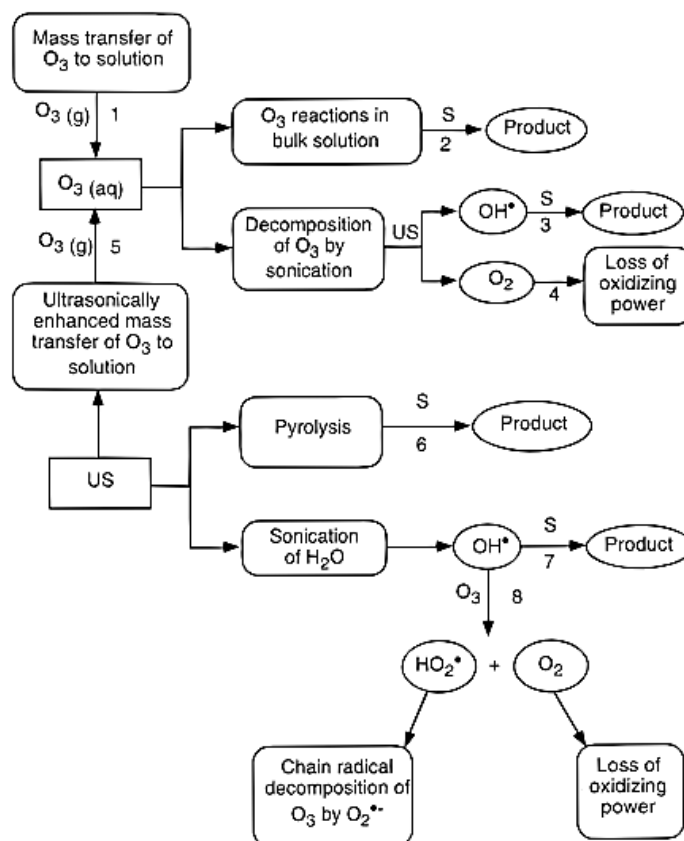


Figure 2.10. Diagram of possible degradation pathways using sonication and ozone.

Figure adapted from (Weavers *et al.*, 1998).

2.2.1.1.2 Advantages/Disadvantages

Advantages of this ultrasonic technique include higher efficiency rates at high frequencies (Gogate and Pandit, 2004a; Pétrier *et al.*, 1994; Weavers *et al.*, 1998). The use of other chemicals for contaminant removal is also not necessary. Ultrasonic systems can also be used in opaque solutions (Ince *et al.*, 2001).

Disadvantages of this method relate to the production and interaction of by-products, both from the contaminants being treated and from other chemicals present in solution. Specifically the role of inorganic compounds and presence of chlorinated compounds are disadvantageous (Weavers *et al.*, 1998; Gogate and Pandit, 2004a). The presence of soil when using ultrasonic methods led to reduced treatment efficiencies (Rababah and Matsuzawa, 2002). Ultra-sonication methods have been proven to be effective at the laboratory scale, however they have been shown to be less effective in

real-world applications like treating waste streams, where complex mixtures of compounds are present (Gogate and Pandit, 2004a). Other disadvantages could be related to energy consumption, which would increase when operating at higher frequencies. Ultrasonic methods have shown to be a possible alternative treatment method however further studies are required in order to be implemented in real-world applications (Gogate and Pandit, 2004a).

2.2.1.2 Ultraviolet Light Process

Photocatalytic methods or photochemical degradation processes, like UV treatment have been used in treat of organic contaminants and have been gaining importance in the area of wastewater treatment (Gogate and Pandit, 2004a; Legrini *et al.*, 1993). UV treatment methods rely on photo-activated chemical reactions. These methods use photons emitted through UV radiation to interact with oxidizing compounds like H_2O_2 and O_3 to produce free radicals (Gogate and Pandit, 2004a; Comninellis *et al.*, 2008; Gan *et al.*, 2009; Legrini *et al.*, 1993). The most commonly used irradiation wavelengths used in UV AOPs are around the 200-370 nm range (Legrini *et al.*, 1993). UV AOPs have been widely studied, usually where UV is coupled with highly oxidizing compounds. Typical examples include $\text{H}_2\text{O}_2/\text{UV}$, O_3/UV , and TiO_2/UV processes (Comninellis *et al.*, 2008; Zhang *et al.*, 2008). The degradation of organic compounds via direct photolysis, without the use of additional oxidants, has also been observed (Burrows *et al.*, 2002). This UV overview will focus on those four UV utilizing examples.

2.2.1.2.1 Mechanism

The mechanism for the $\text{H}_2\text{O}_2/\text{UV}$ process and H_2O_2 photolysis, will be examined first. The most commonly accepted mechanism involves the cleavage of the H_2O_2 molecule into two HO^\bullet radicals due to the interaction with a photon. This process is shown on Equation 2.11 (Legrini *et al.*, 1993). Reactions of hydroxyl radicals with compounds like PAHs would follow the hydrogen abstraction mechanism, where the

resulting organic radical can initiate several chain reactions. An example of these radical propagation reactions are shown on Equations 2.12 and 2.13 (Legrini *et al.*, 1993).



The hydroxyl radical created in Equation 2.11 abstracts a hydrogen from the organic compound (R), yielding a water molecule and an organic radical (R \cdot) (see Eq. 2.12). The organic radical can then react with H₂O₂, forming a hydroxylated organic compound and another HO \cdot radical as illustrated in Equation 2.13. A proposed reaction mechanism for the H₂O₂/UV system is shown below on Figure 2.11.

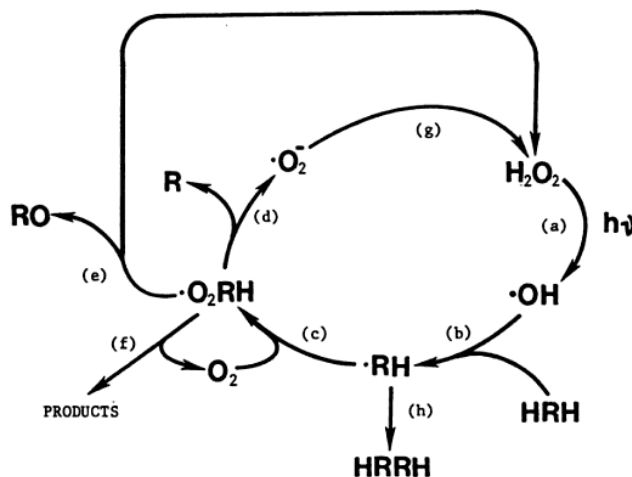


Figure 2.11. Reaction system in the H₂O₂/UV system.

Figure adapted from (Peyton, 1990).

The O₃/UV mechanism, also called O₃ photolysis, consists of the reaction of O₃ dissolved in water, reacting with a photon and eventually leading to the production of H₂O₂. This mechanism has been proposed to be a two-step process involving the homolysis of O₃ and then production of HO \cdot radicals. It has been observed that the

photolysis of dissolved O_3 leads to the production of H_2O_2 in a sequence of reactions, where HO^\bullet does not leave the reaction site. These reactions are shown on Equations 2.14, 2.15 and 2.16, respectively (Legrini *et al.*, 1993).



Work done by Peyton and Glaze (1988) concluded that the HO^\bullet is the primary active species in ozone photolysis, but H_2O_2 is ultimately the final product; in addition, secondary reactions of radicals formed in scavenging processes, driven by O_3 input, maybe be important for sparged systems. The set of organic degradation reaction pathways in the O_3/UV systems is shown in Figure 2.12.

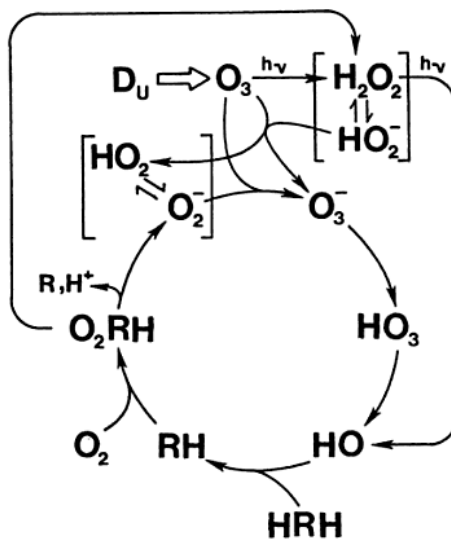
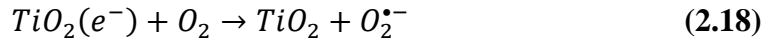


Figure 2.12. Reaction pathways in the O_3/UV system.

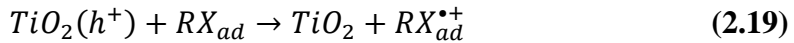
Figure adapted from (Peyton and Glaze, 1988).

The TiO_2/UV process has been utilized for a long time and was first shown to be effective in the degradation of biphenyl and chlorobiphenyls (Carey *et al.*, 1976). Many

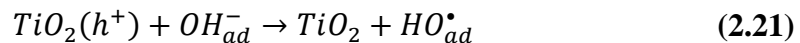
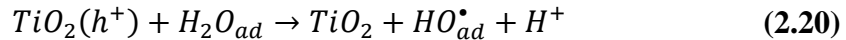
new applications involving titanium dioxide and platinumized TiO₂ powders have also been shown to be effective in degrading organic contaminants in water (Legrini *et al.*, 1993). The TiO₂/UV process utilizes titanium dioxide (TiO₂) particles, which are a semi-conductive material, and irradiates it with UV radiation. Spectral absorption properties of TiO₂ allow can promote and electron (e⁻) from the valence band (VB) to the conduction band (CB), leaving a positive electron hole (h⁺) where the electron was originally located (see Eq. 2.17). This phenomenon then allows oxidation to take place. (Zhang *et al.*, 2008; Legrini *et al.*, 1993). In order for these oxidation processes to take place, molecular oxygen must be present since it serves as the accepting species in the electron-transfer reaction from the conduction band (see Eqs. 2.17 and 2.18) (Legrini *et al.*, 1993).



Two distinct oxidation reaction mechanisms have been observed for the TiO₂/UV process. Mechanism I is an electron transfer mechanism from an adsorbed substrate RX, shown in Equation 2.19 (Fox *et al.*, 1991).



Mechanism II involves an electron transfer reaction from adsorbed solvent molecules, H₂O and HO⁻, as shown on Equations 2.20 and 2.21 (Pichat, 1991).



Mechanism II (see Eqs. 2.20 and 2.21) seems to be of greater significance in oxidation processes. The reasons being: [i] high concentrations of H₂O, and [ii] HO[•] molecules adsorbed at particle surfaces. The addition of H₂O₂ has also been found to considerably enhance photodegradation rates probably due to acting as an accepting species (Alpert *et al.*, 1991; Ollis *et al.*, 1991). The reaction of TiO₂ and H₂O₂ is most probably thought to occur as illustrated in Equation 2.22 (Legrini *et al.*, 1993).



The final mechanism discussed will be direct photolysis. Direct photolysis of organic compounds has been observed as well. For example, Burrows and colleagues (2002) discussed possible degradation of pesticides via direct photolysis without the aid of additional oxidants. Direct photolysis occurs naturally. However, it is highly dependent on the contaminants' exposure to direct sunlight. Compounds that undergo direct irradiation mediated by sunlight can be promoted to excited singlet states, and eventually triplet states. At this point three possible pathways are hypothesized: [i] homolysis, [ii] heterolysis or [iii] photoionization. A diagram depicting these three possible reaction pathways is shown in Figure 2.13 below.

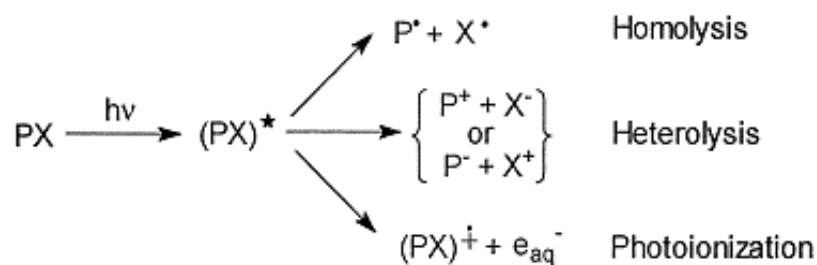


Figure 2.13. Direct photolysis possible reaction pathways.

Figure adapted from (Burrows *et al.*, 2002).

2.2.1.2.2 Advantages/Disadvantages

Research using photocatalytic methods is extensive and is still being done today. The effective destruction of halogenated aliphatic compounds, halophenols, pesticides, and aromatics, has been observed using a variety of photocatalytic methods (Sundstrom *et al.*, 1986; Weir *et al.*, 1987; Burrows *et al.*, 2002; Gogate and Pandit, 2004a). Zhang and colleagues (2008) used the TiO₂/UV process to effectively degrade benzo[a]pyrene, phenanthrene and pyrene. Advantages using photocatalytic oxidation include room: temperature and pressure operating conditions, and natural resources (*i.e.*, sunlight). These resources are freely available, which could result in economic savings, TiO₂ has a low cost, and treatments of organic compounds (including aromatic compounds) have been found to be effective (Gogate and Pandit, 2004a). An advantage of the H₂O₂/UV process is that it is able to completely oxidize a variety of contaminants to innocuous products (Venkatadri and Peters, 1993).

Possible disadvantages are: [i] lower reaction rates compared to conventional chemical reaction rates, [ii] applications to real world effluents are lacking, and [iii] non-uniform radiation at large scales. This leads to inefficient use of energy and economic loss (Gogate and Pandit, 2004a). The presence of soil or other particles, colored by-products and the formation of precipitates greatly reduce treatment efficiencies since they reduce UV light penetration, which could lead to limitations of these applications (Venkatadri and Peters, 1993). The formation of precipitates could be managed by implementing pH controls. However efficiencies of these processes, like the TiO₂/UV and H₂O₂/UV process, have been found to be pH dependent (Zhang *et al.*, 2008; Weir *et al.*, 1987). A disadvantage specific to the O₃/UV process is that O₃ is an unstable gas, and handling of O₃ can prove to be problematic (Weir *et al.*, 1987). This might also be a disadvantage for the H₂O₂/UV process, since H₂O₂ is very reactive. In addition, optimal dosing is an important factor in the H₂O₂/UV process. Any unused H₂O₂ may act as a HO[•] radical scavenger, which can result in lower oxidation efficiencies (Beltrán *et al.*, 1997). A problem relating to direct photodegradation is that natural sunlight reaching the Earth's surface contains small amounts of short-wave UV radiation necessary for photolysis leading to slow reaction rates. This severely limits the potential use of direct photodegradation in environmental applications (Burrows *et al.*, 2002).

2.2.2 Chemical Methods

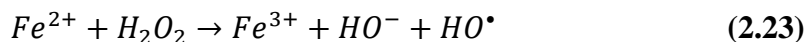
Chemical oxidation processes are the most commonly used oxidation processes, and they can be used to remediate soils contaminated with PAHs (Gan *et al.*, 2009). Many different methods exist. In this literature review four different methods will be reviewed: [i] Fenton's reagent, [ii] ozone, [iii] potassium permanganate and [iv] peroxy-acid process. A general overview will be given and their respective mechanisms with advantages and disadvantages will be discussed below.

2.2.2.1 Fenton's Reagent Process

Fenton's reagent consists of an Fe(II)-H₂O₂ system. Specifically, H₂O₂ and an iron catalyst in solution has been shown to be able to oxidize contaminants (Gan *et al.*, 2009; Gogate and Pandit, 2004a). This technique was first developed by Henry John Horstman Fenton in the 1890s (Fenton, 1894). Fenton's reagent is used to treat PAHs and other contaminants and is considered an accepted technique for environmental use (Gan *et al.*, 2009; Gogate and Pandit, 2004a).

2.2.2.1.1 Mechanism

The major steps in the Fenton's reagent reaction mechanism involve the decomposition of H₂O₂ into two HO• radicals in the presence of ferrous iron (*e.g.*, Fe²⁺). Equation 2.23 illustrates this step (Flotron *et al.*, 2005). The HO• radicals produced can then degrade organic compounds (R, RH) by hydrogen abstraction or by hydroxyl addition as illustrated in Equations 2.24 and 2.25, respectively (Flotron *et al.*, 2005).



The optimum operating pH for Fenton's reagent process is between 3 and 4 for most chemicals. Otherwise HO• radical scavenging by H⁺ and other ions will decrease reaction rates (Gogate and Pandit, 2004a). As the reaction occurs, the concentration of ferrous ions will increase, and this increased salt concentration can also lead to lower reaction rates as investigated by Gogate and Pandit (2004a).

2.2.2.1.2 Advantages/Disadvantages

As mentioned before, Fenton's reagent is widely used and can be advantageous in the field where other AOPs are not feasible (Venkatadri and Peters, 1993). This technique is also very effective in degrading high MW organic compounds, like PAHs, and is not affected by colored organics like UV processes are (Venkatadri and Peters, 1993). The Fenton's reagent process is also more likely to be effective in *in-situ* applications, allowing for on-site treatment. When applied in the field, it has been found that naturally occurring minerals in soils are able to effectively catalyze the reaction, which could simplify design and reduce reagent costs. This, however, is dependent of local geologic conditions (Watts and Teel, 2005).

Ferrarese and colleagues (2008) found that for effective PAH removal, additional catalysts were required, which could increase cost. Also the pH dependency of Fenton's reagent could be problematic not only decreasing reaction rates, but also adding higher costs due to the use of pH buffers (Gogate and Pandit, 2004a). Increases in iron concentration as the reaction occur could also prevent this process from being used in large applications as total dissolved solids (TDS) would increase and the resulting effluent could be potentially non-compliant for discharge limits (Gogate and Pandit, 2004a).

2.2.2.2 Ozone Chemical Oxidation Process

The ozone chemical oxidation process uses O₃, a very powerful oxidizing agent. This process is often coupled with the use of the H₂O₂ and they are commonly used together (Gogate and Pandit, 2004a). The processes discussed will encompass both the

ozone process and the ozone/hydrogen peroxide process since they are very similar in nature resulting often in combination of these two methods (Gogate and Pandit, 2004b).

2.2.2.2.1 Mechanism

For the following mechanism, O_3 must be in solution. Commonly used devices used to transfer O_3 to water include countercurrent bubble columns, packed and plate columns, jet reactors, agitated vessels, static mixers, and electric-discharge ozone generators (Gogate and Pandit, 2004a; O'Mahony *et al.*, 2006). Miller and Olejnik (2004) examined a kinetic study of the O_3 process. These resulting reactions are shown in Equations 2.26 through 2.30 (Miller and Olejnik, 2004). In aqueous solution, O_3 can react with hydroxyl anions as illustrated in Equation 2.26.



This produces a hydroperoxide anion (HO_2^-) (see Eq. 2.26). At this point there are two possible pathways: [i] the hydroperoxide anion can react with a proton, producing H_2O_2 (see Eq. 2.27), or [ii] react with ozone producing a hydroperoxide radical and an ozonide radical anion (see Eq. 2.28). These products then undergo subsequent reactions to form HO^\bullet radicals and the mechanism is shown in Figure 2.14.



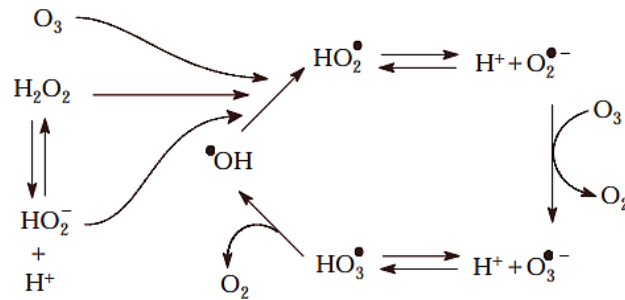


Figure 2.14. Ozonation reaction pathways.

Figure adapted from (Miller and Olejnik, 2004).

As shown in Figure 2.14, the HO^\bullet radicals can then attack O_3 , H_2O_2 or its anion, propagating the reaction by creating hydroperoxide radicals and superoxide radical anions. When organic contaminants (R) are then introduced into this system, these organic contaminants undergo degradation through the direct reaction shown in Equation 2.29, or the radical reaction shown in Equation 2.30.



If these reactions are conducted at low pH, HO^\bullet scavengers will diminish the occurrence of the reaction illustrated Equation 2.30. When reaction time periods are short, the reactions of intermediates consuming O_3 can be neglected (Miller and Olejnik, 2004).

2.2.2.2.2 Advantages/Disadvantages

The use of ozonation is common and is a proven technology used in drinking water treatment. Ozonation is a very effective disinfectant process; this process is capable of destroying bacteria, viruses and is capable of inactivating cryptosporidium (Rochelle *et al.*, 2004). The O_3 generated from air has also been used to remove phenanthrene from spiked soils. In the study by O'Mahony *et al.* (2006), at least 50%

reduction in phenanthrene levels was achieved when soils were air-dried and up to 85% removal in sandy soils (O'Mahony *et al.*, 2006). Phenanthrene degradation was dependent of water and clay content in soils as these clogged pore spaces provided adsorption sites, limiting ozone interaction with the phenanthrene (O'Mahony *et al.*, 2006). Miller and Olejnik (2004) effectively degraded benzo[a]pyrene, chrysene, and flourene in aqueous solutions using ozonation, and found that PAHs were mainly degraded through direct reaction with O₃. The use of ozone has also been proven to be effective in treating groundwater contamination (Watts and Teel, 2005). A benefit of ozonation is that it does not require the use UV light which could prove to be an economic advantage. In addition, O₃ also has potential to be used *in-situ*. However, dewatering might have to be done to contaminated soil in order for ozonation to work (Watts and Teel, 2005; O'Mahony *et al.*, 2006).

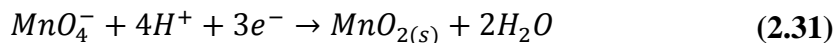
Using O₃ combined with H₂O₂ has not been shown to improve degradation in distillery wastewaters when compared to degradation using O₃ alone (Beltrán *et al.*, 1997). A disadvantage of using O₃, like mentioned in Section 2.2.1.2.2, is the stability of the compound, as O₃ is a very reactive gas. Ozonation is also pH dependent: at low pH hydroxyl radical scavengers led to lower efficiencies, while high pH resulted in ozone reacting almost indiscriminately with organic compounds present (Gogate and Pandit, 2004a; Miller and Olejnik, 2004). Other issues with O₃ relate to contact time, operating temperatures, high dosing and presence of other organics in the medium reacting with incoming ozone, depleting the ozone source (Gan *et al.*, 2009; Gogate and Pandit, 2004a). Ozone technology is easy to adapt to and has proven to be more effective when coupled with other AOP technologies (Gogate and Pandit, 2004a).

2.2.2.3 Potassium Permanganate

Potassium Permanganate (KMnO₄) has been widely used as an oxidant in the treatment of contaminated soils (Brown *et al.*, 2003; Ferrarese *et al.*, 2008). It is a salt consisting of K⁺ and permanganate ions (MnO₄⁻). It also has been used in *in-situ* chemical oxidations, treating chlorinated ethylene, phenol and other aromatic compound contamination (Waldemer and Tratnyek, 2006; Yan and Schwartz, 1999).

2.2.2.3.1 Mechanism

In aqueous systems, the permanganate salts generate MnO_4^- . This decomposition reaction is shown in Equation 2.31 (Ferrarese *et al.*, 2008).



Permanganate salts have a relatively low standard oxidation potential, but they are still considered strong oxidizing agents and are able to break organic molecules containing C-C double bonds, aldehyde groups or hydroxyl groups (Brown *et al.*, 2003). Permanganate oxidation mechanisms, especially in the field, are complex. In addition, numerous reactions can occur. For example, permanganate degradation mechanism of ethylene in neutral and weakly acidic conditions is shown in Figure 2.15.

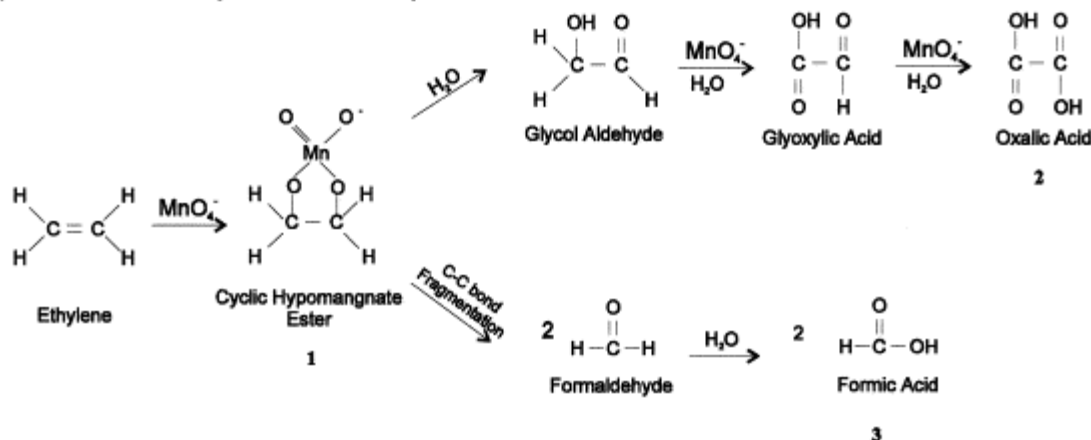


Figure 2.15. Permanganate reaction scheme of ethylene.

Figure adapted from (Yan and Schwartz, 1999).

Degradation of organic compounds using MnO_4^- is dependent on their structure (and functional groups) and it has received little attention as a PAH oxidant, because of its inability to attack the stable benzene ring (Ferrarese *et al.*, 2008). However, in the presence of the MnO_4^- ion, oxidation of PAHs can occur, but it is largely dependent of the PAH structure and amount of aromatic rings (Brown *et al.*, 2003).

2.2.2.3.2 Advantages/Disadvantages

An advantage of using potassium permanganate is that it is not as pH sensitive as other AOPs (Guan *et al.*, 2010). It has also been a proven technology when it comes to treating organic contaminants (Waldemer and Tratnyek, 2006; Brown *et al.*, 2003; Yan and Schwartz, 1999). Handling and transportation of the permanganate salt would prove easier than that of H₂O₂ or O₃, and it is also stable compared to these two materials. The risk of chlorinated by-products will be also minimized when using permanganate (Guan *et al.*, 2010). Problems with potassium permanganate could be due to the precipitation on MnO₂. If applied to water treatment technologies or when used *in-situ*, these solids could be a disadvantage in water treatment systems (Guan *et al.*, 2010). While potassium permanganate has been used in treating organic compounds, more research is needed on using it for specifically for PAH remediation (Ferrarese *et al.*, 2008).

2.2.2.4 Peroxy-Acid Process

Recently, treatment methods that use peroxy-acid to degrade organic contaminants have been gaining more attention (Gan *et al.*, 2009). Peroxy-acids, or peracids, are acids that contain an acidic COOH group. Peracetic acid (PAA) is a type of peroxy-acid with the formula CH₃COOOH. The structure of PAA is shown in Figure 2.16. Peroxy-acids have been shown to be effective in the treatment of organic compounds like PAHs in soils (Alderman and Nyman, 2009; Alderman *et al.*, 2007; N'Guessan, 2005; N'Guessan *et al.*, 2004b; Levitt *et al.*, 2003). This process has also shown to be effective in the disinfection of primary, secondary and tertiary wastewater treatment and in replacing chlorination during wastewater treatment at the pilot-scale level (Koivunen and Heinonen-Tanski, 2005; Dell'Erba *et al.*, 2007).

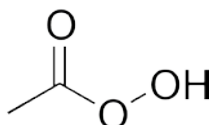
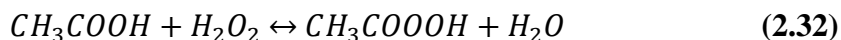


Figure 2.16. Peracetic acid chemical structure.

2.2.2.4.1 Mechanism

The most commonly used method of preparing PAA is by combining H₂O₂, with an organic acid like CH₃OOH, as illustrated in Equation 2.32. This reaction is reversible and a mixture of products and reactants is obtained. (Zhao *et al.*, 2007).



The rate at which equilibrium can be achieved, can be accelerated by adding a strong acid catalyst like sulfuric acid (H₂SO₄). (Zhao *et al.*, 2007; Zhao *et al.*, 2008; Bach *et al.*, 1997). The peroxy-acid method is thought to use the oxidation potential of both HO• radicals and PAA in the system (Alderman and Nyman, 2009). Many mechanisms have been proposed for the degradation of organics using the peroxy-acid process (Shoulder, 2012). Mechanisms of the spontaneous decomposition of PAA have been proposed as well (Zhao *et al.*, 2008). A hypothesized PAA degradation mechanism, using benzo[a]pyrene as a model contaminant is shown on Figure 2.17.

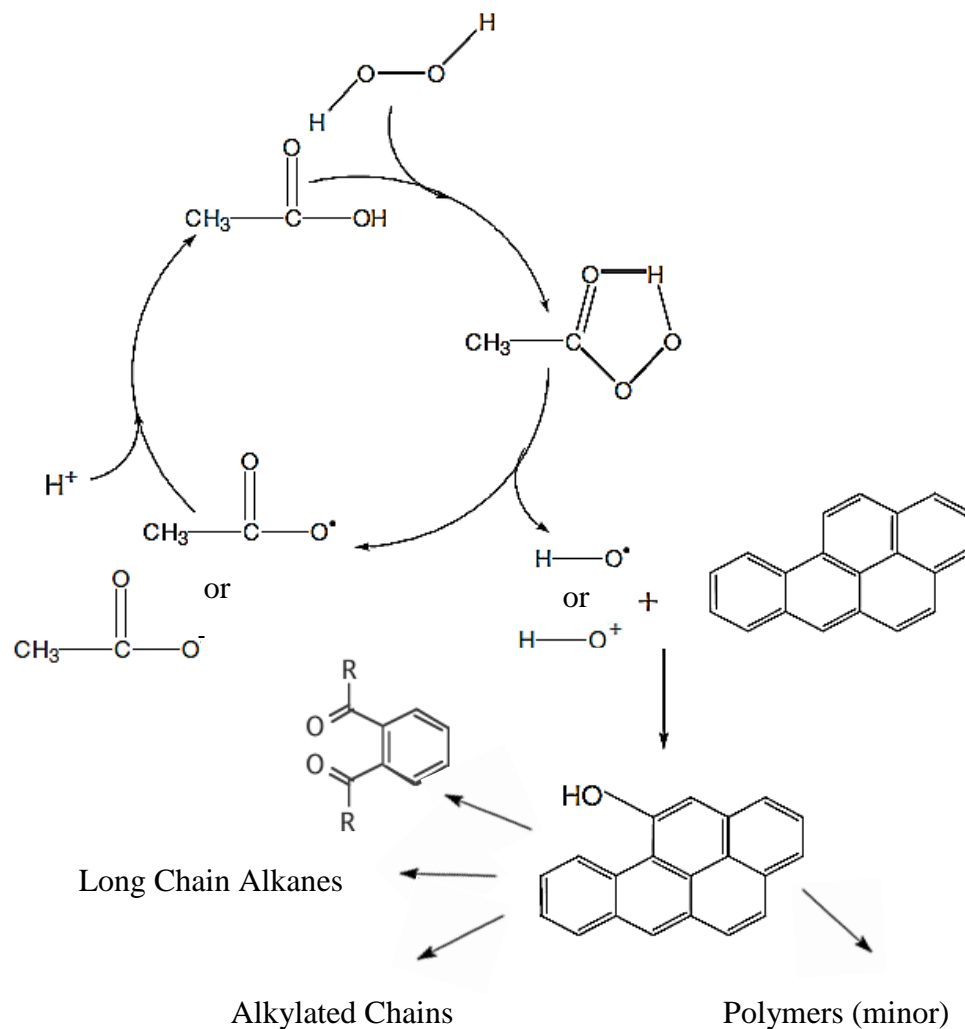


Figure 2.17. Hypothesized peroxy-acid degradation mechanism of a PAH.

Figure adapted from (N'Guessan *et al.*, 2004a; Shoulder, 2012)

In this mechanism H_2O_2 interacts with organic acid, forming PAA. As a result, HO^\bullet radicals or hydroxyl cations (HO^+) are released from that reaction along with an acyloxy radical or the conjugate base of the organic acid as shown in Figure 2.17. Like in other AOPs, the acyloxy radical ($\text{CH}_3\text{COO}^\bullet$) and conjugate base can then further react with an organic or interact with another radical or be protonated in the acidic medium, respectively. Other possible mechanisms of oxidative degradation involve the HO^\bullet radical produced from H_2O_2 or PAA, and epoxidation of double bonds by PAA. The

epoxidation of carbon double bonds using PAA was observed in alkenes and ring structures when peroxy-acids were in solution (Bach *et al.*, 1997). This mechanism, adapted for aromatics is shown in Figure 2.18.

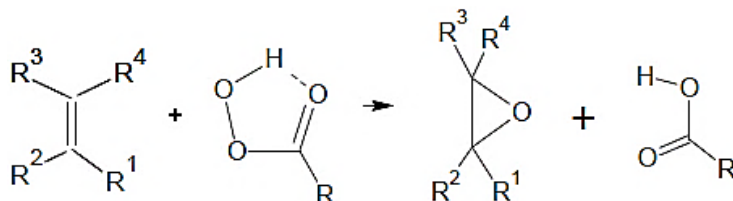
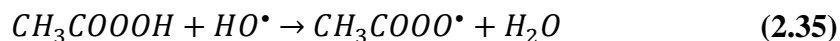
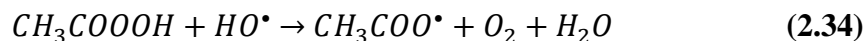
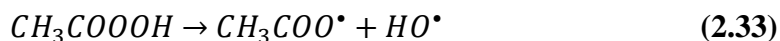


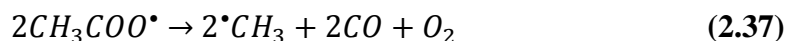
Figure 2.18. PAA epoxidation reaction of a C=C bond.

Figure adapted from (Bach *et al.*, 1997; Shoulder, 2012)

Investigations of the radicals in PAA solutions have been conducted by Rokhina and colleagues (2010). As examined by Rokhina and colleagues (2010), a reaction mechanism of the radical formation in the PAA process proposed by Heywood and colleagues (1961) is shown on Equations 2.33 through 2.38. The formed HO[•] radical in Equation 2.33 can then attack either the organic contaminant present, or the PAA molecule. Two different radical pathways can be observed from the reaction between PAA and the HO[•] radical (see Eqs. 2.34 and 2.35).



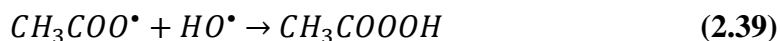
The unstable CH₃COO[•] radical, tends to dissociate to a methyl radical ([•]CH₃) and CO₂ or methyl radical, CO and oxygen as demonstrated in Equations 2.36 and 2.37.



Methyl radicals can react with oxygen as shown in Equation 2.38 (El-Agamey and McGarvey, 2003). However, this is a fast reaction in oxygen-saturated environments and amounts of $\cdot\text{CH}_3$ in solution are fairly limited (Shi and Li, 2007). The $\cdot\text{CH}_3$ radical chain can also be terminated via hydrogen abstraction (Heywood *et al.*, 1961).



Also, $\text{HO}\cdot$ radicals that are formed as primary radicals will react with $\text{CH}_3\text{COO}\cdot$, generating a new organic molecule and restarting a new oxidation cycle (Rokhina *et al.*, 2010). This reaction is shown in Equation 2.39 (Ciotti *et al.*, 2008).



As shown in Equations 2.33 through 2.39, different radical species (*i.e.*, $\text{HO}\cdot$, $\cdot\text{CH}_3$, $\cdot\text{CH}_3\text{CO}$, $\text{CH}_3\text{OO}\cdot$, and $\text{CH}_3\text{COO}\cdot$) have been found present in solution in the peroxy-process. However $\text{HO}\cdot$ radical was found to be the most predominant species and this can lead to thinking that the degradation mechanism, in the peroxy-acid process would involve oxidation via $\text{HO}\cdot$, PAA, or $\text{HO}\cdot$ and PAA (Rokhina *et al.*, 2010).

2.2.2.4.2 Advantages/Disadvantages

The peroxy-acid method has been used as an alternative to traditional chlorine-based disinfection techniques at the batch and pilot-scale level, and has been proven to be a suitable alternative for wastewater reuse, both *Escherichia coli* and total coliform inactivation was achieved (Dell'Erba *et al.*, 2004). The hygienic qualities of secondary and tertiary effluent from municipal wastewater plants was improved by using the peroxy-acid process (Koivunen and Heinonen-Tanski, 2005). This method also resulted in negligible concentrations of DBPs at the pilot-scale level leading to well below maximum allowable concentrations of namely aldehydes and halogenated phenols while

brominated phenol levels were only negligible under pH conditions too low for municipal wastewater treatment (Dell'Erba *et al.*, 2007). When using the peroxy-acid treatment at concentrations required for disinfection, it often generated safe, biodegradable and non-toxic DBPs (Colgan and Gehr, 2001; Booth and Lester, 1995; Kitis, 2004). However, the production of brominated organics could be a potential concern when using this process (Booth and Lester, 1995). Unlike in UV processes, colored compounds or cloudy solutions would not interfere with treatment efficiencies when the peroxy-acid treatment process is used.

Like other AOPs, the efficiency of the peroxy-acid method is dependent on temperature and pH, where higher temperatures and lower pH increase disinfection efficiencies as demonstrated by Kitis (2004) (Kitis, 2004). This could affect potential application of this method to existing technologies and increase economic cost. Disadvantages associated with using peroxy-acid treatment as a disinfection agent relate to the increase of organic content in the effluent with potential of microbial regrowth which could limit application in wastewater treatment systems (Kitis, 2004). This would be due to the addition of acetic acid in the peroxy-acid process, which could serve as a food source for microbes in the wastewater solution. Another disadvantage of the PAA process is that it has limited worldwide production leading to the peroxy-acid treatment having a higher cost than sodium hypochlorite. Hypochlorite is widely used in treatments needing chlorination (Kitis, 2004). The peroxy-acid is a process used in many industries including the beverage, textile, pharmaceutical, medical and paper industries (Kitis, 2004). It has also been used in wastewater applications around the world (Dell'Erba *et al.*, 2004; Dell'Erba *et al.*, 2007; Koivunen and Heinonen-Tanski, 2005; Kitis, 2004). Degradation rates of PAHs have been found to be comparable to those of other AOPs (Alderman and Nyman, 2009). The use of peroxy-acid has also shown to have potential in environmental remediation applications, treating compounds like PAHs, chlorinated phenols, substituted aromatics, and alkene compounds (Alderman and Nyman, 2009; N'Guessan *et al.*, 2004b; Levitt *et al.*, 2003; Booth and Lester, 1995; Bach *et al.*, 1997). The peroxy-acid process can also be utilized for the degradation of organic compounds in both the liquid and solid phases, being useful in the treatment of

contaminated soils and sediments (Alderman *et al.*, 2007; N'Guessan *et al.*, 2004a; N'Guessan *et al.*, 2004b; N'Guessan, 2005; Levitt *et al.*, 2003).

3. MATERIALS AND METHODS

3.1 Materials

Anthracene (99%), benzo[a]pyrene (97%), and phenanthrene (99.5%) were purchased from Sigma-Aldrich Chemistry (St. Louis, MO). Pyrene (98.4%) was purchased from ChemService, Inc. (West Chester, PA). All PAH compounds were used as received. Zero grade air, ultra high purity helium, ultra high purity hydrogen and ultra-high purity nitrogen were purchased in compressed cylinder from Noble Gas Solutions (Albany, NY) and Airgas, Inc. (Radnor Township, PA).

Certified ACS acetone, glacial ACS acetic acid, HPLC grade hexanes, 50% (v/v) stabilized hydrogen peroxide, ACS plus sulfuric acid, USP grade potassium permanganate, USP grade manganese sulfate monohydrate, ACS grade potassium iodide, 0.100 N standardized sodium thiosulfate solution, certified ACS sodium sulfite and USP/FCC sodium sulfate were all purchased from Fisher Scientific (Pittsburgh, PA). Primary standard grade sodium oxalate was obtained from J. T. Baker (Phillipsburg, NJ).

3.2 Methods

3.2.1 Peracetic Acid (PAA) Generation Study

3.2.1.1 Experimental Methods

An initial investigation was done using the reaction ratio of 3 mL glacial acetic acid (CH_3COOH) : 3 mL 50% hydrogen peroxide (H_2O_2) : 9 mL of nano-pure distilled water (DI) in order to examine PAA generation and H_2O_2 concentrations in the centrifuge tubes (*e.g.*, T1). All experiments were carried out in 35 mL glass centrifuge tubes capped with Teflon® lined septa. Additionally, 1 mL of sulfuric acid (H_2SO_4) catalyst was added to two sets of the tubes (*e.g.*, T2 and T4) and the volumes of CH_3COOH and H_2O_2 were varied to determine how it would affect PAA generation. For the centrifuge tubes that included 1 mL H_2SO_4 , or differing amounts of the reagents than mentioned above, the amount of DI added was adjusted in order to keep the total volume

amount of the centrifuge tubes the same (*i.e.*, 15 mL) (*e.g.*, T2, T3, and T4). Table 3.1 lists the volumes of the reagents added to the 35 mL centrifuge tubes. The centrifuge tubes were then placed on an orbital shaker at a speed of at least 100 RPM, protected from light for the entirety of the reaction period. The reaction time period for samples indicated in Table 3.1 was close to 4 hours and experiment was conducted at room temperature. The reaction was stopped with the addition of 3 mL of 1M sodium sulfite (NaSO_3) in water solution, and centrifuge tubes were contents were mixed using a vortex mixer.

Table 3.1. Experimental conditions for initial PAA study.

Sample	DI Water (mL)	Acetic Acid (mL)	Hydrogen Peroxide (mL)	Sulfuric Acid (mL)	Total Volume (mL)
T1	9	3	3	-	15
T2	8	3	3	1	15
T3	5	5	5	-	15
T4	4	5	5	1	15

Another study was conducted with the addition of 100 μL of an anthracene stock solution prepared in acetone (approximately 5000 mg L^{-1} , of known concentration), this experimental set-up did not have the addition of the H_2SO_4 catalyst and was used as a model for PAH degradation study discussed in Section 3.2.2. This experiment consisted of one experimental set-up and three control set-ups. Following the addition of the reagents to the centrifuge tubes, 100 μL of the anthracene stock solution were added. The experimental set-up reaction periods were 0, 0.5, 1, 2, 3, 4, 5, and 24 hours. After the addition of all the reagents and the anthracene stock solution, the centrifuge tubes were then placed on an orbital shaker at a speed of at least 100 RPM, protected from light for the entire reaction period. At the end of the desired reaction interval, 3 mL of 1M sodium sulfite in water was added to the centrifuge tubes to stop the reaction and the contents of the centrifuge tubes were mixed using a vortex mixer. All reactions took

place at room temperature. The experimental conditions for this study are shown below on Table 3.2. The amount of H₂O₂ and PAA present in the centrifuge tubes was then determined by performing titrations (see Sections 3.2.1.3 and 3.2.1.4).

Table 3.2. Experimental conditions for initial PAA study, with anthracene.

Set-up	Anthracene			Hydrogen Peroxide (mL)	1M Sodium Sulfite (mL)
	Stock Solution (μL)	DI Water (mL)	Acetic Acid (mL)		
Experimental	100	9	3	3	3
CH ₃ COOH Control	100	12	3	0	3
H ₂ O ₂ Control	100	12	0	3	3
DI Water Control	100	15	0	0	3

3.2.1.2 Controls

The controls consisted of [i] one for DI water, [ii] one for CH₃COOH and [iii] one for the H₂O₂ control. The reaction periods for the H₂O₂ control were 0, 3, and 24 hours. For the DI water control and CH₃COOH control, only one reaction period was done at 0 hours. The controls followed the same procedure as the experimental set-up (see Section 3.2.1.1). The volumes and contents of the controls are shown in Table 3.2. The controls consisted of: [i] CH₃COOH control only acetic acid, DI water and 100 μL of stock solution; [ii] H₂O₂ control consisted of only H₂O₂, DI water and 100 μL of stock solution; and [iii] DI Water control consisted of only DI water and 100 μL of stock solution. More information about PAH calibration and gas chromatographic (GC) methods are provided in Appendices B and C.

3.2.1.3 Titrations

Two titrations were performed for each sample to determine H₂O₂ and PAA concentrations. Sodium thiosulfate (Na₂S₂O₃) was used as a 0.100 N solution and was used in the titration for determining PAA concentration. A 0.10 N solution of potassium permanganate (KMnO₄) was prepared from a 0.50 N KMnO₄ in water solution and diluting it with DI H₂O.

3.2.1.3.1 Potassium Permanganate Standardization

The 0.10 N KMnO₄ titrant solution was standardized using sodium oxalate (Na₂C₂O₄). This process followed instructions outlined by Shoulder (2012). The normality (N) of the prepared KMnO₄ solution was then calculated by using Equation 3.1.

$$N \text{ KMnO}_4 = \frac{\text{weight of Na}_2\text{C}_2\text{O}_4(\text{g})}{\left(\frac{67.0 \text{ g Na}_2\text{C}_2\text{O}_4}{\text{mol. eq. Na}_2\text{C}_2\text{O}_4}\right) (\text{volume KMnO}_4 (\text{L}))} \quad (3.1)$$

The procedure used included two replicate standardizations and the N of the KMnO₄ solution was recorded as the average to the nearest hundredth thousandths unit.

3.2.1.4 Hydrogen Peroxide and Peracetic Acid Determination

This section discusses the hydrogen peroxide and PAA determination. The process follows steps outlined by Shoulder (2012). Approximately one gram (mass known) of the reaction mixture was weighed into a 100 mL volumetric flask and is was then diluted to volume using DI H₂O, 20 mL of this solution was placed in a 125 mL Erlenmeyer flask and 20 mL of DI H₂O were added to this flask. One mL of H₂SO₄ and one mL of 0.2M manganese sulfate (MnSO₄) were also added to the solution in the flask. The solution was then titrated with the prepared standardized KMnO₄ titrant solution to determine the H₂O₂ concentration based on Equation 3.2. The solution was then added until the first pink color appeared, indicating the consumption of H₂O₂ in solution and

the volume of titrant was recorded. Next, 1 mL of a 30% potassium iodide (KI) solution was added to the flask, turning the solution a straw-yellow color. The solution was then titrated with $\text{Na}_2\text{S}_2\text{O}_3$ to a colorless endpoint, and the volume of titrant was again recorded. A set of two aliquots was prepared and titrated from each sample, and the result was reported as the mean value of these two titrations. The weight percent (wt. %) of H_2O_2 was calculated using Equation 3.2, which utilizes the volume of KMnO_4 needed to titrate the solution to the first endpoint.

$$\% \text{H}_2\text{O}_2 = \frac{(L \text{KMnO}_4)(N \text{KMnO}_4) \left(\frac{17.01 \text{ g H}_2\text{O}_2}{\text{mol eq. H}_2\text{O}_2} \right) (DF)(100)}{(g \text{ of sample})} \quad (3.2)$$

DF is the dilution factor, which was equal to 5 for all titrations since a 20 mL aliquot was used from the original 100 mL of solution; and g of sample is the initial weight of the sample weighed into the 100 mL volumetric flask. The wt. % of PAA in the solution was calculated using Equation 3.3, which utilizes the volume of $\text{Na}_2\text{S}_2\text{O}_3$ needed to titrate the solution to the second endpoint. In this equation, DF and g of sample are the same as indicated above for Equation 3.2.

$$\% \text{PAA} = \frac{(L \text{Na}_2\text{S}_2\text{O}_3)(L \text{Na}_2\text{S}_2\text{O}_3) \left(\frac{38.03 \text{ g PAA}}{\text{mol eq. PAA}} \right) (DF)(100)}{(g \text{ of sample})} \quad (3.3)$$

A blank was titrated for both titrations using DI H_2O . The volume of titrants calculated from the blank was then used as a volume correction for the volumes of titrants required to reach the endpoints of the two endpoint titrations.

3.2.1.5 pH Measurements

The pH of all four set-ups shown in Table 3.2, was monitored, pH was initially measured at time $t = 0$ hrs, and after time $t = 24$ hrs corresponding to the end of the time-course study utilized in this research. All set-ups had replicates and the pH value reported was taken as the average of the two replicate measurements. The measurements

were also done at two different temperatures, 25 °C and 40 °C, the two extremes of temperatures done for the PAH and E_a study (see the discussion in Section 3.2.2).

3.2.2 PAH Degradation and Activation Energy

3.2.2.1 Experimental Methods

Individual stock solutions (approximately 5000 mg L⁻¹, of known concentration) were prepared for each of the selected PAH compounds in acetone. All experiments were carried out in 35 mL glass centrifuge tubes capped with Teflon® lined septa. The total volume of the experiments during the reaction period was kept constant at 15 mL and 100 µL of the selected PAH stock solutions were added. The series of experiments consisted of the experimental set-up and three control experiments (same as Section 3.2.1.1). The controls consisted of [i] one for DI water, [ii] one for CH₃COOH and [iii] one for the H₂O₂ control. The ratio of the volumes of the individual reagents within the AOP examined was 3 mL CH₃COOH : 3 mL 50% H₂O₂ : 9 mL of DI water (same ratios as discussed in Section 3.2.2.1). The different ratios and reagents for the experimental and control set-ups are shown on Table 3.3. After the reagents were added to the centrifuge tubes, the contents of the centrifuge tubes were mixed using a vortex mixer, then 100 µL of the selected PAH stock solutions was added and subsequently mixed using a vortex mixer. The centrifuge tubes were placed on an orbital shaker at a speed of at least 100 RPM for the duration of the reaction period. For the experiments conducted at temperatures other than room temperature, all reagents were kept at the specific temperature before and during the experiment took place; this was implemented in order to ensure that the specific reaction temperature was constant throughout the reaction period. The orbital shaker was set to the desired reaction temperature as well and the temperature was measured frequently. The experimental reaction periods were 0, 1, 2, 4, 6, 12, 18, and 24 hours for all 4 selected PAH compounds (*e.g.*, anthracene, benzo[a]pyrene, phenanthrene and pyrene). If other reaction times were needed, these were recorded accurately. The reaction periods for all three controls were 0, 6, and 24 hours (see Section 3.2.2.2). At the end of each desired reaction interval, a quenching

agent to stop the reaction (*e.g.*, 3 mL of 1M sodium sulfite in water) was added to the centrifuge tubes and mixed using a vortex mixer.

3.2.2.2 Controls

Three different types of controls were employed, one accounting for the DI water, one for the CH₃COOH, and one for the H₂O₂. The intent of the controls were to assure that the experimental results were due to the peroxy-acid reaction and not due to the individual chemicals in the peroxy-acid mixture. All controls were made to contain the same final volume amount of liquid as the experimental set up (*e.g.*, 15 mL). Therefore, Control 1 contained DI water and CH₃COOH, Control 2 contained H₂O₂ and DI water and Control 3 contained only DI water. All controls followed the same procedure of the experimental set-up. In addition, the controls also had 100 µL of the selected PAH stock solution, had replicates and the reaction was stopped using the same quenching agent (*e.g.*, 1M sodium sulfite). The experimental set-up and the different controls are shown below in Table 3.3.

Table 3.3. Experimental and control set-up.

Set-up	PAH Stock Solution (µL)	DI Water (mL)	Acetic Acid (mL)	Hydrogen Peroxide (mL)	1M Sodium Sulfite (mL)
Experiment	100	9	3	3	3
Control 1	100	12	3	0	3
Control 2	100	12	0	3	3
Control 3	100	15	0	0	3

Experiment = peroxy-acid experiment; Control 1 = acetic acid control; Control 2 = hydrogen peroxide control; Control 3 = DI water control

3.2.2.3 Extraction Methods

After the addition of the quenching agent (*e.g.*, sodium sulfite), 10 mL of hexanes were added to the vials to extract the PAH compounds from the aqueous liquid phase. The centrifuge tubes were then mixed on a vortex mixer in order to facilitate the extraction of the PAH compounds onto the hexanes containing phase. The solutions were allowed to be mixed on the orbital shaker at least overnight. The hexane extracts were then filtered using sodium sulfate (Na_2SO_4) to remove any excess water. In addition, the samples were then stored in a freezer and only removed until they were analyzed using GC equipped with an FID detector (see Section 3.2.2.4 and Appendix C for more information).

3.2.2.4 Sample Analysis

The concentration of the PAH in the samples was determined by analysis with a GC, using an FID. The GC used was a Shimadzu GC-17A series, equipped with a Shimadzu AOC-20i auto-injector (Columbia, MD). The capillary column used in analysis was a 5 meter Restek Rtx-5 column, with a 0.25 mm inner diameter and a 0.25 μm film thickness (Bellefonte, PA). The software used to analyze the results from the GC was Shimadzu Class-VP7.4. All standards and samples concentrations were analyzed using duplicate injections. A 1 μL volume was injected for sample extracts and calibration standards. Sample concentrations were determined from the peak areas of the 1 μL hexane extract injection, utilizing the prepared calibration curves from the standards with known concentrations. PAH GC oven methods followed the general format shown on Table 3.4. The initial oven temperature was 150°C, with an equilibration time of 1 minute. The temperature was then ramped at a rate of 20°C/min until reaching 300°C, where it was held for 3 minutes. The oven program time was around 10 minutes. For detailed GC oven programs for each specific PAH please see Appendix C.

Table 3.4. Example gas chromatograph oven program.

Equilibration Time (min)	Initial Temperature (°C)	Ramp Rate (°C/min)	Final Temperature (°C)	Final Temperature Dwell Time (min)	Program Time (min)
1	150	25	300	3	10

3.2.2.5 Rate Constants and Activation Energy

For the four selected PAH compounds (*e.g.*, anthracene, benzo[a]pyrene, phenanthrene, and pyrene) pseudo-first order rate constants (k) were calculated. Pseudo-first order reaction kinetics was most appropriate because any of the selected PAHs and/or HO \cdot and PAA were the limiting reagent in this investigation. The rate constants were derived from the negative slope of linear equation fit of the plot of $\ln(m/m_0)$ vs. time in hours. The m/m_0 refers to the mass of PAH in solution in mg for the given reaction time and m_0 was the initial mass of PAH in the solution in mg at time zero, respectively (see Section 4.2). These rate constants were then plotted for each of the PAHs as $\ln(k)$ vs. $1/T$. The k was in units of s^{-1} and T was in Kelvin. The E_a and frequency factor A was then determined from the equation for the slope of the line of the reaction rate values (see Section 4.2 for more information).

4. RESULTS AND DISCUSSION

4.1 Hydrogen Peroxide and Peracetic Acid Study Results

4.1.1 Initial H₂O₂ and PAA Study Results

The results of the initial H₂O₂ and PAA study shown for the set-up shown on Table 2.1, times are 0 hrs and results are given below in Table 4.1.

Table 4.1. Results of the initial H₂O₂ and PAA study.

Sample Id	% H ₂ O ₂	% PAA
T1	11.356	0.240
T2	7.610	3.130
T3	16.396	0.086
T4	12.561	10.292

Sample T1 contained 9 mL of DI water, 3 mL of acetic acid and 3 mL H₂O₂. This T1 sample was the same as those in the PAH degradation studies. As seen in Table 4.1, the % H₂O₂ in solution was 11.37 and % PAA in solution was 0.24. Sample T2 followed the same set-up as sample T1 only that this T2 sample had 1 mL of H₂SO₄ catalyst and 8 mL of DI water instead of 9 mL in T1 sample. This set-up showed a decreased % H₂O₂ concentration in solution resulting in 7.61 % from 11.37 % and an increased % PAA concentration in solution increasing from 0.24 % to 3.13 %. The addition of an acid catalyst resulted in higher PAA values and decreased H₂O₂ values since chemicals were used in making the PAA from H₂O₂ and acetic acid in solution. Similar findings correlate to other studies (Zhao *et al.*, 2007; Zhao *et al.*, 2008; Shoulder, 2012). Sample T3 contained increased values of acetic acid and H₂O₂, and decreased value of DI water. All three chemical volumes were equal to 5 mL. For sample T3, values % H₂O₂ in solution was increased to a value of 16.30 % while % PAA in solution was decreased to a value of 0.09 %. Increased % H₂O₂ were due to higher volume amount of H₂O₂ added

to the system, while the lower % PAA value could be due reduced PAA production efficiency with HO[•] radicals acting as radical scavengers and limiting PAA formation. Sample T4 contained the same ratios of acetic acid, H₂O₂, and DI water as sample T3, with the addition of 1 mL of H₂SO₄ catalyst and reduction of DI water to 4 mL to ensure the same sample volume (*e.g.*, 15 mL) throughout the selected experiments. Like with sample T2, the addition of the acid catalyst increased the amount of % PAA in solution to a value of 10.29 % from 3.13 %. The % H₂O₂ increased to 12.56 % from 7.61%. However, this was lower than the % H₂O₂ value of sample T3, but in this case it resulted in much higher PAA amounts due to the addition of the acid catalyst (see Table 4.1). Appendix E provides more information about the PAA generation studies.

4.1.1.1 pH Results

The pH values of the peroxy-acid solutions, without the addition of PAH stock solution, stayed consistent over time. Measurements were done at time $t = 0$ and $t = 24$ hrs for two selected extreme temperatures of 25 and 40 °C. The pH values for the experimental set-up are shown below on Table 4.2.

Table 4.2. Solution pH values of experimental set-up.

Temperature (°C)	Time (hrs)	pH
25	0	1.81
	24	1.89
40	0	1.78
	24	1.77

The values of the solution at 25 °C and 40 °C for both times 0 and 24 hrs, was consistently around a pH value of 1.8. Very little change was observed in both temperatures and times. The controls exhibited the same behavior where little change was observed. Acetic acid control pH values stayed close to a pH value of 2.10, while

that of H_2O_2 was around 3.5 (see Appendix E for more details on the pH results in the control set-ups).

4.1.2 Behavior of H_2O_2 and PAA in PAH Degradation Set-up

Following the findings in Section 4.1.1, an H_2O_2 and PAA determination study in the set-up used for PAH degradation (see Section 4.2) was implemented. All reagents (see Section 3.2.1.1) were added, including 100 μL of an anthracene stock solution. The reaction was then allowed to take place at 25 $^\circ\text{C}$, and the concentration in vol % of H_2O_2 and PAA were determined at reaction periods ranging from 0 to 24 hours, by performing titrations (see Section 3.2.1.3). The values of % H_2O_2 and % PAA of the reaction are shown in Figure 4.1 and Figure 4.2, respectively.

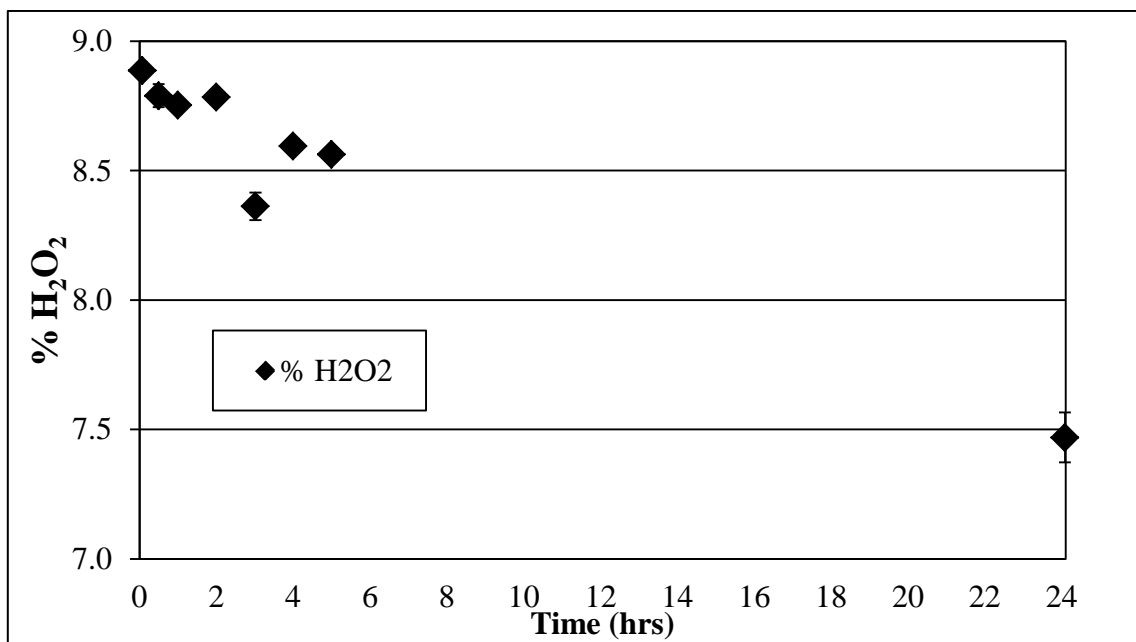


Figure 4.1. Values of H_2O_2 (%), vs. time (hrs) for PAH degradation.

The value of % H_2O_2 decreased as reaction times went on, the reaction started with a concentration of % H_2O_2 equal to 8.8 %, but steadily decreased to a value of 7.4 % after 24 hours. This could be due to H_2O_2 interacting with acetic acid, creating PAA and degrading anthracene molecules as discussed in Section 4.1.1.

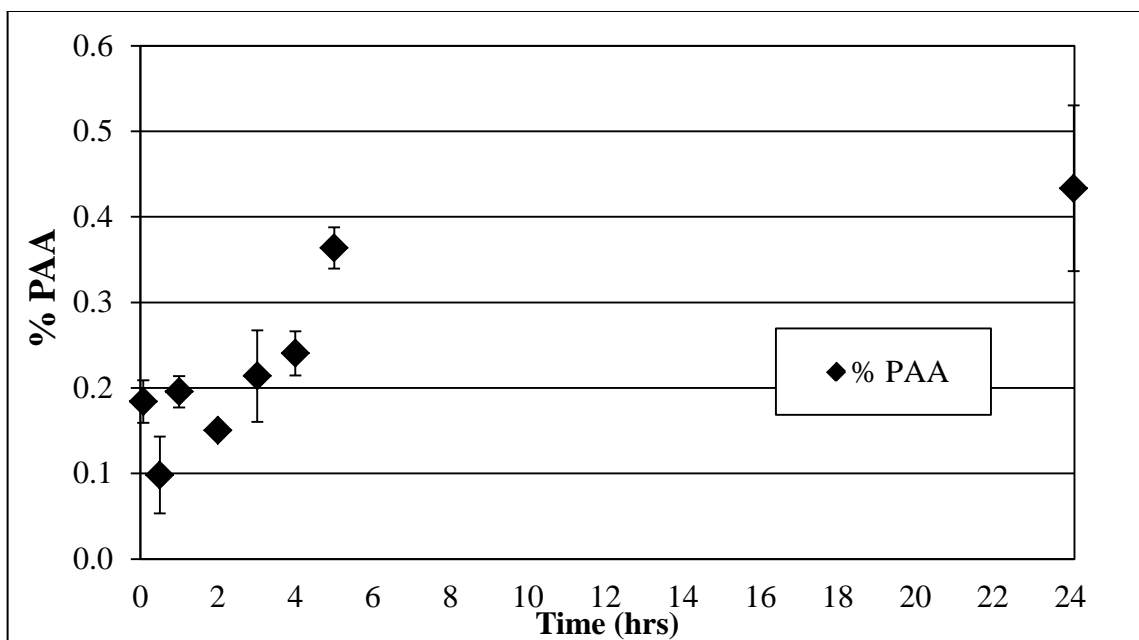


Figure 4.2. Values of PAA (%) vs. time (hrs) for PAH degradation.

At the same time, the concentration of PAA (%) in the reaction vessels steadily increased, starting with an initial value of 0.18 % and with a value of 0.43 % after 24 hour reaction period. Increase in PAA values indicated and increase in oxidation potential for the reaction and resulted in lower amounts of PAH present at increased reaction times (See Section 3.2.2).

The controls done for this set up showed consistent results, for the DI, Acetic acid and % H₂O₂ blanks, % H₂O₂ and % PAA values did not change with the increasing reaction time period went on, indicating that the increase in % PAA and reduction of % H₂O₂ in solution as the reaction time increased was due to the interaction of H₂O₂ and acetic acid (see Appendix E for more information). The decomposition of H₂O₂ and PAA was taken into account to see if the degradation mechanism could change at different temperatures. The thermal decomposition of H₂O₂ and spontaneous decomposition of PAA were negligible at these temperatures (Zhao *et al.*, 2007). H₂O₂ is stable even at higher temperatures, while the thermal homolysis of PAA becomes obvious only at temperatures higher than 80 °C (Zhao *et al.*, 2007; Kadla and Chang, 2001). The spontaneous decomposition of PAA was also negligible below 55 °C (Zhao *et al.*, 2008)

4.2 PAH Degradation and Activation Energy Experimental Results

Rate constants were calculated for four PAH compounds investigated in this study. Anthracene, benzo[a]pyrene, phenanthrene, and pyrene degradation using the peroxy-acid process were measured at three different temperatures (*e.g.*, 25, 32 and 40 °C). The E_a for the reactions also calculated and these results will be shown in the following sections. Values of k were derived from the negative slope of the plot of $\ln(m/m_0)$ vs. time (hrs). The equation used to calculate the values of k is shown as Equation 4.1:

$$\ln\left(\frac{m}{m_0}\right) = -kt \quad (4.1)$$

where m is the initial mass (mg) of PAH spiked and m_0 is mass (mg) of PAH following the reaction time interval. Concentrations at given reaction times were analyzed using a GC equipped with a FID, and with the use of external standards (see Section 3.2.2.4 and Appendices B and C for more information). Reaction rate constants vary as an exponential function of temperature. Therefore, after the values of k were calculated for each of the three selected temperatures, the E_a was calculated for the reaction with each of the PAHs at the three different selected temperatures using the *Arrhenius* equation, Equation 4.2:

$$k = Ae^{-E_a/RT} \quad (4.2)$$

Where A is the pre-exponential factor (hr^{-1}), commonly called the frequency factor for first-order kinetics, E_a is activation energy (kJ mol^{-1}), R is the universal gas constant ($8.3144621 \text{ J K}^{-1} \text{ mol}^{-1}$) and T is the temperature (K). When Equation 4.2 is used to calculate rates, assumptions are that A and E_a are temperature independent, reasonable for a small temperature range (25-40 °C) and that one reaction is causing the compound to disappear (Schwarzenbach *et al.*, 1993). The *Arrhenius* equation can be derived for a given reaction by performing a linear regression of a plot of $\ln(k)$ vs. $1/T(\text{K})$, this is shown on Equation 4.3.

$$\ln(k) = \ln(A) - E_a/RT \quad (4.3)$$

When computing the E_a , the PAH degradation reaction rates obtained using Equation 4.1 were converted from hrs^{-1} to s^{-1} . The value of E_a was then calculated from the slope of the line, which was equal to $-E_a/R$, the units of A correspond to the units of the rate constant corresponding to case s^{-1} in this case.

4.2.1 Anthracene Degradation Results

The peroxy-acid process effectively degraded anthracene and the experimental set-up showed consistent anthracene degradation results at the three selected temperatures. Set-ups will be referred to the same as indicated in Table 3.3. Degradation rate increased as temperature increased. The three control set-ups (DI Water, CH_3COO and H_2O_2) experienced little to no degradation of anthracene (see Appendix D for more information).

4.2.1.1 Degradation and Reaction Rate at $T = 25\text{ }^\circ\text{C}$

At $T = 25\text{ }^\circ\text{C}$, anthracene was degraded by the peroxy-acid process. Anthracene control sample concentrations experienced little change, indicating little to no degradation at $25\text{ }^\circ\text{C}$. Degradation of anthracene and anthracene concentrations of the controls 1, 2, and 3 (*e.g.*, experimental (\blacklozenge), and H_2O_2 (\square), acetic acid (Δ), and DI water (\circ) blanks) are shown on Figure 4.3 (*e.g.*, plotted as m/m_0 versus time in hours). Mass amounts of anthracene left with respect to initial added amounts were 85.6 % after 6 hours, 86.5 % after 12 hours, 76.8 % after 18 hours and 69.5 % after 24 hours. The slightly high value at time $t = 12$ hours could be due to experimental error. These results were then plotted following the process discussed at the beginning of Section 4.2 and Equation 4.1. The reaction rate was calculated and these results are shown in Figure 4.4, plotted as $\ln(m/m_0)$ versus time in hours. The computed reaction rate value for anthracene at $T = 25\text{ }^\circ\text{C}$, was 0.0107 hr^{-1} ($2.972 \times 10^{-6}\text{ s}^{-1}$). Again here time value for time = 12 hours was high with respect to the other data points but the plot had a value of $R^2 = 0.9156$. Detailed results of the degradation of anthracene and controls at $T = 25\text{ }^\circ\text{C}$ are shown in Tables D.1 and D.2 in Appendix D.

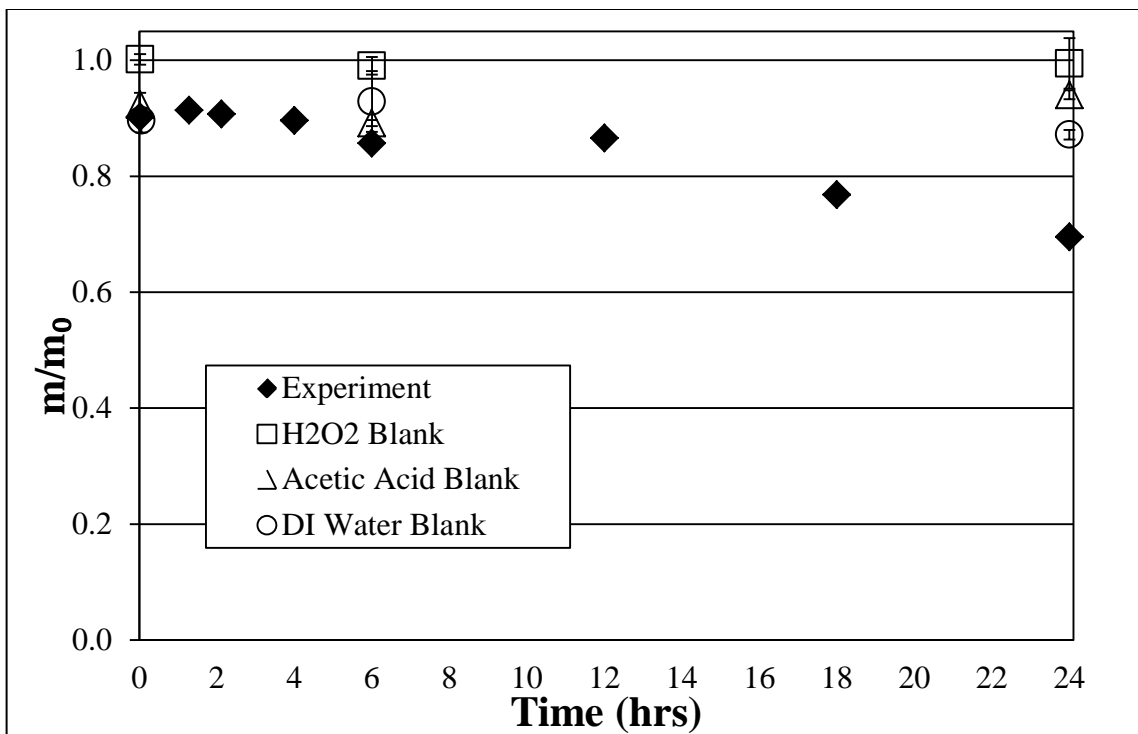


Figure 4.3. Anthracene degradation plotted as mass (m/m_0) vs. time (hrs), 25 °C.

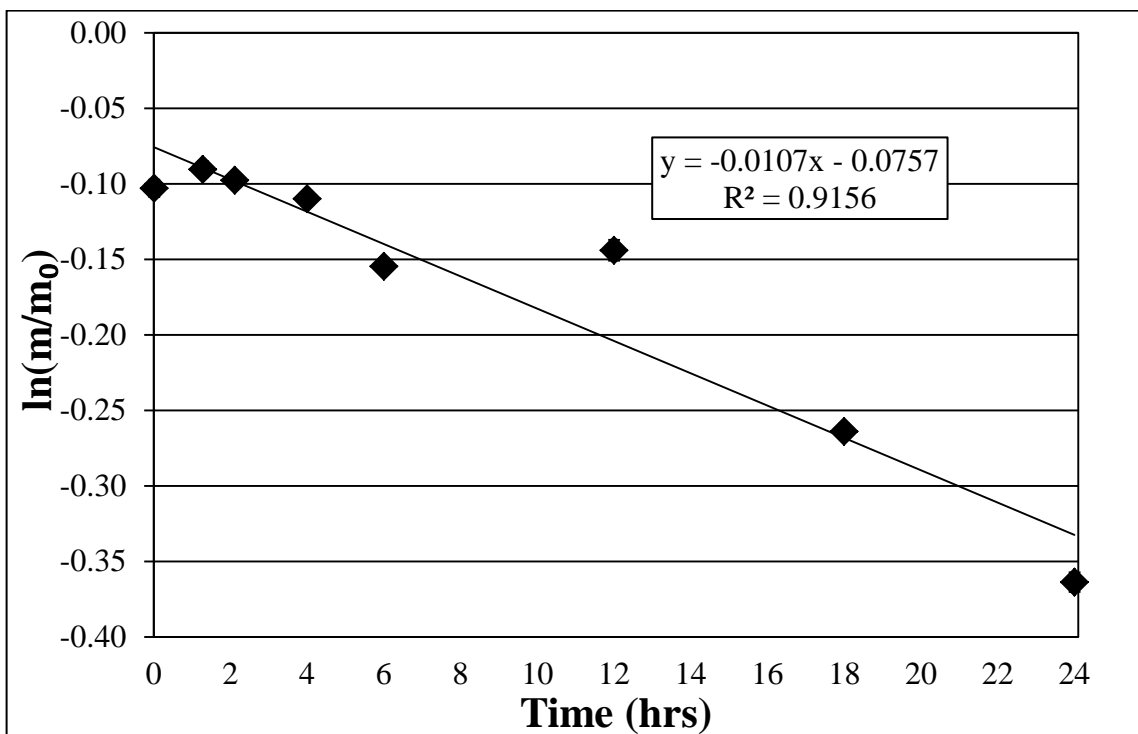


Figure 4.4. Anthracene reaction rate plotted as $\ln(m/m_0)$ vs. time (hrs) at 25 °C.

4.2.1.2 Degradation and Reaction Rate at T = 32 °C

Anthracene was degraded by the peroxy-acid process at T = 32 °C, at an increased rate compared to anthracene degradation at T = 25 °C. Anthracene concentrations for all control samples had very little discernible change as illustrated in Figure 4.5, indicating little to no degradation of anthracene in the control samples. Most controls had 90% of the mass at the beginning of the reaction period and at the end of the 24-hour reaction period.

The degradation of anthracene (◆) and the anthracene concentrations of the control set-ups (*e.g.*, H₂O₂ control (□), acetic acid control (Δ), and DI water control (○)) are shown on Figure 4.5. In this figure, the anthracene disappearance is plotted as m/m_0 , mass of benzo[a]pyrene over initial mass versus time in hours. The percent of anthracene left with respect to initial added amounts was 83.6 % after 6 hours, 74.8 % after 12 hours, 69.2 % after 18 hours and 55.4 % after a 24 hour reaction period. Degradation of anthracene at this temperature was also consistent like it was at 25 °C, with increased degradation rate at 32 °C. These results were then plotted utilizing the same process discussed in the beginning of Section 4.2. The reaction rate was computed; and these results are shown in Figure 4.6 (*e.g.*, plotted as $\ln(m/m_0)$ versus time in hours to obtain the k from the slope). The calculated reaction rate value for anthracene at T = 32 °C, was 0.0182 hr^{-1} (or $5.056 \times 10^{-6} \text{ s}^{-1}$), an increase compared to 25 °C. The R^2 value of the computed reaction rate of anthracene at 32 °C was 0.9473. Detailed results of the degradation of anthracene and controls at T = 32 °C are shown on Tables D.3 and D.4 in Appendix D.

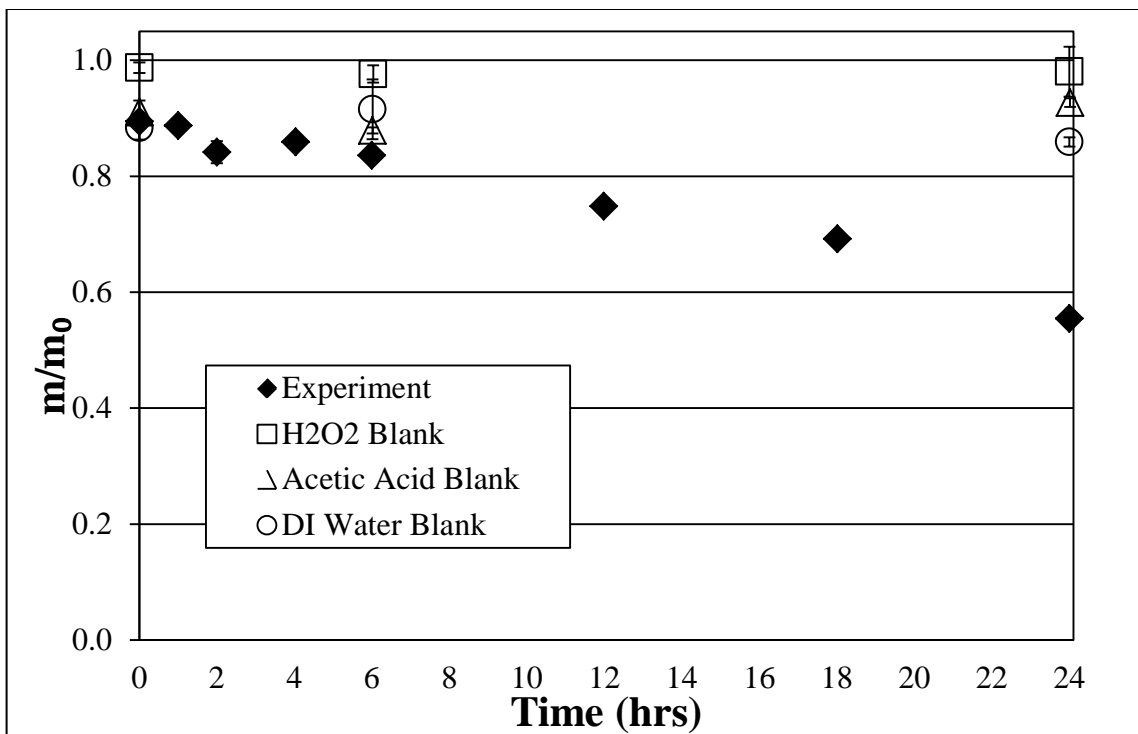


Figure 4.5. Anthracene degradation plotted as mass (m/m_0) vs. time (hrs), 32 °C.

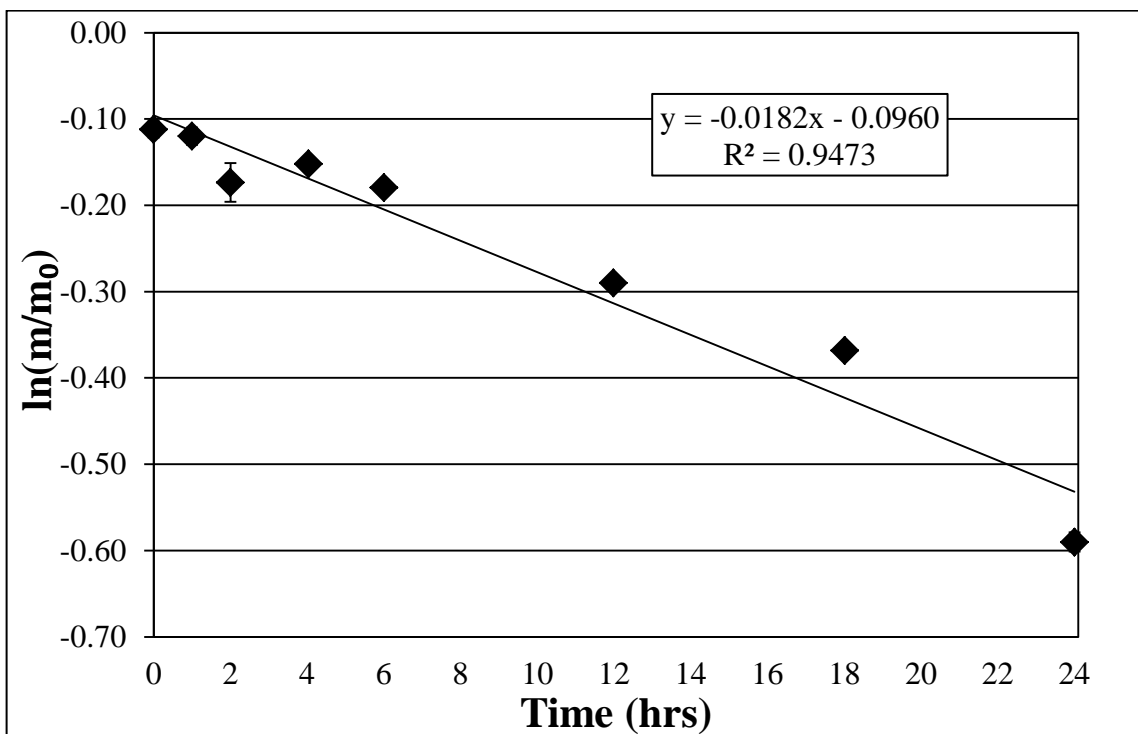


Figure 4.6. Anthracene reaction rate plotted as $\ln(m/m_0)$ vs. time (hrs) at 32 °C.

4.2.1.3 Degradation and Reaction Rate at T = 40 °C

Anthracene was virtually completely degraded by the peroxy-acid process at T = 40 °C. Anthracene concentrations for all control samples experienced little change as observed as open symbols in the figure, with the amounts of anthracene present after 24 hours being consistent with that of 0 hours (or in the beginning of the experiment), indicating very little to no degradation of anthracene in the H₂O₂, acetic acid and DI water controls

The degradation of anthracene including the anthracene concentrations in the controls are shown in Figure 4.7. The data is plotted as m/m_0 (e.g., mass of benzo[a]pyrene (mg) over initial mass (mg) spiked into the system) versus time (hrs). After 6 hours, the amount of anthracene left with respect to initial amount of anthracene at time $t = 0$ hours was 73.3 %, 43.1 % after 12 hours, 12.1 % after 18 hours and finally 1.86 % after 24 hours, respectively, resulting in virtually complete degradation of anthracene at 40 °C. These results were then plotted following the process discussed in the beginning of Section 4.2, the reaction rate was calculated, and these results are shown on Figure 4.8 as $\ln(m/m_0)$ plotted versus time (hrs). The estimated first-order reaction rate for anthracene at T = 40 °C was 0.154 hr^{-1} (or $4.267 \times 10^{-5} \text{ s}^{-1}$). As it can be compared from Figures 4.4 and 4.6, much faster reaction rate of anthracene in v/v/v 3:3:9 H₂O₂ : acetic acid : DI water was obtained (see Fig. 4.8). The value of R^2 for obtaining the reaction rate at this temperature was 0.909 (detailed results of the degradation of anthracene and controls at T = 40 °C are shown in Tables D.5 and D.6 in Appendix D).

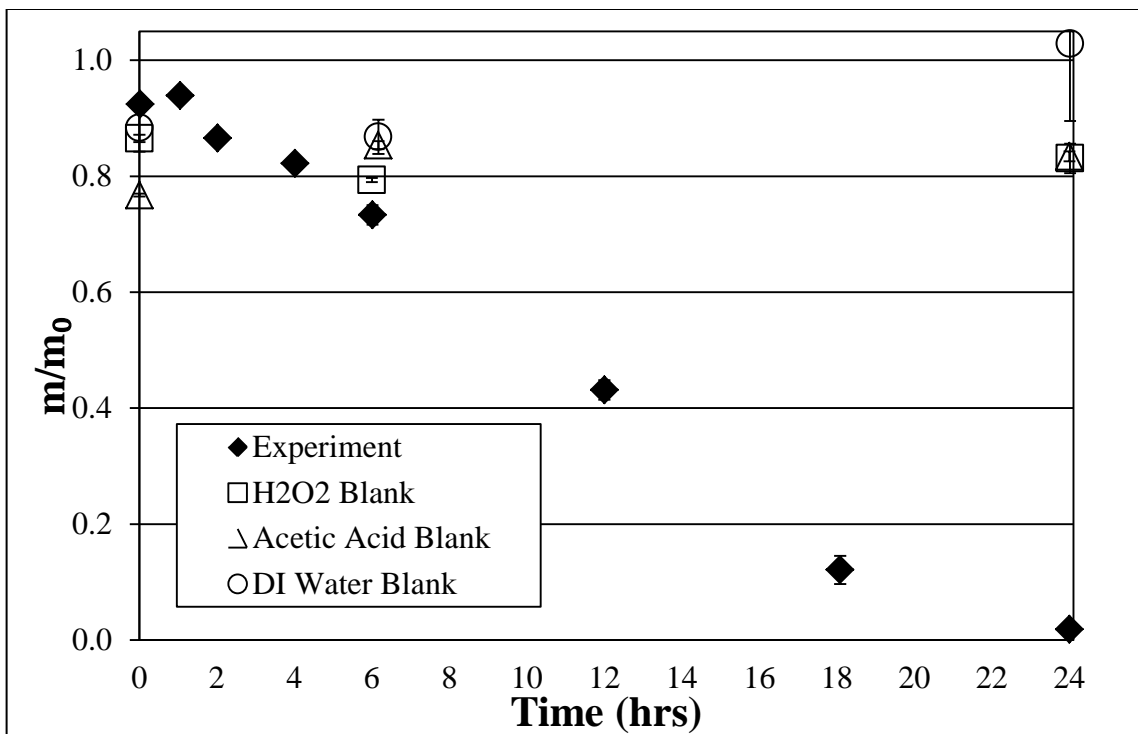


Figure 4.7. Anthracene degradation plotted as mass (m/m_0) vs. time (hrs), 40 °C.

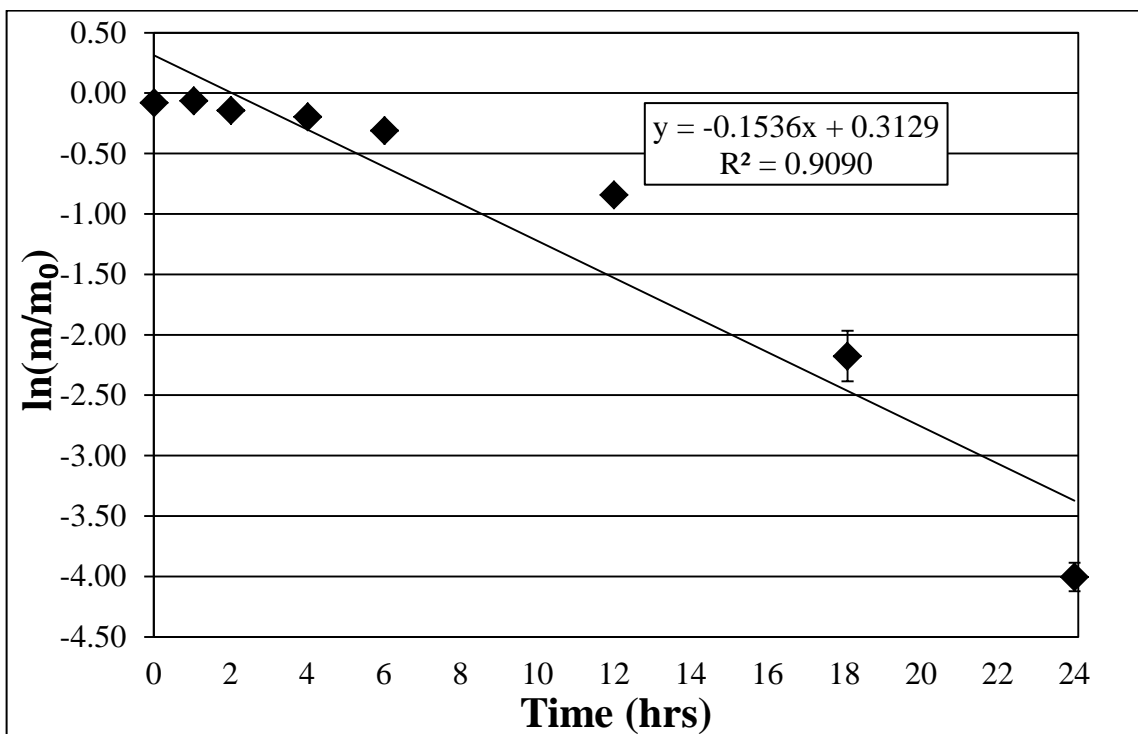


Figure 4.8. Anthracene reaction rate plotted as $\ln(m/m_0)$ vs. time (hrs) at 40 °C.

4.2.1.4 Reaction Rates and Activation Energy

The pseudo first-order reaction rates in (hr^{-1} and s^{-1}) at temperatures $T = 25, 32$ and 40 °C for the degradation of anthracene using the peroxy-acid process are illustrated in Table 4.3 below and plotted as $\ln(k)$ versus $1/T$ in Figure 4.9 (see also Eq. 4.2).

Table 4.3. Anthracene reaction rates for the selected temperatures.

Temperature (°C)	Reaction Rate (hr^{-1})	Reaction Rate (s^{-1})
25	0.0107	2.972×10^{-6}
32	0.0182	5.056×10^{-6}
40	0.1536	4.267×10^{-5}

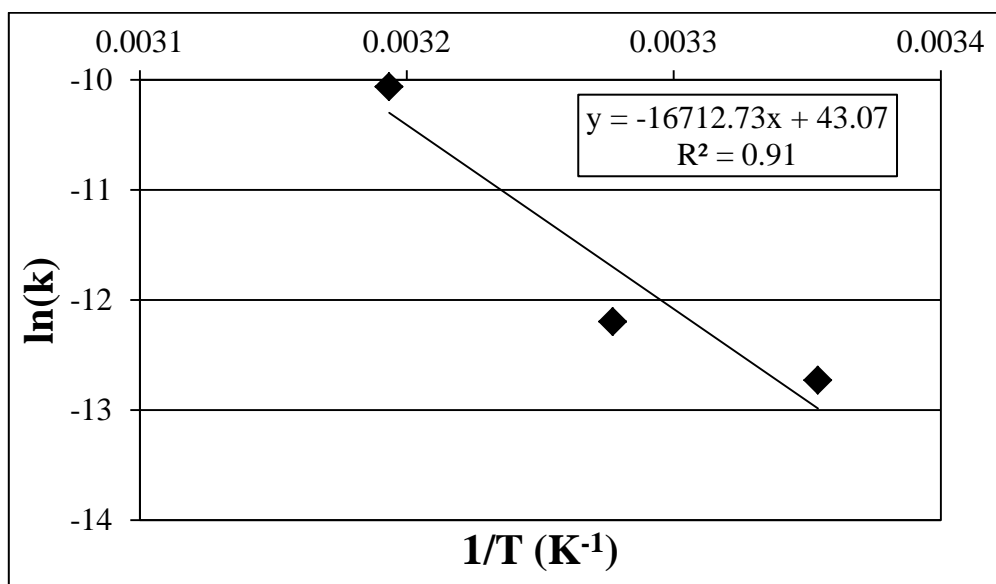


Figure 4.9. Reaction rates (s^{-1}) and activation energy of anthracene, $\ln(k)$ vs. $1/T$.

The plotted values of the natural log of the reaction rates of anthracene degradation are shown in Figure 4.9. Reaction rates for anthracene exhibited a good correlation with an R^2 value of 0.91. From the slope of the line, the E_a for this reaction was calculated to be $138.96 \text{ kJ mol}^{-1}$ (see Section 4.2.5 for a more in-depth discussion on E_a and reaction rates and Appendix F for more information on degradation).

4.2.2 Benzo[a]pyrene Degradation Results

The peroxy-acid process was found to effectively degrade benzo[a]pyrene. The experimental set-ups will be referred to as indicated in Table 3.3. The experimental set-up showed consistent benzo[a]pyrene degradation results at the three different temperatures with degradation rate increasing as temperature increased from 25 to 40 °C. The three controls (*e.g.*, H₂O₂, CH₃COOH and DI water controls) experienced little to no degradation of anthracene (see Appendices D, E, and F).

4.2.2.1 Degradation and Reaction Rate at T = 25 °C

At T = 25 °C, benzo[a]pyrene was degraded by the peroxy-acid process like anthracene (see Section 4.2.1). The change in benzo[a]pyrene concentrations for all control samples during the time-course study had very little discernible change at this selected temperature retaining most of the original amounts of benzo[a]pyrene added at the initial time (*e.g.*, t = 0 hrs). The degradation of benzo[a]pyrene and the benzo[a]pyrene concentrations of the corresponding controls are shown in Figure 4.10. This figure is obtained by plotting m/m₀ (*e.g.*, mass of benzo[a]pyrene (mg) over initial mass (mg)) versus time (hrs).

The mass amounts of benzo[a]pyrene left with respect to the initial amount of benzo[a]pyrene added to the reaction vessels were 92.2% after 6 hours, 87.7 % after 13 hours, 84.0 % after 18 hours and 79.9 % after a 24-hour reaction period. These amounts corresponded to less than those of anthracene at the same temperature (see Section 4.2.1.1), with benzo[a]pyrene undergoing less degradation resulting in lower reaction rates. These results were then plotted following the same process as discussed in Section 4.2. The reaction rate at this temperature was calculated and these results are shown on Figure 4.11 plotted as ln(m/m₀) versus time in hours. The calculated reaction rate value for benzo[a]pyrene at T = 25 °C was 0.0080 hr⁻¹ (or corresponding to 2.222 x 10⁻⁵ s⁻¹) with correlation coefficient of R² = 0.994. Detailed results of the degradation of benzo[a]pyrene and controls at T = 25 °C are shown in Tables D.7 and D.8 in Appendix D.

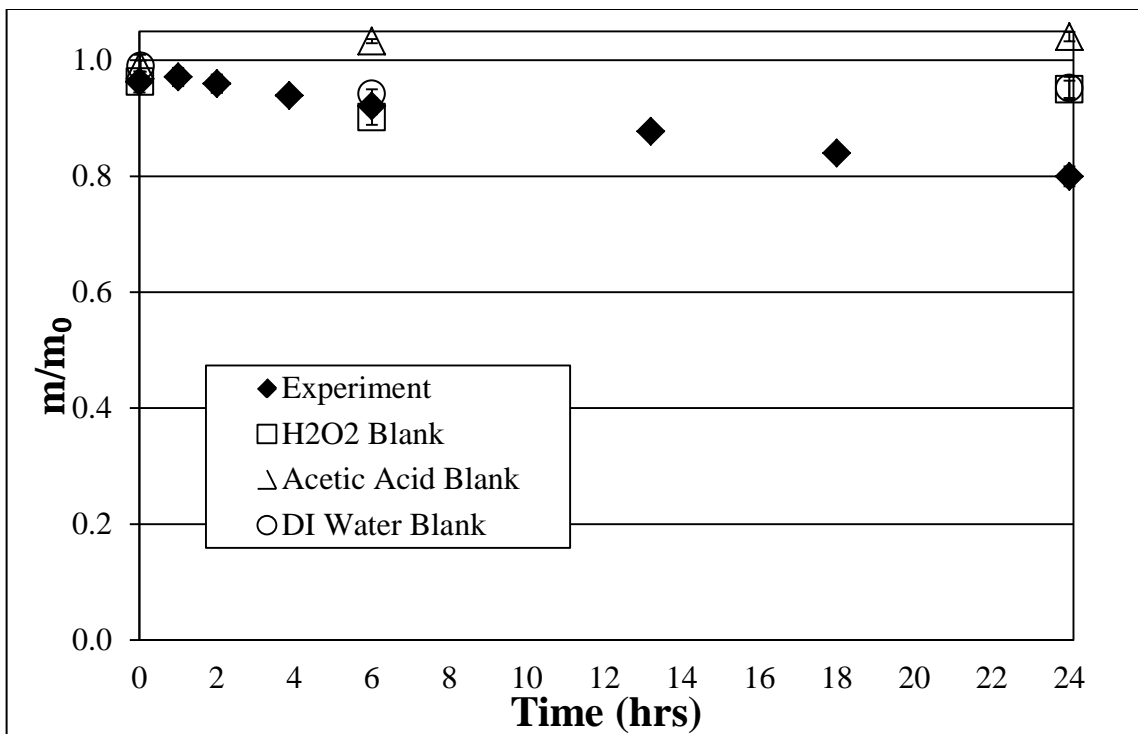


Figure 4.10. Benzo[a]pyrene degradation plotted as mass (m/m_0) vs. time (hrs), 25 °C.

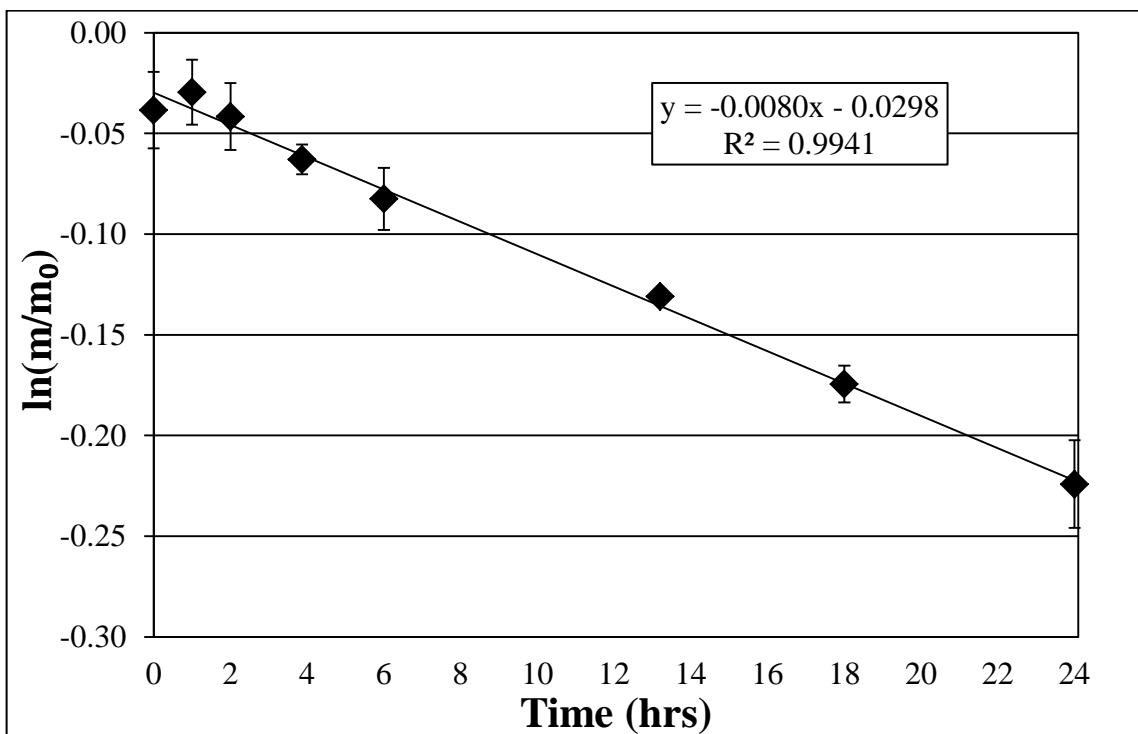


Figure 4.11. Benzo[a]pyrene reaction rate plotted as $\ln(m/m_0)$ vs. time (hrs) at 25 °C.

4.2.2.2 Degradation and Reaction Rate at T = 32 °C

Benzo[a]pyrene was degraded to a higher degree at 32 °C than at 25 °C by utilizing the peroxy-acid process. Benzo[a]pyrene concentrations for all control samples illustrated in Figure 4.12 as open symbols demonstrated very little discernible change from t = 0 to t = 24 hours.

The degradation of benzo[a]pyrene and the benzo[a]pyrene concentrations of the controls are shown in Figure 4.12. The Figure 4.12 is shown as mass of benzo[a]pyrene (mg) over initial mass (mg) (*e.g.*, m/m_0) versus time (hrs). After a time period of 6 hours, benzo[a]pyrene was degraded to 79.5 % of the initial added amount, 75.3 % after 12 hours, 69.4 % after 18 hours and 61.9 % after a time period of 24 hours, respectively, leading to an overall disappearance of approximately 39 % at the end of the time-course study. Benzo[a]pyrene was found to have a higher degree of degradation at 32 °C than that of at 25 °C (see Figs. 4.10 and 4.12). As illustrated in Figure 4.12, H₂O₂ (□), acetic acid (Δ), and DI water (○) blanks remained constant at approximately 80% between t = 0 hrs and 24 hrs.

These results were then plotted following the process discussed in the beginning of Section 4.2. The reaction rate for this temperature (*e.g.*, 32 °C) was calculated, and these results are shown in Figure 4.13 plotted as $\ln(m/m_0)$ versus time in hours. The calculated reaction rate for benzo[a]pyrene at T = 32 °C was 0.0133 hr⁻¹ (or converted to 3.694 x 10⁻⁶ s⁻¹) with an R² value of 0.985. Anthracene experienced a higher degree of degradation at this selected temperature (see Figs. 4.5 and 4.13). Detailed results can be found of the degradation of benzo[a]pyrene and the corresponding controls at T = 32 °C in Tables D.9 and D.10 in Appendix D.

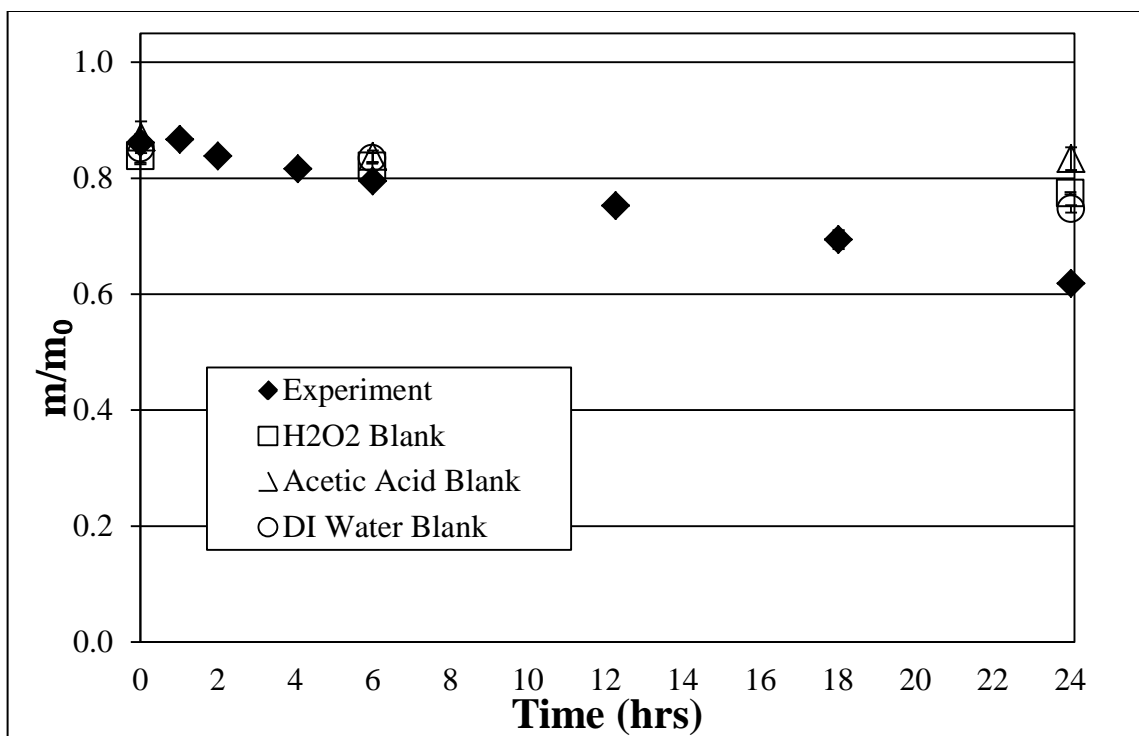


Figure 4.12. Benzo[a]pyrene degradation plotted as mass (m/m_0) vs. time (hrs), 32 °C.

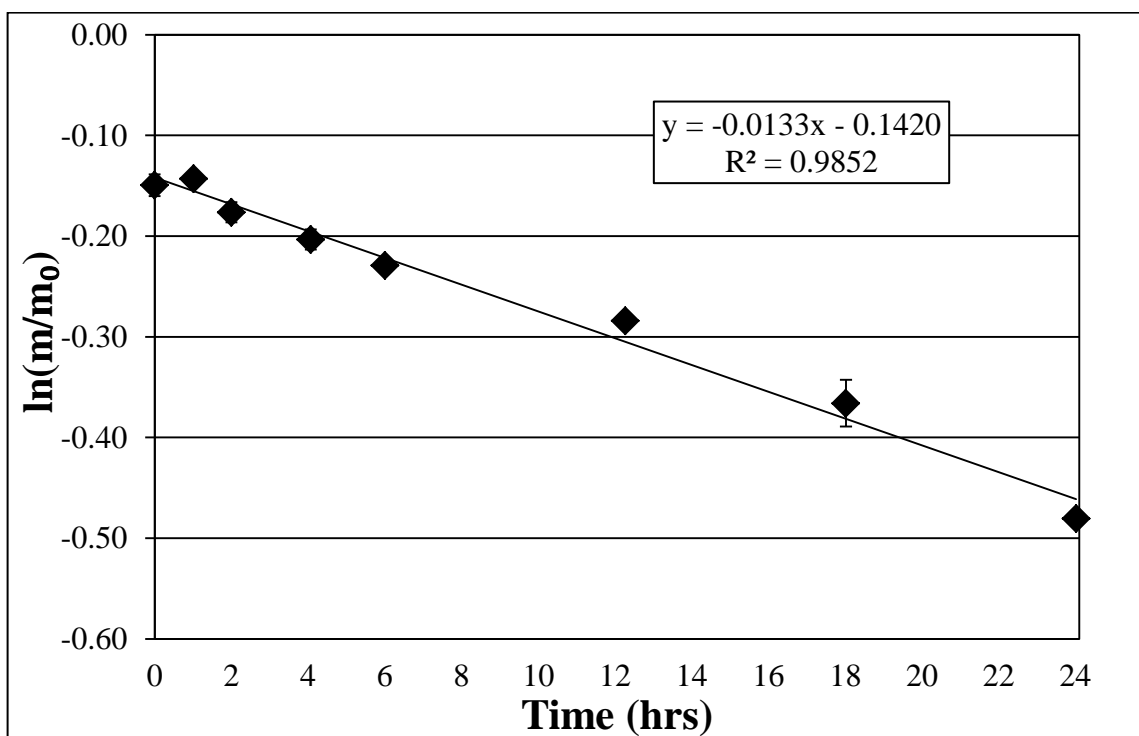


Figure 4.13. Benzo[a]pyrene reaction rate plotted as $\ln(m/m_0)$ vs. time (hrs) at 32 °C.

4.2.2.3 Degradation and Reaction Rate at T = 40 °C

At T = 40 °C, benzo[a]pyrene was almost completely degraded by the peroxy-acid process. Benzo[a]pyrene concentrations for all three control samples demonstrated again very little discernible change with amounts remaining fairly constant ranging from 90 – 100 % of the initial mass added throughout the duration of the reaction periods (*e.g.*, 24 hrs).

The degradation of benzo[a]pyrene and the benzo[a]pyrene concentrations of the controls are shown in Figure 4.14. This figure illustrates the m/m_0 , or mass of benzo[a]pyrene (mg) over initial mass (mg) of benzo[a]pyrene added at $t = 0$ hrs, versus time in hours. The observed mass benzo[a]pyrene left with respect to the original added amount was 72.1 % after 6 hours, 60.5 % after 12 hours, 15.8 % after 18 hours and 7.61 % after 24 hours, respectively, achieving a good percentage of degradation (*e.g.*, 92.39 %) of the benzo[a]pyrene after 24 hours. However, these results demonstrated that benzo[a]pyrene still had some amount left (*e.g.*, approximately 8 %) in the solution at the end of the reaction period. Anthracene was found to virtually have complete degradation (*e.g.*, approximately 98 %) at 40 °C. The value for time $t = 12$ hours was higher compared to the rest of the degradation rates, but this data point was still following the general degradation trend; this slightly higher result could have been due to an experimental error. These results were then plotted as $\ln(m/m_0)$ versus time in hours following the same process discussed at the beginning of Section 4.2. The reaction rate was obtained from the figure and these results are shown in Figure 4.15. The calculated reaction rates for benzo[a]pyrene at T = 40 °C was 0.1027 hr^{-1} (or $2.853 \times 10^{-5} \text{ s}^{-1}$) with a corresponding correlation coefficient of $R^2 = 0.907$. Anthracene demonstrated higher degradation rates than benzo[a]pyrene and a larger reaction rate constant at this temperature (*e.g.*, 40 °C) (see Figs. 4.8 and 4.14). Detailed results of the degradation of benzo[a]pyrene and corresponding controls at T = 40 °C are provided in Tables D.11 and D.12 in Appendix D.

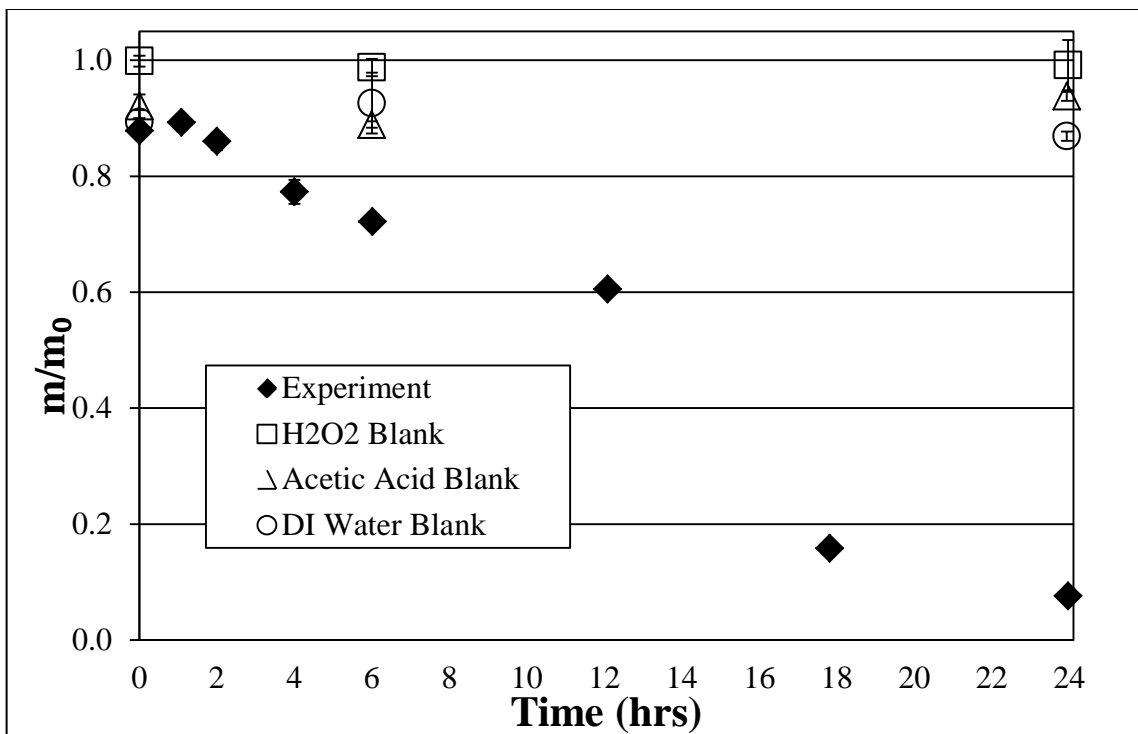


Figure 4.14. Benzo[a]pyrene degradation plotted as mass (m/m_0) vs. time (hrs), 40 °C.

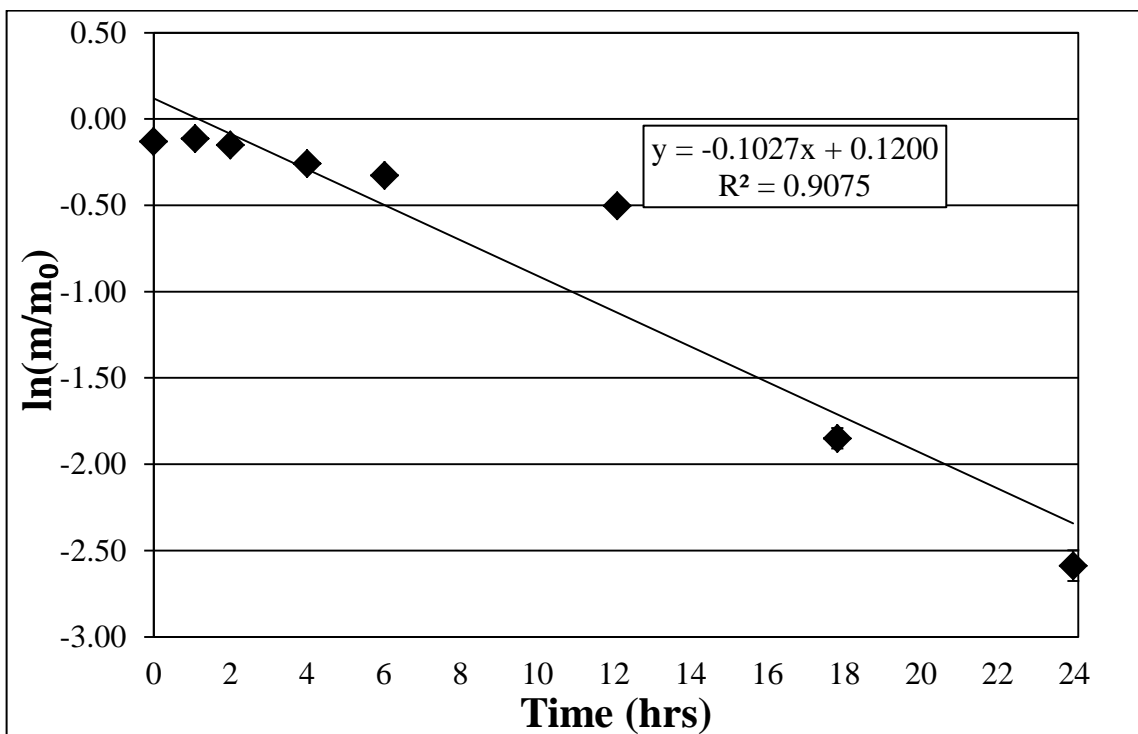


Figure 4.15. Benzo[a]pyrene reaction rate plotted as $\ln(m/m_0)$ vs. time (hrs) at 40 °C.

4.2.2.4 Reaction Rates and Activation Energy

The pseudo-first-order reaction rates in (hr^{-1} and s^{-1}) at temperatures $T = 25, 32$ and $40\text{ }^\circ\text{C}$ for the degradation of benzo[a]pyrene using v/v/v 3:3:9 H_2O_2 : acetic acid : DI water are shown on below on Table 4.4.

Table 4.4. Benzo[a]pyrene reaction rates for the selected temperatures.

Temperature ($^\circ\text{C}$)	Reaction Rate (hr^{-1})	Reaction Rate (s^{-1})
25	0.0080	2.222×10^{-6}
32	0.0133	3.694×10^{-6}
40	0.1027	2.853×10^{-5}

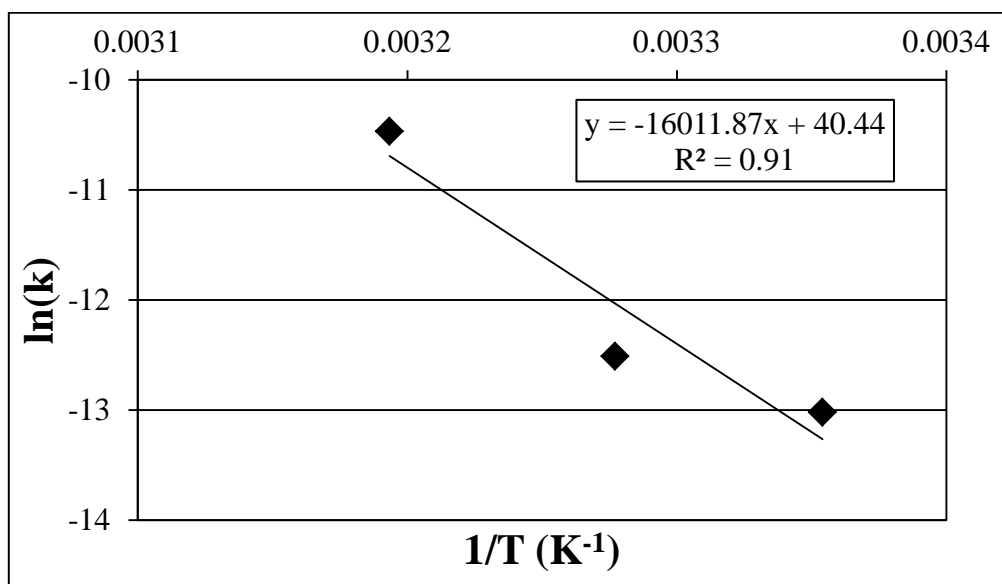


Figure 4.16. Reaction rates and activation energy of benzo[a]pyrene, $\ln(k)$ vs. $1/T$.

The plotted values of the reaction rates of benzo[a]pyrene degradation are shown on Figure 4.16. Reaction rates for benzo[a]pyrene exhibited a good correlation between the temperatures investigated with a correlation coefficient R^2 value of 0.91. From the slope of the line, the E_a for this reaction was calculated to be $133.13\text{ kJ mol}^{-1}$ (see Section 4.2.5 for a more in-depth discussion on E_a and reaction rates and Appendix F for more information on degradation results).

4.2.3 Phenanthrene Degradation Results

The peroxy-acid process was found to effectively degrade phenanthrene as well. The experimental conditions will be referred to the same as indicated in Table 3.3. The experimental set-up showed consistent phenanthrene degradation results at the three selected different temperatures (*e.g.*, 25, 32, and 40 °C) with degradation rate increasing as temperature increased from 25 to 40 °C. The three controls (*e.g.*, DI Water, acetic acid and H₂O₂) experienced little to no degradation of phenanthrene during the 24-hr reaction period.

4.2.3.1 Degradation and Reaction Rate at T = 25 °C

Phenanthrene degradation was observed when subjected to the peroxy-acid process at 25 °C. Phenanthrene concentrations for all control samples experienced almost no change at all after 24 hours with values staying fairly constant around 100 % of the initial mass of phenanthrene added indicating no degradation of phenanthrene during the 24-hr reaction period. The degradation of phenanthrene and the phenanthrene concentrations in the H₂O₂, acetic acid and DI water controls are shown in Figure 4.17, where m/m_0 (*e.g.*, mass of phenanthrene (mg) over initial mass (mg) phenanthrene added) is plotted versus time (hrs). The mass phenanthrene left with respect to the original added amount was 96.4 % after 6 hours, 91.2 % after 12 hours, 89.4 % after 18 hours and 82.1 % after the 24-hour reaction period, respectively, indicating that approximately 18 % of phenanthrene was degraded over the 24-hr time-course study. These results were then plotted following the process discussed at the beginning of Section 4.2. Specifically, $\ln(m/m_0)$ was plotted versus time in hours (see Eq. 4.1). The reaction rate for this temperature was then calculated. These plotted results are shown in Figure 4.18. The calculated reaction rate for phenanthrene at T = 25 °C was 0.0068 hr⁻¹ (or 1.889 x 10⁻⁶ s⁻¹). Phenanthrene had the lowest reaction rate and demonstrated the least amount of degradation of all four PAHs investigated in this study. The reaction rate of phenanthrene at this temperature had an R² value of 0.922. Detailed results of the degradation of phenanthrene and the corresponding controls at T = 25 °C are provided in Tables D.13 and D.14 in Appendix D.

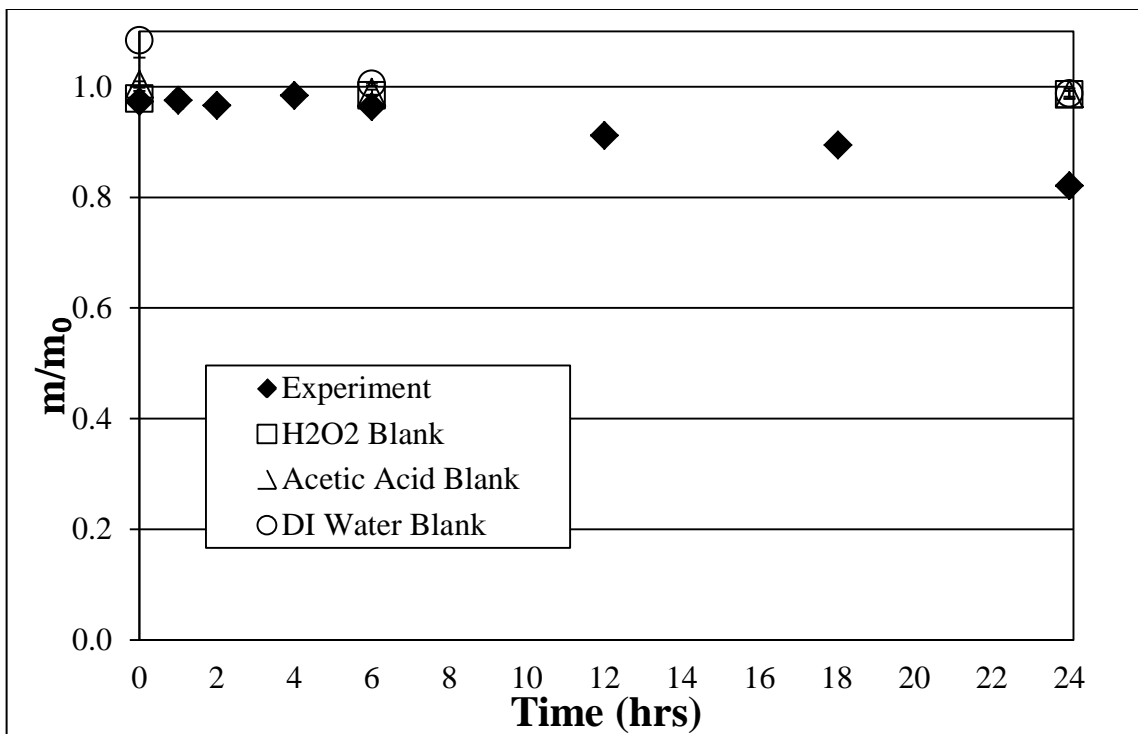


Figure 4.17. Phenanthrene degradation plotted as mass (m/m_0) vs. time (hrs), 25 °C.

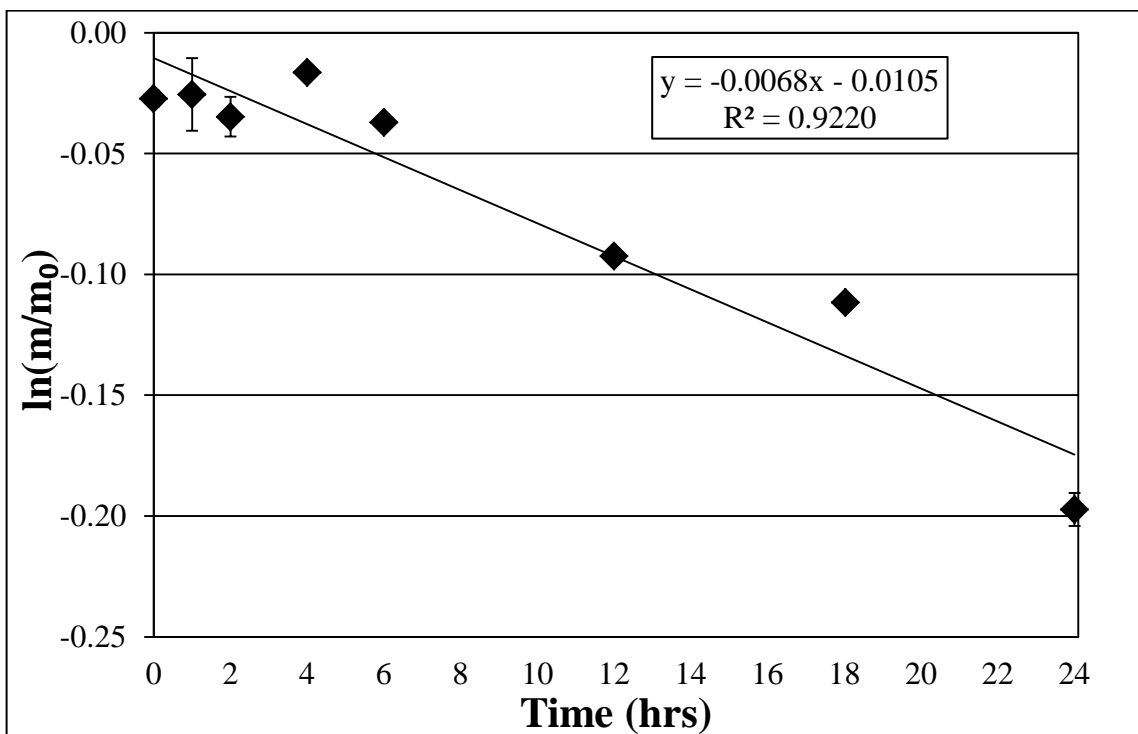


Figure 4.18. Phenanthrene reaction rate plotted as $\ln(m/m_0)$ vs. time (hrs) at 25 °C.

4.2.3.2 Degradation and Reaction Rate at T = 32 °C

Phenanthrene was degraded by the peroxy-acid process at T = 32 °C. Phenanthrene concentrations for all control samples had very little discernible change compared to the initial added amounts with most samples retaining over 95% of the initial amount of phenanthrene added after 24 hours of reaction period.

The degradation of phenanthrene and the phenanthrene concentrations of the controls are shown in Figure 4.19. Again, the m/m_0 is mass of phenanthrene (mg) over initial mass (mg) of phenanthrene is plotted versus elapsed time in hours. The values of phenanthrene left with respect to the original added amount of the elapsed reaction times were 88.3 % after 6 hours, 85.4 % after 12 hours, 78.4 % after 18 hours and 72.3 % after 24 hours, respectively. Phenanthrene demonstrated the least amount of degradation out of all four PAHs investigated in this study for this selected reaction temperature (*e.g.*, 32 °C). These results were then plotted following the process discussed in Section 4.2. In other words, the data was plotted as $\ln(m/m_0)$ versus time in hours. The reaction rate was obtained from Figure 4.20 and these results are shown below (see Figure 4.20). The calculated reaction rate value for phenanthrene at T = 32 °C was 0.112 hr^{-1} (or $3.111 \times 10^{-6} \text{ s}^{-1}$) with correlation coefficient value of $R^2 = 0.981$. Phenanthrene also had the lowest reaction rate of the four PAH compounds investigated in this study at this reaction temperature of 32 °C (see detailed results of the degradation of phenanthrene and corresponding controls at T = 32 °C shown in Tables D.15 and D.16 in Appendix D.

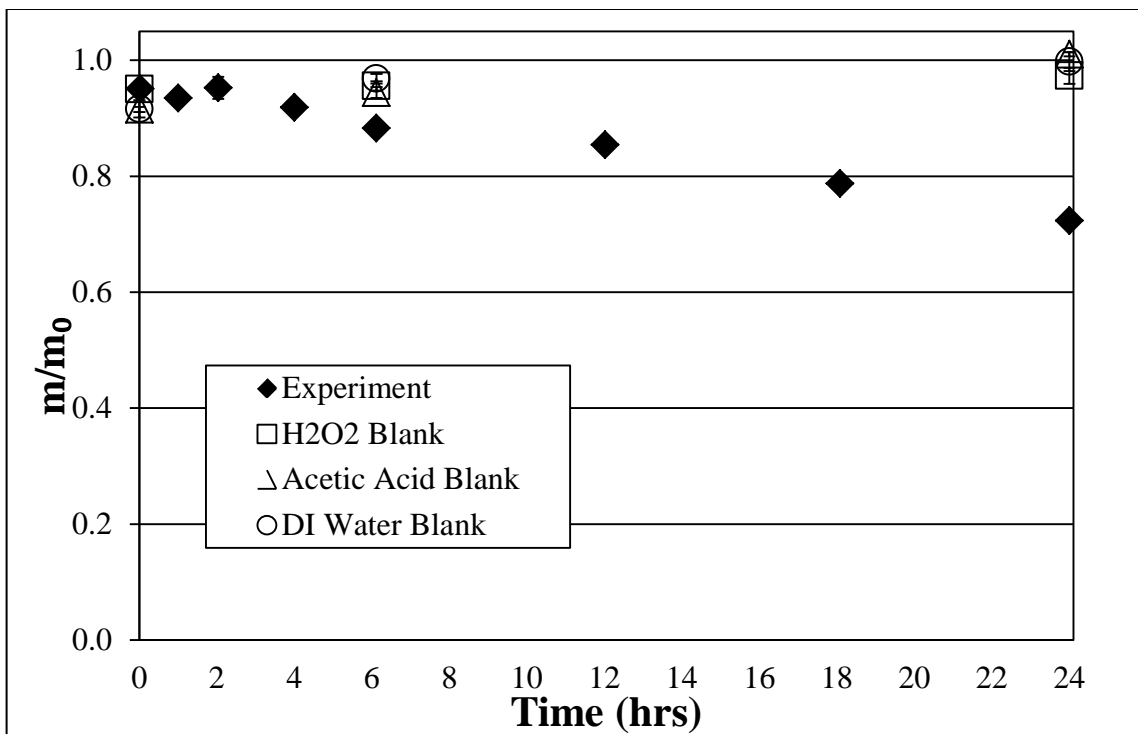


Figure 4.19. Phenanthrene degradation plotted as mass (m/m_0) vs. time (hrs), 32 °C.

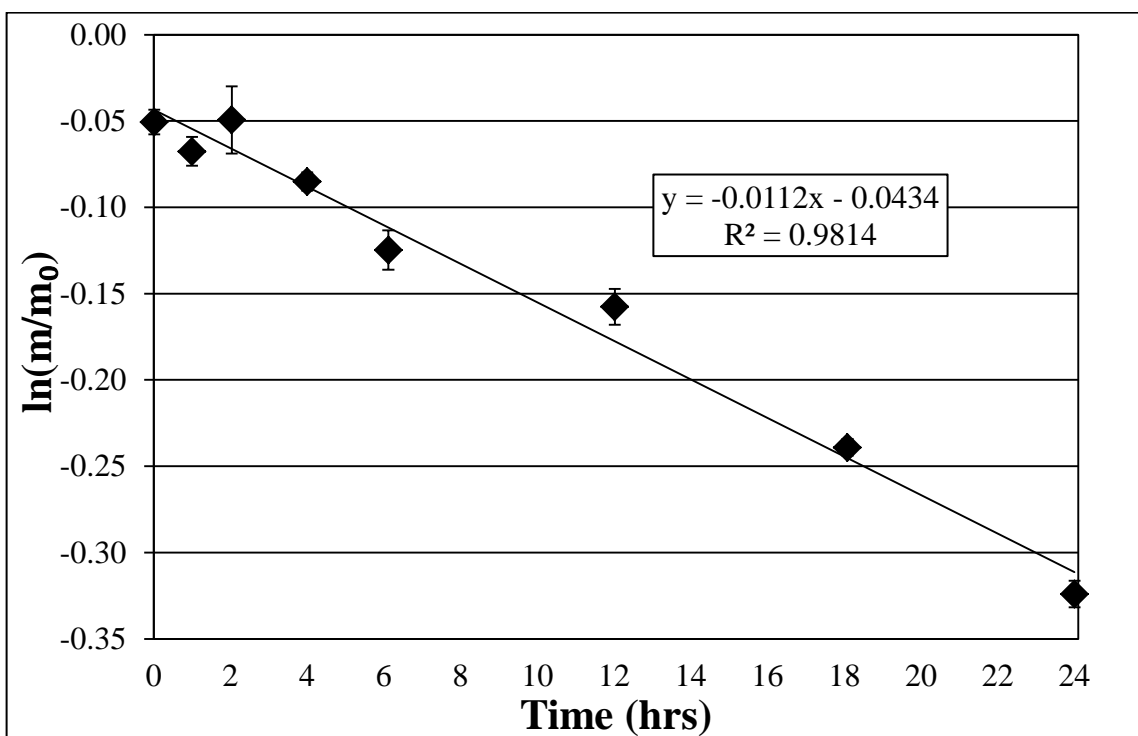


Figure 4.20. Phenanthrene reaction rate plotted as $\ln(m/m_0)$ vs. time (hrs) at 32 °C.

4.2.3.3 Degradation and Reaction Rate at T = 40 °C

Phenanthrene was also degraded by the peroxy-acid process like anthracene, benzo[a]pyrene and pyrene. Phenanthrene concentrations for all three control samples had again very little discernible change, with most of the mass of phenanthrene with respect to the initial added amounts over 90% during the 24-hr reaction period.

The degradation of phenanthrene and the phenanthrene concentrations of the controls are shown on Figure 4.21 (*e.g.*, shown as a plot of m/m_0 , mass of phenanthrene over initial added mass, versus elapsed time in hours). The experimental degradation values are provided as black diamonds in Figure 4.21. The H₂O₂, acetic acid, and DI water controls are provided as open squares, triangles and circles, respectively. Percentage values of m/m_0 for phenanthrene at this reaction temperature were 72.3 % after 6 hours, 70.07 % after 12 hours, 63.3 % after 18 hours and 38.7 % after 24 hours, respectively. This resulted in approximately 61 % overall degradation of phenanthrene at 40 °C. While phenanthrene degraded leaving almost a third of the initial concentration of phenanthrene left in reaction vessels after 24-hr reaction period, this selected compound still had the lowest amount of degradation observed for the four selected PAHs for this reaction temperature. These results were then plotted as $\ln(m/m_0)$ versus time in hours (see Section 4.2). The reaction rate was calculated and these results are shown in Figure 4.22. The observed reaction rate for phenanthrene at T = 40 °C was 0.336 hr⁻¹ (or 9.333 x 10⁻⁶ s⁻¹) with a correlation coefficient value of R² = 0.905. Phenanthrene also had the smallest reaction rate at this temperature out of all the four PAH compounds investigated in this study. Detailed results of the degradation of phenanthrene and corresponding controls at T = 40 °C are shown in Tables D.17 and D.18 in Appendix D.

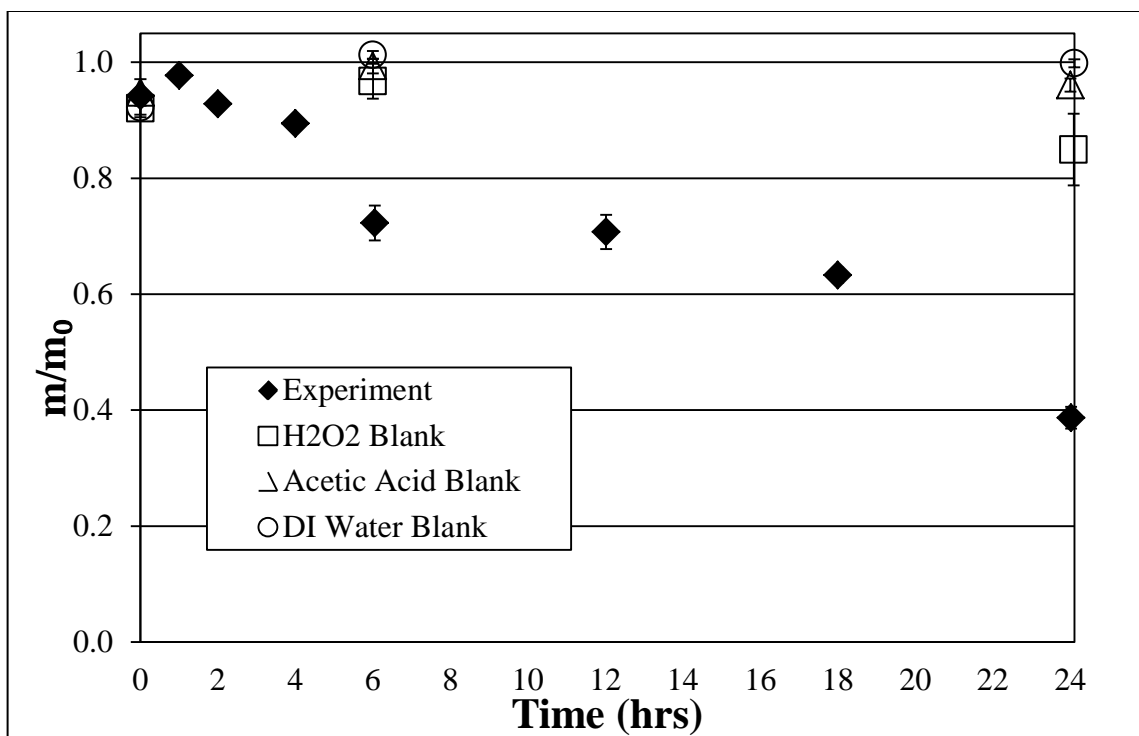


Figure 4.21. Phenanthrene degradation plotted as mass (m/m_0) vs. time (hrs), 40 °C.

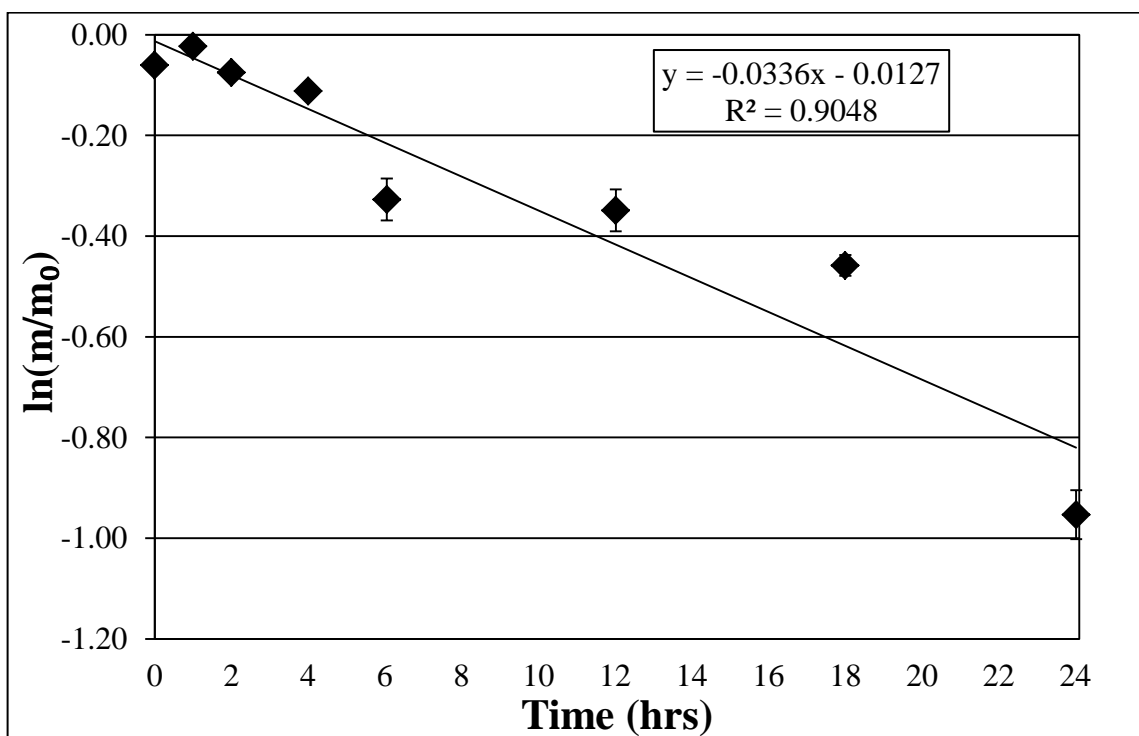


Figure 4.22. Phenanthrene reaction rate plotted as $\ln(m/m_0)$ vs. time (hrs) at 40 °C.

4.2.3.4 Reaction Rates and Activation Energy

The pseudo-first-order reaction rates in (hr^{-1} and s^{-1}) at temperatures $T = 25, 32$ and $40\text{ }^{\circ}\text{C}$ for the degradation of phenanthrene using the peroxy-acid process are shown on below on Table 4.5.

Table 4.5. Phenanthrene reaction rates for the selected temperatures.

Temperature ($^{\circ}\text{C}$)	Reaction Rate (hr^{-1})	Reaction Rate (s^{-1})
25	0.0068	1.889×10^{-6}
32	0.0112	3.111×10^{-6}
40	0.0336	9.333×10^{-6}

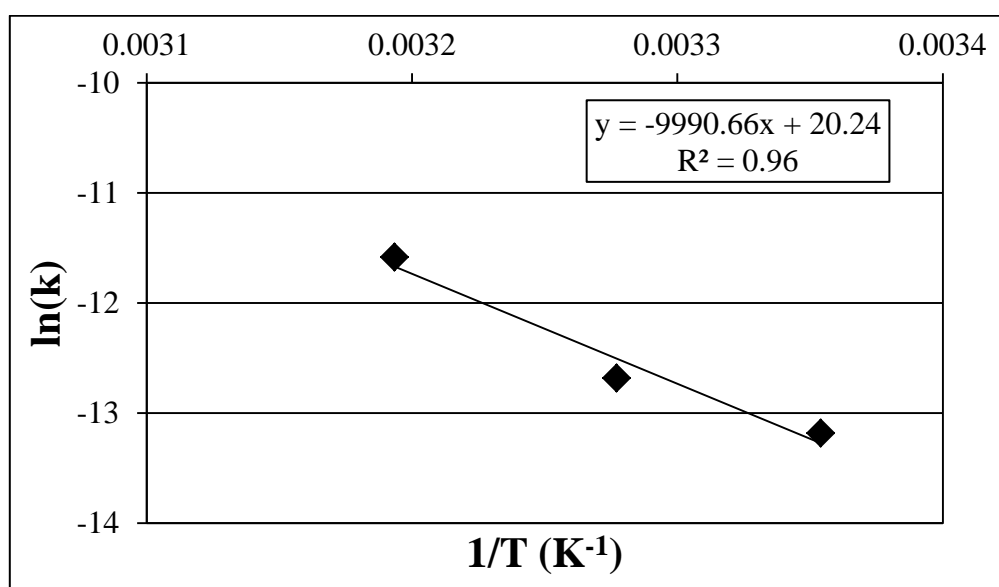


Figure 4.23. Reaction rates and activation energy of phenanthrene, $\ln(k)$ vs. $1/T$.

The plotted values of the reaction rates of phenanthrene degradation are shown on Figure 4.23. Reaction rates for phenanthrene exhibited a good correlation with a correlation coefficient (*e.g.*, R^2) value of 0.96. From the slope of the line, the E_a for this reaction was calculated to be 83.07 kJ mol^{-1} (see Section 4.2.5 for a more in-depth discussion on E_a and reaction rates and Appendix F for more information on degradation).

4.2.4 Pyrene Degradation Results

The peroxy-acid process was found to effectively degrade also pyrene. The set-ups will be referred to the same as indicated in Table 3.3. The experimental set-up showed consistent pyrene degradation results at the three selected different temperatures investigated with degradation rate increasing as temperature increased from 25 to 40 °C. The three controls (*e.g.*, H₂O₂, acetic acid and DI water) experienced little to no degradation of pyrene (see Figs. 4.24, 4.26, and 4.28).

4.2.4.1 Degradation and Reaction Rate at T = 25 °C

At T = 25 °C, pyrene like all the other PAHs investigated in this study was degraded by the peroxy-acid process utilizing 3:3:9 v/v/v H₂O₂ : acetic acid : DI water. Pyrene concentrations for all control samples had very little discernible change and stayed fairly constant in the 24-hour reaction time period as illustrated in Figure 4.24.

The results for pyrene degradation and the pyrene concentrations of the controls are shown in Figure 4.24 and illustrated in Appendix D. The Figure 4.24 illustrates a plot of m/m_0 , or mass of phenanthrene (mg) over initial added mass (mg) pyrene added, versus elapsed time (hrs). After the reaction time periods, the values of m/m_0 were found to be 88.1 % after 6 hours, 84.0 % after 12 hours, 82.7 % after 18 hours and 80.2 % after 24 hours, respectively. In terms of PAH degradation amounts, pyrene demonstrated less degradation than anthracene and benzo[a]pyrene but more than phenanthrene for this selected reaction temperature (*e.g.*, 25 °C). The point for time at $t = 2$ hours had a large mass variability between the two replicate values. However, as an average, this value was still following the overall pyrene degradation trend for this selected temperature.

These results were then plotted following the process provided at the beginning of Section 4.2 (see also Eq. 4.1). The $\ln(m/m_0)$ versus time in hours was plotted as seen in Figure 4.25. The reaction rate of pyrene degradation was calculated for this selected temperature; these results are also shown on Figure 4.25. The observed reaction rate for pyrene at T = 25 °C was 0.0074 hr⁻¹ (or corresponding to 2.056 x 10⁻⁶ s⁻¹) with an R² value of 0.896 (see detailed results of the degradation of pyrene and controls at T = 25 °C are shown in Tables D.19 and D.20 in Appendix D).

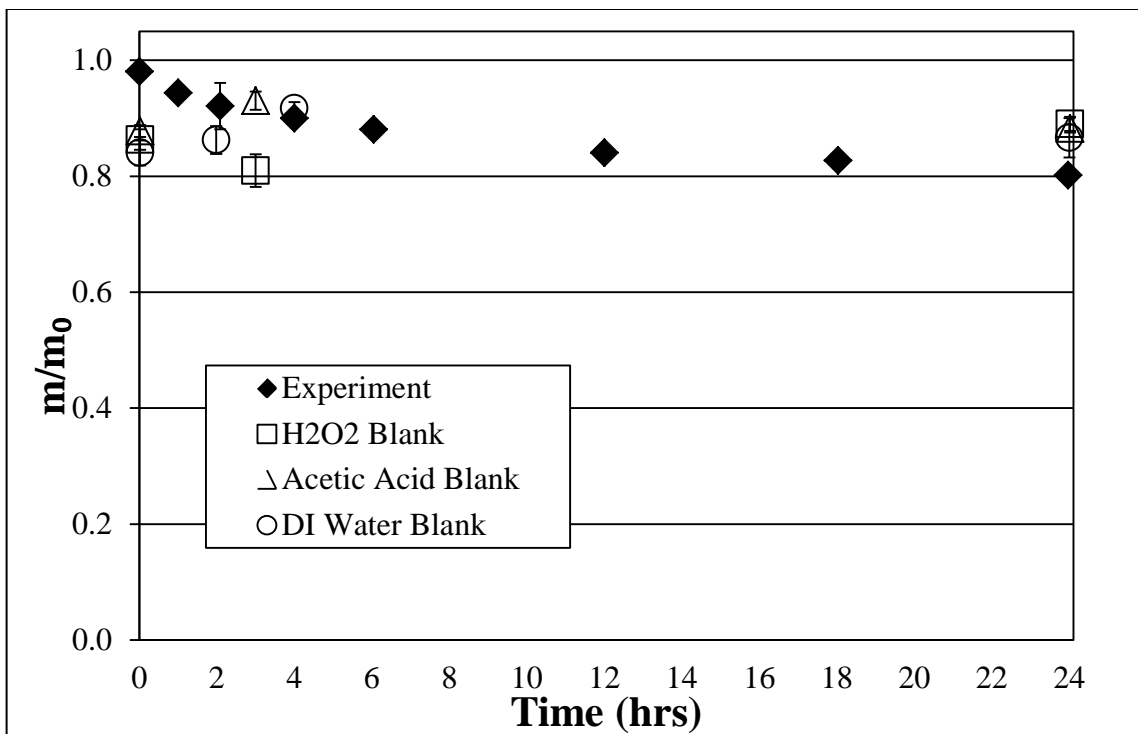


Figure 4.24. Pyrene degradation plotted as mass (m/m_0) vs. time (hrs), 25 °C.

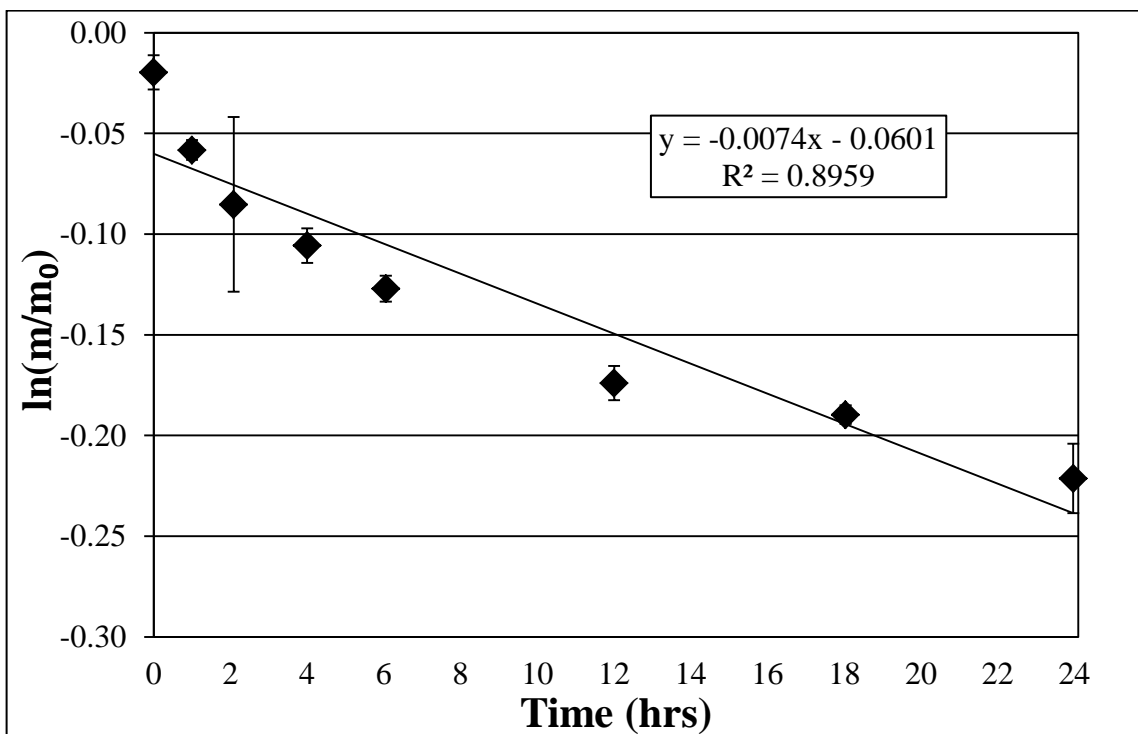


Figure 4.25. Pyrene reaction rate plotted as $\ln(m/m_0)$ vs. time (hrs) at 25 °C.

4.2.4.2 Degradation and Reaction Rate at T = 32 °C

At T = 32 °C reaction temperature, pyrene was degraded by the peroxy-acid process to a higher degree than the 25 °C reaction temperature. Pyrene concentrations for all control samples experienced very little discernible change from t = 0 to t = 24 hours, indicating little to no observed degradation in the blanks (see Fig. 4.26).

The degradation values of pyrene and the pyrene concentrations of the controls are illustrated in Figure 4.26 (*e.g.*, shown as a plot of m/m_0 , mass of phenanthrene over initial added mass, versus elapsed time in hours). The amounts of m/m_0 for pyrene, expressed as a percent of pyrene left in the reaction vessel, after the reaction time period were 83.7 % after 6 hours, 73.1 % after 12 hours, 67.5 % after 18 hours and 60.3 % after the 24-hour reaction time period as seen in Figure 4.26. Pyrene experienced the highest degradation rate out of all the four PAH compounds investigated in this study at this reaction temperature, followed by anthracene, benzo[a]pyrene and phenanthrene.

These results were then plotted again following the procedure discussed in Section 4.2. As described in Section 4.2, the $\ln(m/m_0)$ versus time in hours was plotted to obtain the equation of the line. The reaction rate was then calculated and obtained from this data set and these results are shown on Figure 4.27. The calculated reaction rate for pyrene was 0.0194 hr^{-1} (or $5.389 \times 10^{-6} \text{ s}^{-1}$) with a value of $R^2 = 0.982$ at T = 32 °C (see detailed results of the degradation of pyrene and the controls utilized in these experiments at T = 32 °C are shown in Tables D.21 and D.22 in Appendix D).

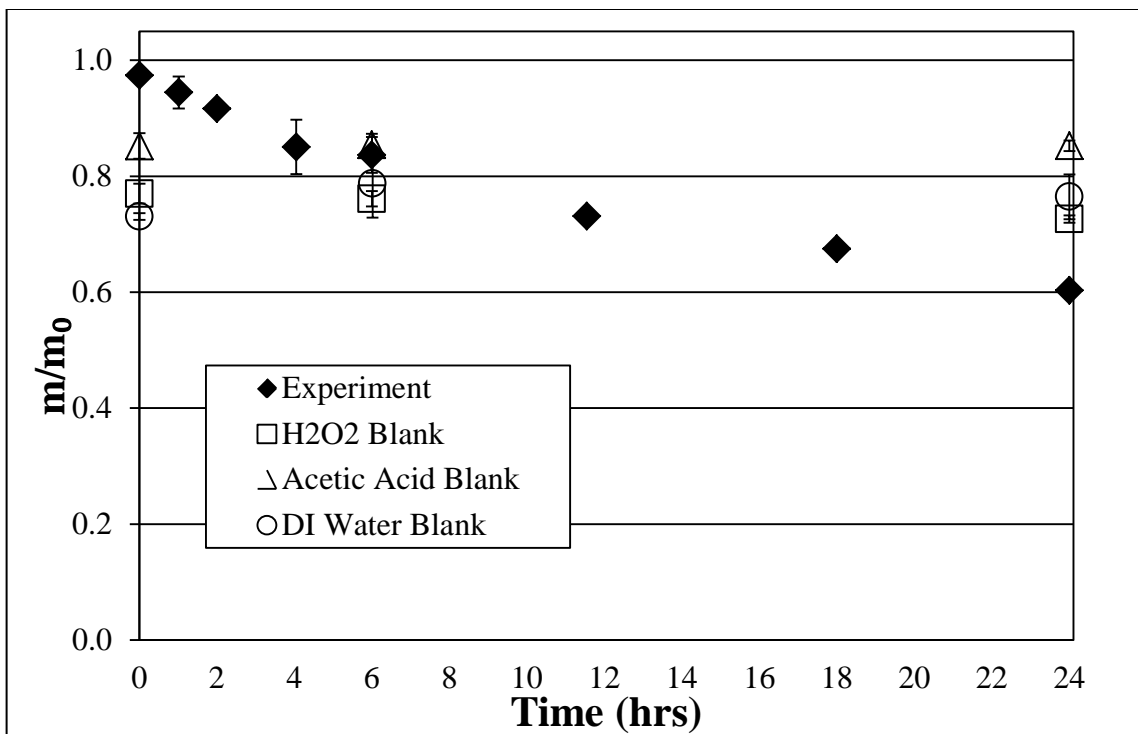


Figure 4.26. Pyrene degradation plotted as mass (m/m_0) vs. time (hrs), 32 °C.

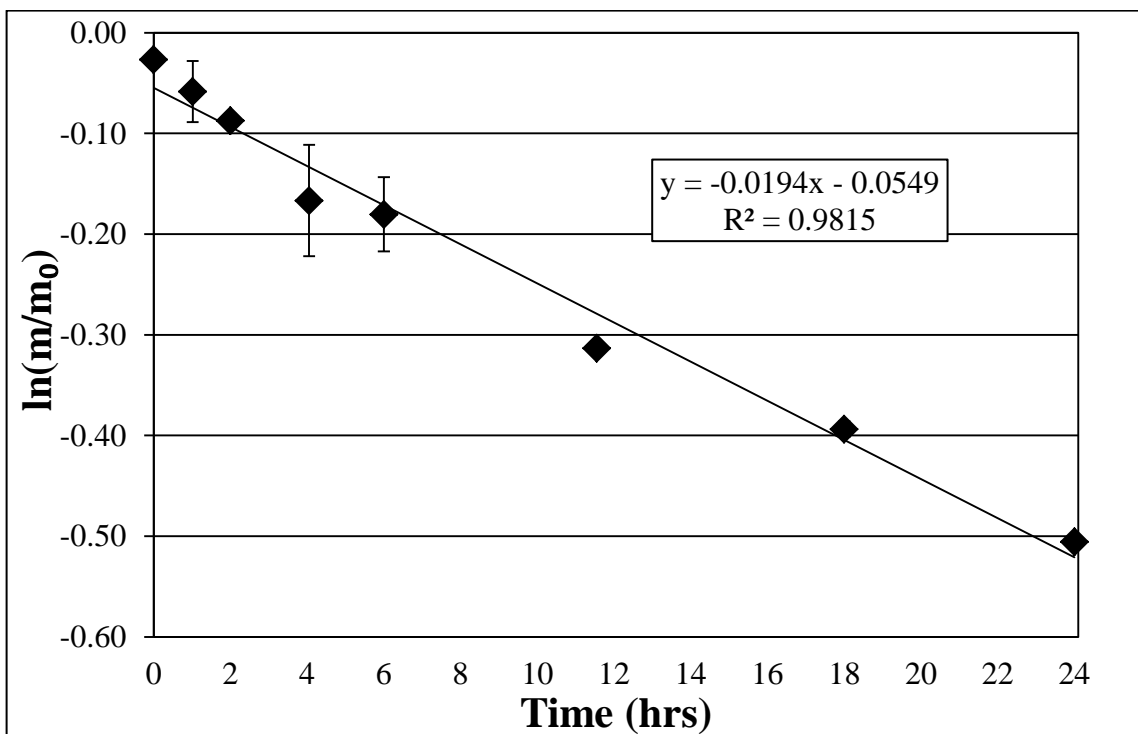


Figure 4.27. Pyrene reaction rate plotted as $\ln(m/m_0)$ vs. time (hrs) at 32 °C.

4.2.4.3 Degradation and Reaction Rate at T = 40 °C

At T = 40 °C, pyrene was almost completely degraded by the peroxy-acid process as illustrated in Appendix D. The pyrene concentrations for all control samples experienced little change after a 24-hour reaction time period, indicating very little to no degradation of pyrene in the control samples at 40 °C. The three controls (*e.g.*, H₂O₂, acetic acid and DI water controls) demonstrated between 0 and 10 % degradation during the 24-hr reaction period.

Pyrene degradation and the pyrene concentrations of the controls are shown in Figure 4.28. A plot of m/m_0 (*e.g.*, mass of pyrene (mg) over initial added mass (mg) of pyrene added to the reaction vessels) versus elapsed time in hours was produced. After a time period of 6 hours, pyrene was degraded to 83.7 % of the initial added amount, 56.1 % after 12 hours, 31.5 % after 18 hours and 10.4 % after a time period of 24 hours, respectively, demonstrating a higher degree of degradation of pyrene at 40 °C than at 32 °C. Based on Figure 4.28, the peroxy-acid solution in contact with pyrene resulted in about 90 % degradation of pyrene during the 24-hr time-course study. These results are consistent with increase in the magnitude of pyrene rate constants with increasing temperature (*e.g.*, from 25 to 40 °C). At this selected temperature, pyrene experienced lower degradation rates than anthracene and benzo[a]pyrene but higher degradation rate than phenanthrene.

These results were then plotted following Equation 4.1 and the process discussed at the beginning of Section 4.2 (*e.g.*, as $\ln(m/m_0)$ versus time in hours). The reaction rate for pyrene at T = 40 °C was then calculated. The results from these calculations are shown on Figure 4.29. The calculated reaction rate value for pyrene at T = 40 °C, was 0.0852 hr^{-1} (or $2.367 \times 10^{-5} \text{ s}^{-1}$) which was a lower degradation rate than anthracene and benzo[a]pyrene but higher than phenanthrene was observed to have at 40 °C. The results used in the reaction rate calculation and the obtained trend line resulted in a correlation coefficient of 0.884 Detailed results of the degradation of pyrene and controls at T = 40 °C can be found in Tables D.23 and D.24 in Appendix D.

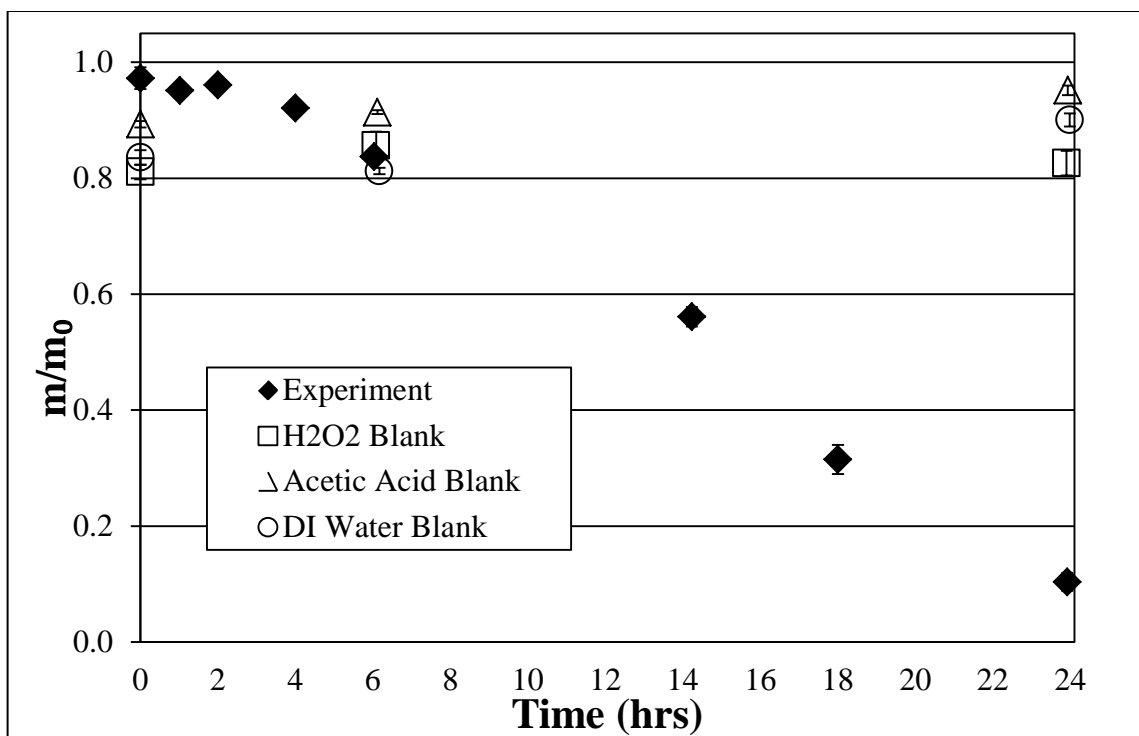


Figure 4.28. Pyrene degradation plotted as mass (m/m_0) vs. time (hrs), 40 °C.

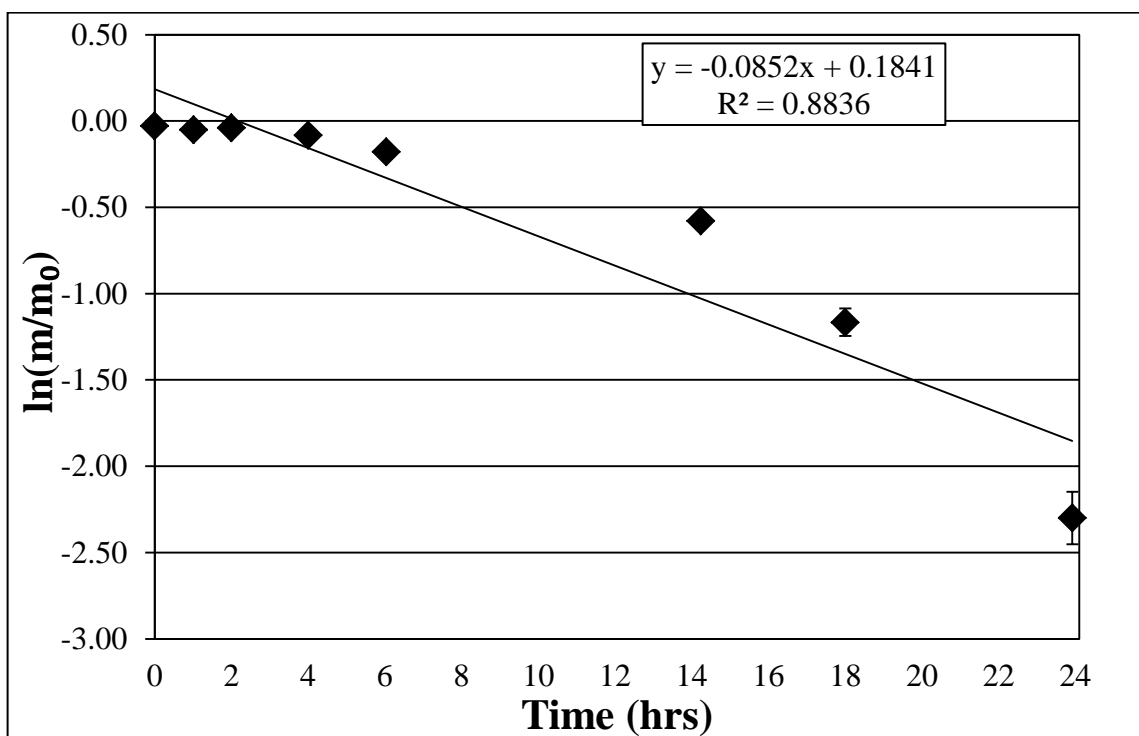


Figure 4.29. Pyrene reaction rate plotted as $\ln(m/m_0)$ vs. time (hrs) at 40 °C.

4.2.4.4 Reaction Rates and Activation Energy

The pseudo-first-order reaction rates in (hr^{-1} and s^{-1}) at temperatures $T = 25, 32$ and 40 °C for the degradation of pyrene using the peroxy-acid process (e.g., 3:3:9 v/v/v H_2O_2 : acetic acid : DI water) are shown on below on Table 4.6.

Table 4.6. Pyrene reaction rates for the selected temperatures.

Temperature (°C)	Reaction Rate (hr^{-1})	Reaction Rate (s^{-1})
25	0.0074	2.056×10^{-6}
32	0.0194	5.389×10^{-6}
40	0.0852	2.367×10^{-5}

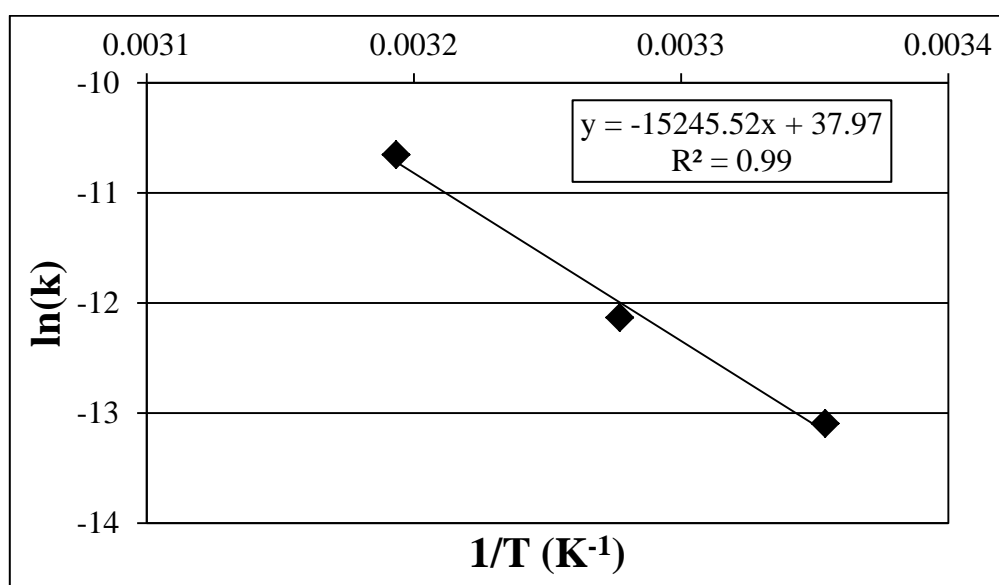


Figure 4.30. Reaction rates and activation energy of pyrene, $\ln(k)$ vs. $1/T$.

The plotted values of the reaction rates of pyrene degradation are shown on Figure 4.30. Reaction rates for pyrene exhibited a good correlation with an R^2 value of 0.99. From the slope of the line through these points, the E_a for this reaction was calculated to be $126.76 \text{ kJ mol}^{-1}$ (see Eq. 4.2). Section 4.2.5 provides a more in-depth discussion on E_a and reaction rates and Appendix F provides more information on degradation.

4.2.5 Summary of Results

All PAHs exhibited good degradation efficiencies when treated with the peroxy-acid process. As temperature increased, reaction rates and degradation efficiencies increased as well. In terms of mass, the final amounts of mass of PAH left after 24 hours of degradation for temperatures of 25, 32, and 40 °C were: [i] anthracene 69.5 %, 55.4 %, and 1.86 %; [ii] benzo[a]pyrene 79.9 %, 61.9 %, and 7.61 %; [iii] phenanthrene 82.1 %, 72.3 %, and 38.7 %; and [iv] pyrene 80.2 %, 60.3 % and 10.4 %, respectively. The above mentioned values for the mass % of PAH left after degradation times of 24 hours for all four PAH compounds in this study versus temperature in °C can be obtained in Figure 4.31 below.

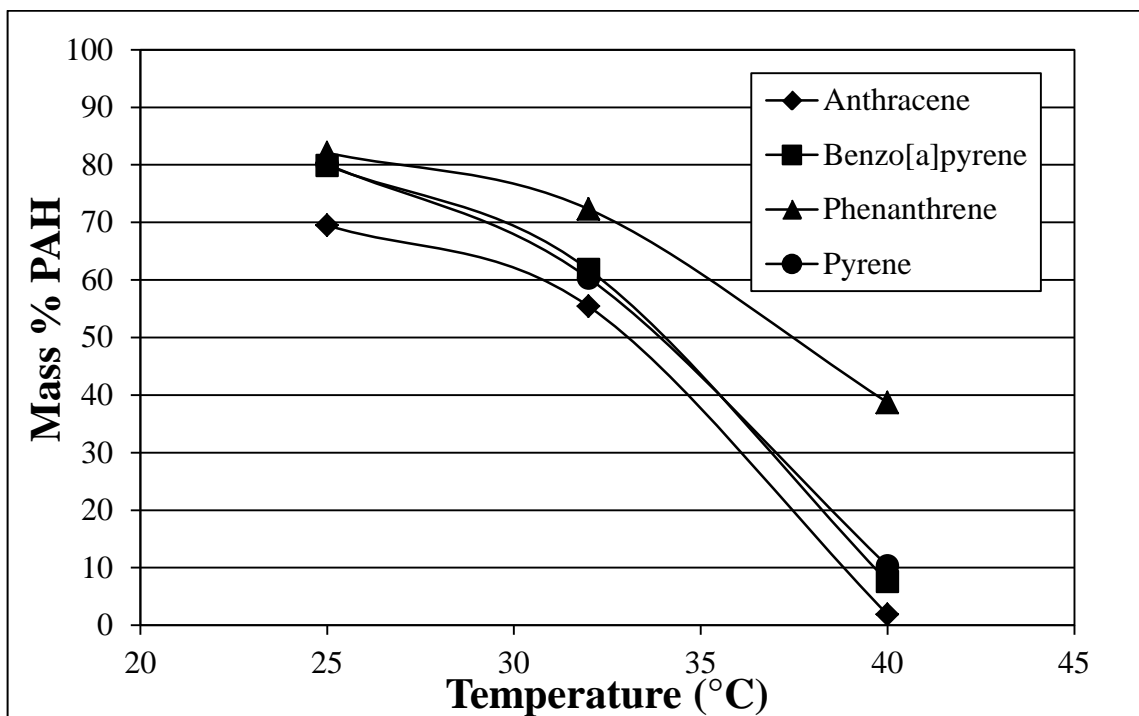


Figure 4.31. Mass % values all four PAHs, degradation after 24 hours vs. T (°C).

Anthracene had the highest decrease in % PAH values for all three temperatures, benzo[a]pyrene had the second highest overall, with pyrene third, while phenanthrene had the lowest for all four PAH compounds. Pyrene did have a slightly better % PAH degradation than benzo[a]pyrene (60.3% vs. 61.8 % mass left) but this could be due to

experimental or analytical error. General trend of increased treatment efficiencies at higher temperatures was observed. As the temperature increased the reaction seemed to accelerate, this can be observed in Figure 4.31, and this could be due to increased efficiency due to higher PAA concentrations in solution as time elapsed, see Section 4.1.2. Increased efficiencies and PAA concentrations were also observed by Shoulder (2012) when reagents were allowed to undergo an “equilibration period” of 48 hours before the addition of aniline to the reaction vessels.

The natural log of the reaction rates (in units of s^{-1}) vs. $1/T$ in units of (K) for all four PAH compounds in this study are also presented in Figure 4.32, the reaction rate values of the PAHs can be found in Sections 4.2.1.4, 4.2.2.4, 4.2.3.4, 4.2.4.4 and Appendix F.

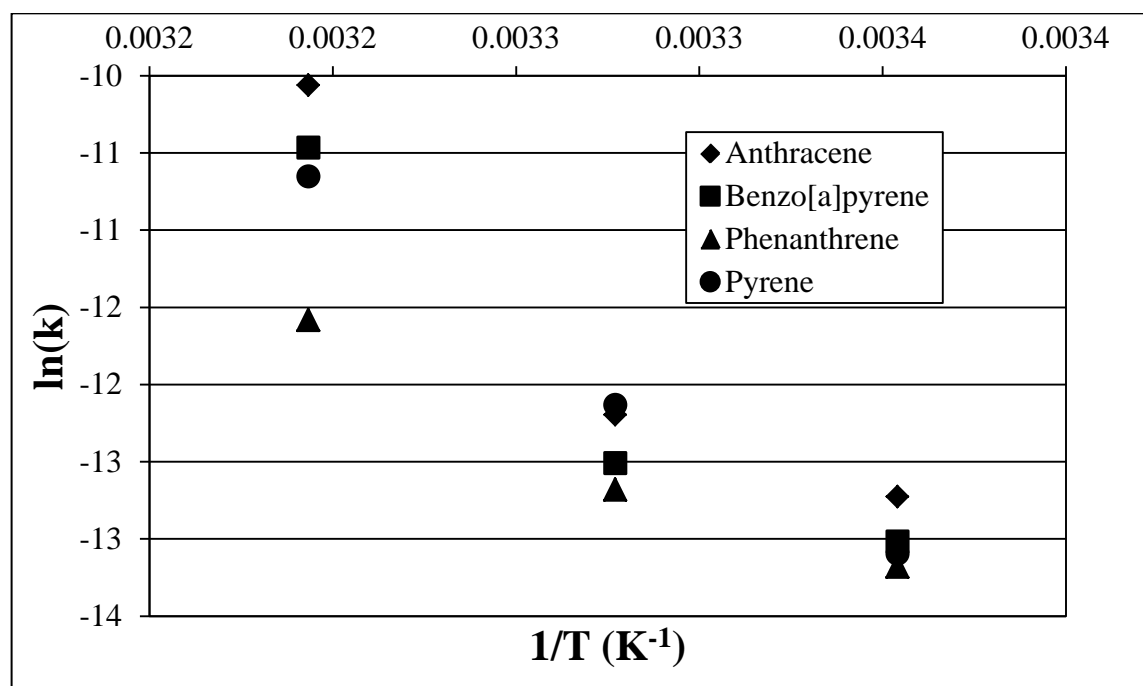


Figure 4.32. Natural log of all rate constants for all four PAH compounds.

Activation energies for anthracene, benzo[a]pyrene, phenanthrene and pyrene ranged from 83.07 to 138.96 kJ mol^{-1} . The trend followed in Figure 4.31 is the same for the trend in E_a . Anthracene had the highest E_a with a value of 138.96 kJ mol^{-1} , followed by benzo[a]pyrene with 133.13 kJ mol^{-1} , then pyrene with 126.76 kJ mol^{-1} , and finally

phenanthrene with the lowest E_a value of 83.07 kJ mol⁻¹. All these activation energy values and corresponding frequency factors, A, are show in Table 4.7 below.

Table 4.7. Summary of activation energies for the four selected PAHs.

PAH Compound	E_a (kJ mol ⁻¹)	A (s ⁻¹)
Anthracene	138.96	5.07×10^{18}
Benzo[a]pyrene	133.13	3.65×10^{17}
Phenanthrene	83.07	6.17×10^8
Pyrene	126.76	3.09×10^{16}

The pre-exponential factor or in this case frequency factor A, followed the same trend as E_a , with anthracene having the highest followed by benzo[a]pyrene, pyrene, and phenanthrene with a much lower value. This helps explain why anthracene had the highest E_a , but still experienced the most degradation since it had a value of $A = 5.07 \times 10^{18} \text{ s}^{-1}$, the highest for all four compounds. Benzo[a]pyrene had the second highest activation energy, came second in terms of most degradation and it had the second highest value of A, with $A = 3.65 \times 10^{17} \text{ s}^{-1}$. Pyrene was third in terms of degradation rate, E_a and pre-exponential factor with a value of $A = 3.09 \times 10^{16} \text{ s}^{-1}$; while phenanthrene had the lowest E_a , but experienced the least amount of degradation, and this could be due to its frequency factor, much lower than those of the other PAHs with a value of $A = 6.17 \times 10^8 \text{ s}^{-1}$.

Going back to Equation 4.2, the frequency factor A accounts for the total number of collisions leading to a reaction, while the term $e^{-E_a/RT}$ is the probability that a collision will result in the reaction proceeding (Schwarzenbach *et al.*, 1993). Perhaps physico-chemical properties like S_w or the chemical structure and arrangement of the rings of the PAHs, like the “well-structure” or also called “bay-area”, present in the arrangement of the rings of phenanthrene could be reasons for these trends in A and E_a .

5. CONCLUSIONS

The peroxy-acid process proved to be effective in treating PAH compounds in solutions and achieved results comparable to other AOPs. The presence of an H_2SO_4 catalyst was found to increase the concentration of PAA more than tenfold. This suggested that H_2SO_4 could prove to be a successful catalyst when used in small amounts in the peroxy-acid process for increasing PAA production in solution and, hence, increase the efficiency of the peroxy-acid process. The wt. % of PAA in solution was also found to increase as time elapsed and the wt. % of H_2O_2 decreased. This could be due to interactions between the H_2O_2 producing HO^\bullet and the added CH_3COOH present in solution, producing PAA. PAA was also found to be present in the peroxy-acid process by confirming the presence with the titrimetric method.

The peroxy-acid process was able to degrade all four PAH compounds (*i.e.*, anthracene, benzo[a]pyrene, phenanthrene, and pyrene) effectively at 25, 32, and 40 °C. None of the controls for displayed significant degradation of the PAHs; since H_2O_2 was found in the blanks, this could indicate that the presence of PAA is required for degradation of PAHs using the peroxy-acid process. Anthracene and phenanthrene have the same molecular weights but were at the highest and lowest ends in terms of degradation, respectively. Benzo[a]pyrene demonstrated the second and phenanthrene the third highest reaction rates utilizing 3:3:9 v/v/v H_2O_2 : acetic acid : Di water. Reaction rates and mass % degraded using the peroxy-acid process to degrade PAHs for temperatures $T = 25, 32$ and 40 °C were found as follows: [i] anthracene 0.0107, 0.0182, and 0.1536 hr^{-1} with degradations of 30.5 %, 44.6 %, and 98.14 %; [ii] benzo[a]pyrene 0.0080, 0.0133, and 0.1027 hr^{-1} with degradations of 20.1 %, 38.2 %, and 92.39 %; [iii] phenanthrene 0.0068, 0.0112 and 0.0336 hr^{-1} with degradations of 17.9 %, 27.7 %, and 61.3 %; and [iv] pyrene 0.0074, 0.0194, and 0.0852 hr^{-1} with degradations of 19.9 %, 39.7 % and 89.7 %, respectively.

The E_a and frequency factors computed for the scenarios mentioned above were: [i] for anthracene $E_a = 138.96 \text{ kJ mol}^{-1}$ and $A = 5.07 \times 10^{18} \text{ s}^{-1}$; [ii] for benzo[a]pyrene $E_a = 133.13 \text{ kJ mol}^{-1}$ and $A = 3.65 \times 10^{17} \text{ s}^{-1}$; [iii] for phenanthrene $E_a = 83.07 \text{ kJ mol}^{-1}$ and $A = 6.17 \times 10^8 \text{ s}^{-1}$; and [iv] for pyrene $E_a = 126.76 \text{ kJ mol}^{-1}$ and $A = 3.09 \times 10^{16} \text{ s}^{-1}$. The

compounds that exhibited the best degradation rates, highest E_a and frequency factors in the following order: anthracene, benzo[a]pyrene, pyrene and phenanthrene.

6. FUTURE WORK

This work could be potentially useful in helping determine the reaction mechanism of PAA and organics, like PAHs. While the peroxy-acid has proven useful to treat soils contaminated with PAHs, this type of investigation could be performed with soils present to inspect any possible difference in mechanics and behavior (Alderman *et al.*, 2007; Levitt *et al.*, 2003; N'Guessan *et al.*, 2004a; N'Guessan *et al.*, 2004b).

Molecular modeling based on the rates calculated in this work could also be performed to compare the E_a values between the peroxy-acid process and HO^\bullet or PAA. Predictive models developed from these experiments could help predict the applicability of remediation methods to different solutions and help determine the most viable and cost effective method. Production of PAA could also be investigated further, to determine the amount of PAA produced to the amount of H_2O_2 added to the reaction vessels. Other work to help understand process mechanics would be to study the degradation products from PAHs undergoing the peroxy-acid methods. Identification of these by-products could also be useful for determining if the peroxy-acid method is a viable AOP, as these by-products could prove to be more harmful than the initial contaminant. Finally, the methods used in this work could also be applied to other organic contaminants to see if the peroxy-acid process is a proper treatment method for those as well.

REFERENCES

- Achten, C. and Hofmann, T. (2009) 'Native polycyclic aromatic hydrocarbons (PAH) in coals - A hardly recognized source of environmental contamination', *Science of the Total Environment*, no. 407, pp. 2641-2473.
- Alderman, N.S. (2009) 'The peroxy-acid treatment process: An investigation of process mechanics', *Ph.D. Dissertation, Rensselaer Polytechnic Institute, Troy, New York, USA*.
- Alderman, N.S., N'Guessan, A.L., Nyman, M.C. (2007) 'Effective treatment of PAH contaminated Superfund site soil with the peroxy-acid process', *Journal of Hazardous Materials*, no. 146, pp. 652-660.
- Alderman, N.S. and Nyman, M.C. (2009) 'Oxidation of PAHs in a simplified system using peroxy-acid and glass beads: Identification of oxidizing species', *Journal of Environmental Science and Health, Part A*, vol. 44, no. 11.
- Alpert, D.J., Sprung, J.L., Pacheco, J.E., Prairie, M.R., Reilly, H.E., Milne, T.A., Nimlos, M.R. (1991) 'Sandia National Laboratories' work in solar detoxification of hazardous wastes', *Solar Energy Materials*, vol. 24, no. 1-4, December, pp. 594-607.
- ATSDR (1995) *Toxicological profile for polycyclic aromatic hydrocarbons (PAHs)*, August, [Online], Available: <http://www.atsdr.cdc.gov/toxprofiles/tp69.pdf> [2 March 2013].
- Bach, R.D., Canepa, C., Winter, J.E., Blanchette, P.E. (1997) 'Mechanism of acid-catalyzed epoxidation of alkenes with peroxy acids', *Journal of Organic Chemistry*, vol. 62, no. 15, pp. 5191-5197.

Beltrán, F.J., Encinar, J.M., González, J.F. (1997) 'Industrial wastewater advanced oxidation. Part 2. Ozone combined with hydrogen peroxide or UV radiation', *Water Research*, vol. 31, no. 10, October, pp. 2415-2428.

Boffetta, P., Jourenkova, N., Gustavsson, P. (1997) 'Cancer risk from occupational and environmental exposure to polycyclic aromatic hydrocarbons', *Cancer Causes & Control*, vol. 8, no. 3, pp. 444-472.

Booth, R.A. and Lester, J.N. (1995) 'The potential formation of halogenated by-products during peracetic acid treatment of final sewage effluent', *Water Research*, vol. 29, no. 7, July, pp. 1793-1801.

Bossert, I., Kachel, W.M., Bartha, R. (1984) 'Fate of hydrocarbons during oily sludge disposal in soil', *Applied Environmental Microbiology*, vol. 47, no. 4, April, pp. 763-767.

Brown, G.S., Barton, L.L., Thomson, B.M. (2003) 'Permanganate oxidation of sorbed polycyclic aromatic hydrocarbons', *Waste Management*, vol. 23, no. 8, pp. 737-740.

Burrows, H.D., Canle L, M., Santaballa, J.A., Steenken, S. (2002) 'Reaction pathways and mechanisms of photodegradation of pesticides', *Journal of Photochemistry and Photobiology B: Biology*, vol. 67, no. 2, June, pp. 71-108.

Carey, J.H., Lawrence, J., Tosine, H.M. (1976) 'Photodechlorination of PCB's in the presence of titanium dioxide in aqueous suspensions', *Bulletin of Environmental Contamination and Toxicology*, vol. 16, no. 6, pp. 697-701.

Chang, B.V., Shiung, L.C., Yuan, S.Y. (2002) 'Anaerobic biodegradation of polycyclic aromatic hydrocarbon in soil', *Chemosphere*, vol. 48, no. 7, August, pp. 717-724.

Ciotti, C., Baciocchi, R., Cleriti, G., Chiavola, A. (2008) 'Peroxy-acid as an innovative oxidant for the remediation contaminated sediments', *10th International UFZ. In TNO Conference on Soil-Water Systems (CONSOIL)*.

Colgan, S. and Gehr, R. (2001) 'Disinfection', *Water Environment & Technology*, vol. 13, no. 11, November, pp. 29-33.

Collin, G., Höke, H., Talbiersky, J. (2000) 'Anthracene', in *Ullmann's Encyclopedia of Industrial Chemistry*, Weinheim: Wiley-VCH Verlag GmbH & Co. KGaA.

Comninellis, C., Kapalka, A., Malato, S., Parsons, S.A., Poulios, I., Mantzavinos, D. (2008) 'Advanced oxidation processes for water treatment: advances and trends for R&D', *Journal of Chemical Technology and Biotechnology*, vol. 83, no. 6, pp. 769-776.

Costa, H.J. and Sauer, T.C. (2005) 'Forensics approaches and consideration in identifying PAH background', *Environmental Forensics*, no. 6, pp. 9-16.

Cunningham, S.D. and Berti, W.R. (1993) 'Remediation of contaminated soils with green plants: an overview', *In Vitro Cellular & Developmental Biology-Plant*, vol. 29, no. 4, pp. 207-212.

Cunningham, S.D., Berti, W.R., Huang, J.W. (1995) 'Phytoremediation of contaminated soils', *Trends in Biotechnology*, vol. 13, no. 9, September, pp. 393-397.

Dell'Erba, A., Falsanisi, D., Liberti, L., Notarnicola, M., Santoro, D. (2004) 'Disinfecting behaviour of peracetic acid for municipal wastewater reuse', *Desalination*, vol. 168, August, pp. 435-442.

Dell'Erba, A., Falsanisi, D., Liberti, L., Notarnicola, M., Santoro, D. (2007) 'Disinfection by-products formation during wastewater disinfection with peracetic acid', *Desalination*, vol. 215, no. 1-3, September, pp. 177-186.

Deshpande, S., Shiau, B.J., Wade, D., Sabatini, D.A., Harwell, J.H. (1999) 'Surfactant selection for enhancing ex situ soil washing', *Water Research*, vol. 33, no. 2, February, pp. 351-360.

Dzombak, D.A. and Luthy, R.G. (1984) 'Estimating adsorption of polycyclic aromatic hydrocarbons on soils', *Soil Science*, no. 137, pp. 292-308.

El-Agamey, A. and McGarvey, D.J. (2003) 'Evidence for a lack of reactivity of carotenoid addition radicals towards oxygen: A laser flash photolysis study of the reactions of carotenoids with acylperoxyl radicals in polar and non-polar solvents', *Journal of the American Chemical Society*, vol. 125, no. 11, pp. 3330-3340.

Emsbo-Mattingly, S.D. (2003) 'Creosote and other PAH sources', Proceedings - Annual Meeting of the American Wood-Preservers' Association, 245-252.

Emsbo-Mattingly, S.D., Uhler, A.D., Stout, S.A., McCarthy, K.J. (2001) 'Identifying creosote at contaminated sites: An environmental forensics overview', *Contaminated Soil Sediment & Water*, Feb, pp. 9-12.

Fenton, H.J.H. (1894) 'Oxidation of tartaric acid in presence of iron', *Journal of the Chemical Society, Trans.*, vol. 65, pp. 899-819.

Ferrarese, E., Andreottola, G., Oprea, I.A. (2008) 'Remediation of PAH-contaminated sediments by chemical oxidation', *Journal of Hazardous Materials*, vol. 152, no. 1, March, pp. 128-139.

Flotron, V., Delteil, C., Padellec, Y., Camel, V. (2005) 'Removal of sorbed polycyclic aromatic hydrocarbons from soil, sludge and sediment samples using the Fenton's reagent process', *Chemosphere*, vol. 59, no. 10, June, pp. 1427-1437.

Flowers, L., Rieth, S.H., Cogliano, V.J., Foureman, G.L., Hertzberg, R., Hofmann, E.L., Murphy, D.L., Nesnow, S., Schoeny, R.S. (2002) 'Health assesment of polycyclic aromatic hydrocarbon mixtures: current practices and future directions', *Polycyclic Aromatic Compounds*, no. 22, pp. 811-821.

Fox, M.A., Draper, R.B., Dulay, M., O'Shea, K. (1991) 'Control of photocatalytic oxidative selectivity on irradiated titania powders: A diffuse reflectance kinetic study', in Pelizzetti, E. and Schiavello, M. (ed.) *Photochemical Conversion and Storage of Solar Energy, Proc. Int. Conf., 8th*, Dordrecht: Kluwer.

Gan, S., Lau, E.V., Ng, H.K. (2009) 'Remediation of soils contaminated with polycyclic aromatic hydrocarbons (PAHs)', *Journal of Hazardous Materials*, vol. 172, no. 2-3, December, pp. 532-549.

Gerard, C. and Gustafsson, Ö. (2006) 'Effects of added PAHs and precipitated humic acid coatings on phenanthrene sorption to environmental Black carbon', *Environmental Pollution*, no. 141, pp. 526-531.

Ghosal, S. and Luthy, R.G. (1996) 'Bioavailability of hydrophobic organic compounds from nonaqueous-phase liquids: The biodegradation of naphthalene from coal tar', *Environmental Toxicology and Chemistry*, vol. 15, no. 11, pp. 1894-1900.

Gogate, P.R. and Pandit, A.B. (2004a) 'A review of imperative technologies for wastewater treatment I: oxidation technologies at ambient conditions', *Advances in Environmental Research*, vol. 8, no. 3-4, March, pp. 501-551.

Gogate, P.R. and Pandit, A.B. (2004b) 'A review of imperative technologies for wastewater treatment II: hybrid methods', *Advances in Environmental Research*, vol. 8, no. 3-4, March, pp. 553-597.

Guan, X., He, D., Ma, J., Chen, G. (2010) 'Application of permanganate in the oxidation of micropollutants: A mini review', *Frontiers of Environmental Science & Engineering in China*, vol. 4, no. 4, December, pp. 405-413.

Gustafson, P., Östman, C., Sällsten, G. (2008) 'Indoor levels of polycyclic aromatic hydrocarbons in homes with or without wood burning for heating', *Environmental Science & Technology*, vol. 42, no. 14, pp. 5074-5080.

Gustafsson, Ö., Haghseta, F., Chan, C., Gschwend, P.M. (1997) 'Quantification of the dilute sedimentary soot phase: Implications for PAH speciation and bioavailability', *Environmental Science & Technology*, no. 31, pp. 203-209.

Harmon, T.C., Burks, G.A., Aycaguer, A.-C., Jackson, K. (2001) 'Thermally enhanced vapor extraction for removing PAHs from Lampblack-contaminated soil', *Journal of Environmental Engineering*, vol. 127, no. 11, pp. 986-993.

Hecht, S.S. (1999) 'Tobacco smoke carcinogens and lung cancer', *Journal of the National Cancer Institute*, vol. 91, no. 14, July, pp. 1194-1210.

Henner, P., Schiavon, M., Morel, J.-L., Lichtfouse, E. (1997) 'Polycyclic aromatic hydrocarbons (PAH) occurrence and remediation methods', *Analisis* 25, no. 9-10.

Heywood, D., Phillips, B., Stansbury, Jr., H. (1961) 'Communications. Free radical hydroxylations with peracetic acid', *The Journal of Organic Chemistry*, vol. 26, no. 1, p. 281.

IARC (2010) *Monographs on the evaluation of carcinogenic risks to humans Vol. 92: Some non-heterocyclic polycyclic aromatic hydrocarbons and some related exposures*, IARC Working Group on the evaluation of carcinogenic risks to humans, [Online], Available: <http://monographs.iarc.fr/ENG/Monographs/vol92/mono92.pdf> [1 March 2013].

Ince, N.H., Belen, R.K., Apikyan, Ī.G. (2001) 'Ultrasound as a catalyzer of aqueous reaction systems: the state of the art and environmental applications', *Applied Catalysis B: Environmental*, vol. 29, no. 3, February, pp. 167-176.

Kadla, J.F. and Chang, H.-M. (2001) 'The reactions of peroxides with lignin and lignin model compounds', in Argyropoulos, D., (ed.) *Oxidative Delignification Chemistry*, ACS Symposium Series, Vol. 785.

Khalili, N.R., Scheff, P.A., Holsen, T.M. (1995) 'PAH source fingerprints for coke ovens, diesel and gasoline engines, highway tunnels and wood combustion emissions', *Atmospheric Environment*, vol. 29, no. 4, pp. 533-542.

Kitis, M. (2004) 'Disinfection of wastewater with peracetic acid: a review', *Environment International*, vol. 30, no. 1, March, pp. 47-55.

Koivunen, J. and Heinonen-Tanski, H. (2005) 'Peracetic acid (PAA) disinfection of primary, secondary and tertiary treated municipal wastewaters', *Water Research*, vol. 39, no. 18, November, pp. 4445-4453.

Lau, K.L., Tsang, Y.Y., Chiu, S.W. (2003) 'Use of spent mushroom compost to bioremediate PAH-contaminated samples', *Chemosphere*, vol. 52, no. 9, September, pp. 1539-1546.

Law, R.J., Dawes, V.J., Woodhead, R.J., Matthiessen, P. (1997) 'Polycyclic aromatic hydrocarbons (PAH) in seawater around England and Wales', *Marine Pollution Bulletin*, vol. 34, no. 5, pp. 306-322.

Legrini, O., Oliveros, E., Braun, A.M. (1993) 'Photochemical processes for water treatment', *Chemical Review*, vol. 93, pp. 671-698.

Levitt, J.S., N'Guessan, A.L., Rapp, K.L., Nyman, M.C. (2003) 'Remediation of α -methyl-naphthalene-contaminated sediments using peroxy acid', *Water Research*, vol. 37, no. 12, pp. 3016-3022.

Luthy, R.G., Aiken, G.R., Brusseau, M.L., Cunningham, S.D., Gschwend, P.M., Pignatello, J.J., Reinhard, M., Traina, S.J., Webber, Jr., W.J., Westall, J.C. (1997) 'Sequestration of hydrophobic organic contaminants by geosorbents', *Environmental Science & Technology*, vol. 31, no. 12, pp. 3341-3347.

Ma, Y.-G., Lei, Y.D., Xiao, H., Wania, F., Wang, W.-H. (2010) 'Critical review and recommended values for the physical-chemical property data of 15 polycyclic aromatic hydrocarbons at 25 °C', *J. Chem. Eng. Data*, no. 55, pp. 819-825.

Marczynski, B., Pesch, B., Wilhelm, M., Rossbach, B., Preuss, R., Hahn, J.-U., Rabstein, S., Raulf-Heimsoth, M., Seidel, A., Rihs, H.-P., Adams, A., Scherenberg, M., Erkes, A., Engelhardt, B., Straif, K., Kafferlein, H.U., Angerer, J., Bruning, T. (2009) 'Occupational exposure to polycyclic aromatic hydrocarbons and DNA damage by industry: a nationwide study in Germany', *Archives of Toxicology*, vol. 83, no. 10, October, pp. 947-957.

Miller, J.S. and Olejnik, D. (2004) 'Ozonation of polycyclic aromatic hydrocarbons in water solution', *Ozone: Science and Engineering*, vol. 26, no. 5, October, pp. 453-464.

Mulligan, C.N., Yong, R.N., Gibbs, D.F. (2001) 'Surfactant-enhanced remediation of contaminated soil: A review', *Engineering Geology*, vol. 60, no. 1-4, June, pp. 371-380.

N'Guessan, A.L. (2005) 'Remediation of PAH-contaminated soils and sediments; the peroxy-acid process', *Ph.D. Dissertation, Rensselaer Polytechnic Institute, Troy, New York, USA*.

N'Guessan, A.L., Carignan, T., Nyman, M.C. (2004a) 'Optimization of the peroxy acid treatment of α -methyl-naphthalene and benzo[a]pyrene in sandy and silty-clay sediments', *Environmental Science & Technology*, no. 38, pp. 1554-1560.

N'Guessan, A.L., Levitt, J.S., Nyman, M.C. (2004b) 'Remediation of benzo(a)pyrene in contaminated sediments using peroxy-acid', *Chemosphere*, vol. 55, no. 10, June, pp. 1413-1420.

NYS DEC (2013) *Contamination at MGP sites - NYS Dept. of Environmental Conservation*, [Online], Available: <http://www.dec.ny.gov/chemical/24922.html> [15 Feb 2013].

Ollis, D.F., Pelizzetti, E., Serpone, N. (1991) 'Photocatalyzed destruction of water contaminants', *Environmental Science & Technology*, vol. 25, no. 9, pp. 1522-1529.

O'Mahony, M.M., Dobson, A.D.W., Barnes, J.D., Singleton, I. (2006) 'The use of ozone in the remediation of polycyclic aromatic hydrocarbon contaminated soil', *Chemosphere*, vol. 63, no. 2, April, pp. 307-314.

Périer, C., Lamy, M.-F., Francony, A., Benahcene, A., David, B., Renaudin, V., Gondrexon, N. (1994) 'Sonochemical degradation of phenol in dilute aqueous solutions: Comparison of the reaction rates at 20 and 487 kHz', *Journal of Physical Chemistry*, vol. 98, no. 41, pp. 10514-10520.

Peyton, G.R. (1990) 'Oxidative treatment methods for removal of organic compounds from drinking water supplies', in Ram, N.M., Christman, R.F., Cantor, K.P. *Significance and Treatment of Volatile Organic Compounds in Water Supplies*, Chelsea: Lewis Publisher.

Peyton, G.R. and Glaze, W.H. (1988) 'Destruction of pollutants in water with ozone in combination with ultraviolet radiation. 3. Photolysis of aqueous ozone', *Environmental Science & Technology*, vol. 22, no. 7, pp. 761-767.

Pichat, P. (1991) 'Photocatalysis: Heterogeneous regime. Catalysts, adsorption and new Techniques', in Pelizzetti, E. and Schiavello, M. (ed.) *Photochemical Conversion and Storage Solar Energy, Proc. Int. Conf., 8th*, Dordrecht: Kluwer.

Rababah, A. and Matsuzawa, S. (2002) 'Treatment system for solid matrix contaminated with fluoranthene. I—Modified extraction technique', *Chemosphere*, vol. 46, no. 1, January, pp. 39-47.

Rochelle, P.A., Fallar, D., Marshall, M.M., Montelone, B.A., Upton, S.J., Woods, K. (2004) 'Irreversible UV inactivation of *Cryptosporidium* spp. despite the presence of UV repair genes', *Journal of Eukaryotic Microbiology*, vol. 51, no. 5, pp. 553-562.

Rokhina, E.V., Makarova, K., Golovina, E.A., Van As, H., Virkutyte, J. (2010) 'Free radical reaction pathway, thermochemistry of peracetic acid homolysis, and its application for phenol degradation: Spectroscopic study and quantum chemistry calculations', *Environmental Science & Technology*, vol. 44, no. 17, pp. 6815-6821.

Sauer, T.C. and Costa, H.J. (2003) 'Fingerprinting of gasoline and coal tar NAPL volatile hydrocarbons dissolved in groundwater', *Environmental Forensics*, vol. 4, no. 4, pp. 319-329.

Schulte, A., Ernst, H., Peters, L., Heinrich, U. (1994) 'Induction of squamous cell carcinomas in the mouse lung after long-term inhalation of polycyclic aromatic hydrocarbon-rich exhausts', *Experimental and Toxicologic Pathology*, vol. 45, no. 7, pp. 415-421.

Schwarzenbach, R.P., Gschwend, P.M., Imboden, D.M. (1993) *Environmental organic chemistry*, 1st edition, New York: John Wiley & Sons, Inc.

Shi, H.-C. and Li, Y. (2007) 'Formation of nitroxide radicals from secondary amines and peracids: A peroxy radical oxidation pathway derived from electron spin resonance detection and density functional theory calculation', *Journal of Molecular Catalysis A: Chemical*, vol. 271, no. 1-2, June, pp. 32-41.

Shoulder, J.M. (2012) 'Hydrophobic organic compounds reaction rates with peroxy-acid treatment in engineered systems: Prediction of reactivity using modeling and PEST', *Ph.D. Dissertation, Rensselaer Polytechnic Institute, Troy, New York, USA*.

Silva, A., Delerue-Matos, C., Fiúza, A. (2005) 'Use of solvent extraction to remediate soils contaminated with hydrocarbons', *Journal of Hazardous Materials*, vol. 124, no. 1-3, September, pp. 224-229.

Sims, R.C. and Overcash, M.R. (1983) 'Fate of polynuclear aromatic compounds (PNAs) in soil-plant systems', *Residue Reviews*, vol. 88, pp. 1-68.

Speight, J.G. (1994) *The chemistry and technology of coal*, 2nd edition, New York: Marcel Dekker, Inc.

Straif, K., Baan, R., Grosse, Y., Secretan, B., El Ghissassi, F., Coglianò, V. (2005) 'On behalf of the WHO International Agency for Research on Cancer Monograph Working Group, carcinogenicity of polycyclic aromatic hydrocarbons', *The Lancet Oncology*, vol. 6, no. 12, December, pp. 931-932.

Sundstrom, D.W., Klei, H.E., Nalette, T.A., Reidy, D.J., Weir, B.A. (1986) 'Destruction of halogenated aliphatics by ultraviolet catalyzed oxidation with hydrogen peroxide', *Hazardous Waste & Hazardous Materials*, vol. 3, no. 1, pp. 101-110.

Swords, C. and Strange, J. (2006) 'Active containment system for a former industrial site in East London', *Engineering Geology*, vol. 85, no. 1-2, May, pp. 204-211.

U.S. EPA (2001) *EPCRA - Section 313: Guidance for reporting toxic chemicals: Polycyclic aromatic compounds category*, Washington: Office of Environmental Information.

U.S. EPA (2008) *Polycyclic aromatic hydrocarbons (PAHs)*, January, [Online], Available: <http://www.epa.gov/osw/hazard/wastemin/priority.htm> [27 January 2013].

Venkatadri, R. and Peters, R.W. (1993) 'Chemical oxidation technologies: Ultraviolet light/hydrogen peroxide, Fenton's reagent and titanium dioxide-assisted photocatalysis', *Hazardous Waste & Hazardous Materials*, vol. 10, no. 2, pp. 107-150.

Waldemer, R.H. and Tratnyek, P.G. (2006) 'Kinetics of contaminant degradation by permanganate', *Environmental Science & Technology*, vol. 40, no. 3, pp. 1055-1061.

Watts, R.J. and Teel, A.L. (2005) 'Chemistry of modified Fenton's reagent (catalyzed H₂O₂ propagations-CHP) for in situ soil and groundwater remediation', *Journal of Environmental Engineering*, vol. 141, no. 4, April, pp. 612-622.

Weavers, L.K., Ling, F.H., Hoffmann, M.R. (1998) 'Aromatic compound degradation in water using a combination of sonolysis and ozonolysis', *Environmental Science & Technology*, vol. 32, no. 18, pp. 2727-2733.

Weir, B.A., Sundstrom, D.W., Klei, H.E. (1987) 'Destruction of benzene by ultraviolet light-catalyzed oxidation with hydrogen peroxide', *Hazardous Waste & Hazardous Materials*, vol. 4, no. 2, pp. 165-176.

Wilcke, W. (2000) 'Polycyclic aromatic hydrocarbon (PAHs) in soil – A review', *Journal of Plant Nutrition and Soil Science*, vol. 163, no. 2, pp. 229-248.

Woodhead, J.R., Law, J.R., Matthiessen, P. (1999) 'Polycyclic aromatic hydrocarbons (PAH) in marine sediments around England and Wales and their possible biological significance', *Marine Pollution Bulletin*, vol. 38, no. 9, pp. 773-790.

Xie, B., Lv, Z., Lv, B.Y., Gu, Y.X. (2010) 'Treatment of mature landfill leachate by biofilters and Fenton oxidation', *Waste Management*, vol. 30, no. 11, November, pp. 2108-2112.

Yan, Y.E. and Schwartz, F.W. (1999) 'Oxidative degradation and kinetics of chlorinated ethylenes by potassium permanganate', *Journal of Contaminant Hydrology*, vol. 37, no. 3-4, April, pp. 343-365.

Zhang, L., Li, P., Gong, Z., Li, X. (2008) 'Photocatalytic degradation of polycyclic aromatic hydrocarbons on soil surfaces using TiO₂ under UV light', *Journal of Hazardous Materials*, vol. 158, no. 2-3, October, pp. 478-484.

Zhang, Y. and Tao, S. (2009) 'Global atmospheric emission inventory of polycyclic aromatic hydrocarbons (PAHs) for 2004', *Atmospheric Environment*, no. 43, pp. 812-819.

Zhao, X., Cheng, K., Hao, J., Liu, D. (2008) 'Preparation of peracetic acid from hydrogen peroxide, part II: Kinetics for spontaneous decomposition of peracetic acid in the liquid phase', *Journal of Molecular Catalysis A: Chemical*, vol. 284, no. 1-2, April, pp. 58-68.

Zhao, X., Zhang, T., Zhou, Y., Liu, D. (2007) 'Preparation of peracetic acid from hydrogen peroxide: Part I: Kinetics for peracetic acid synthesis and hydrolysis', *Journal of Molecular Catalysis A: Chemical*, vol. 271, no. 1-2, June, pp. 246-252.

APPENDICES

Appendix A: ABBREVIATIONS

Abbreviation	Definition
°C	degrees Celsius
$\cdot\text{CH}_3$	methyl radical
A	pre-exponential factor, units same as k
AOP	advanced oxidation process
C	concentration
C=C	carbon-carbon double bond
C_0	concentration at time $t = 0$
CB	conduction band
$\text{CH}_3\text{COO}\cdot$	acycloxy radical
CH_3COOH	acetic acid
CH_3COOOH	peracetic acid
CO	carbon monoxide
CO_2	carbon dioxide
DBP	disinfection by-product
DF	dilution factor
DI H_2O	nano-pure deionized water
DNAPL	dense non-aqueous phase liquid
e^-	electron
E_a	activation energy in kJ mol^{-1} ;
Fe(II)- H_2O_2	Fenton's reagent
Fe^{2+}	ferrous iron
Fe^{3+}	ferric iron
FID	flame ionization detector
g	grams
GC	gas chromatograph
H^+	hydrogen ion, proton
h^+	electron hole
H_2O	water
H_2O_2	hydrogen peroxide

H_2SO_4	sulfuric acid
HO^-	hydroxide ion
HO^+	hydroxyl cation
HO^\bullet	hydroxyl radical
HO_2^-	hydroperoxide anion
HO_2^\bullet	hydroperoxide radical
HOC	hydrophobic organic contaminants
HOO^\bullet	hydroperoxy radical
hrs	hours
J	joule, $1 \text{ kg m}^2 \text{ s}^{-2}$
k	rate constant (s^{-1} or hr^{-1})
K	kelvin
kHz	kilohertz
KI	potassium iodide
kJ	kilojoule
KMnO_4	potassium permanganate
L	liters
M	molarity, mol L^{-1}
m	mass at time = t
m_0	initial mass, at $t = 0$
mg	milligrams
MGP	manufactured gas plants
mL	milliliters
MnO_2	manganese dioxide
MnO_4^-	permanganate
MnSO_4	manganese sulfate
mol	mole
MW	molecular weight
MW	molecular weight
N	normality, $\text{mol equivalents L}^{-1}$
$\text{Na}_2\text{C}_2\text{O}_4$	sodium oxalate

$\text{Na}_2\text{S}_2\text{O}_3$	sodium thiosulfate
Na_2SO_4	sodium sulfate
NaSO_3	sodium sulfite
nm	nanometer
O^\bullet	monatomic oxygen
O_2	molecular oxygen
$\text{O}_2^{\bullet-}$	superoxide radical anion
O_3	ozone
$\text{O}_3^{\bullet-}$	ozone radical anion
OC	organic carbon
OM	organic matter
PAA	peracetic acid
PAA	peracetic acid
PAH	polycyclic aromatic hydrocarbon
PM	particulate matter
R	alkane or alkyl group
R	universal gas constant, $\text{J K}^{-1} \text{mol}^{-1}$
R^\bullet	organic radical
R^\bullet	alkane or alkyl group radical
SOM	soil organic matter
S_w	solubility in water
t	time
T	temperature
T_b	boiling point
TDS	total dissolved solids
t_f	final time
t_i	initial time
TiO_2	titanium dioxide
T_m	melting point
US EPA	US Environmental Protection Agency
UV	ultraviolet

VB	valence band
v_p	vapor pressure
wt. %	weight percent
Δt	change in time
μg	microgram
μL	microliter
μm	micrometer

Appendix B: PAH CALIBRATION INFORMATION

Appendix B.1: Calibration Standards and Calibration Curve for anthracene.

Table B.1. Anthracene standard concentrations and standard curve area count.

Anthracene (06/21/2011)	
Concentration (mg/L)	Area
10.46	14243.0
20.12	27593.5
60.00	82764.0
100.60	138707.0
160.96	220697.0
201.20	277730.0

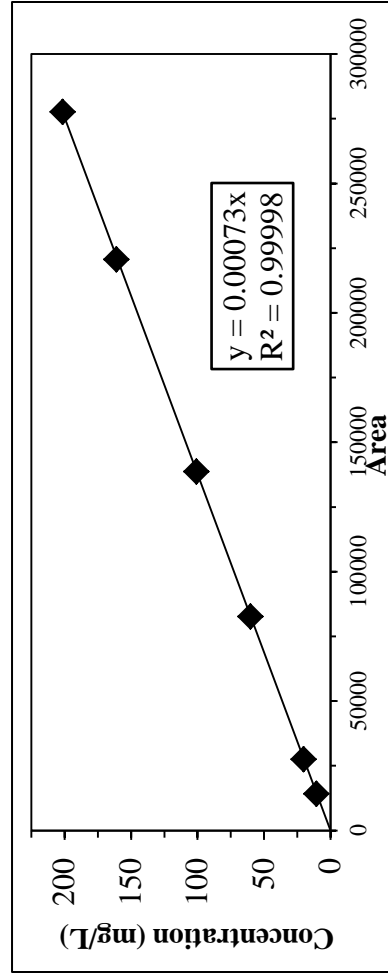


Figure B.1. Sample anthracene calibration curve.

Appendix B.2: Calibration Standards and Calibration Curve for benzo[a]pyrene.

Table B.2. Benzo[a]pyrene standard concentrations and standard curve area count.

Benzo[a]pyrene (07/18/2011)	
Concentration (mg/L)	Area
10.46	11878.0
20.12	23734.0
60.36	70633.0
100.60	121311.0
160.96	205133.0
201.12	240450.0

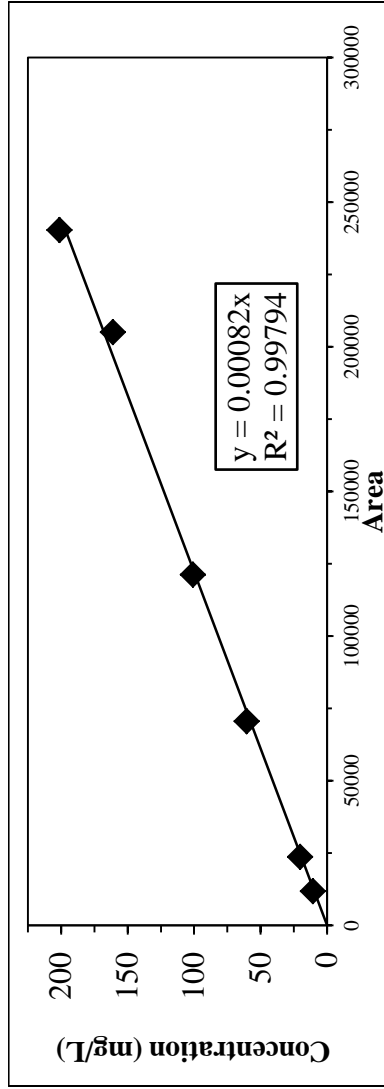


Figure B.2. Sample benzo[a]pyrene calibration curve.

Appendix B.3: Calibration Standards and Calibration Curve for phenanthrene.

Table B.3. Phenanthrene standard concentrations and standard curve area count.

Phenanthrene (07/29/2011)	
Concentration (mg/L)	Area
10.12	14562.0
20.24	29765.5
50.60	74180.5
101.20	148689.0
151.80	226550.0
202.40	304762.0

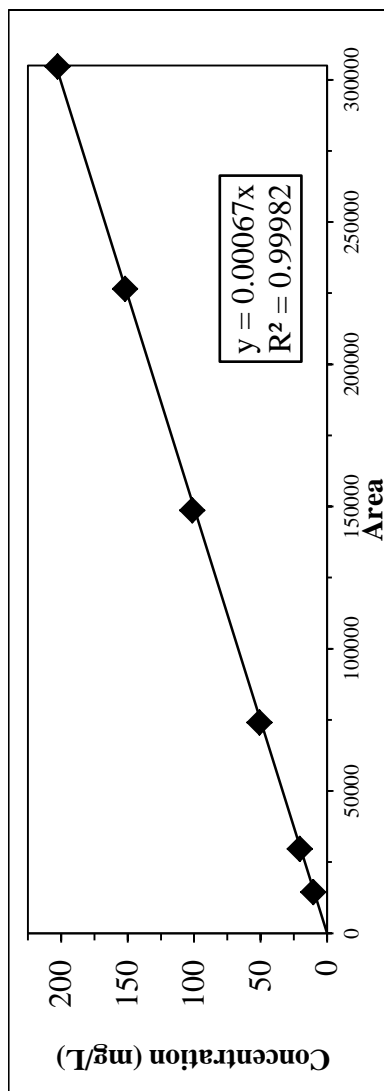


Figure B.3. Sample phenanthrene calibration curve.

Appendix B.4: Calibration Standards and Calibration Curve for pyrene.

Table B.4. Pyrene standard concentrations and standard curve area count.

Pyrene (07/11/2011)	
Concentration (mg/L)	Area
10.40	15595.5
20.00	29312.0
60.00	85846.5
100.20	141438.0
160.30	243959.0
200.40	284874.0

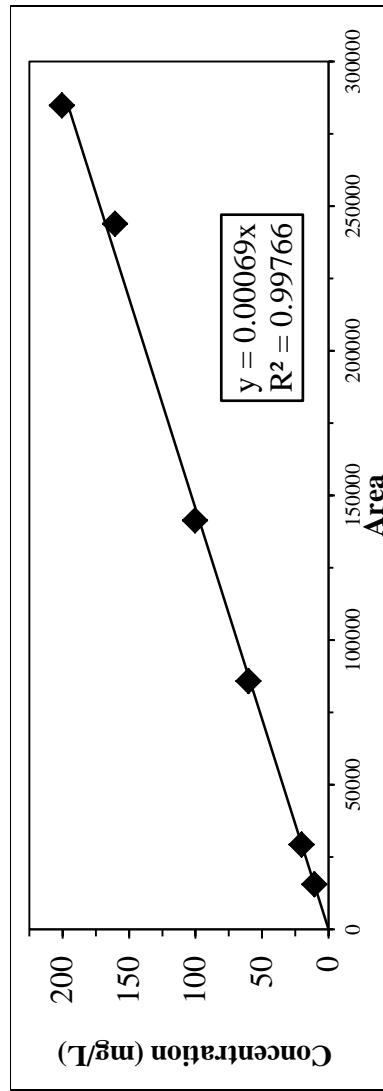


Figure B.4. Sample pyrene calibration curve.

Appendix B.5: 100 μL pipet calibrations for anthracene experiments.

Table B.5. Pipet calibration for anthracene experiments, $T = 25\text{ }^{\circ}\text{C}$.

Stock Solution (mg/L)	DI Water (mL)	m_0 (mg)
5010	0.1020	0.5054
	0.1008	
	0.1003	
	0.1001	
	0.1008	
	0.1003	
	0.1014	
	0.1004	
	0.1018	
	0.1008	
Average =	0.1009	
$m_0 = \text{mass of PAH added from } 100\text{ }\mu\text{L stock}$		

Table B.6. Pipet calibration for anthracene experiments, $T = 32\text{ }^{\circ}\text{C}$.

Stock Solution (mg/L)	DI Water (mL)	m_0 (mg)
5090	0.1015	0.5127
	0.1007	
	0.0990	
	0.0995	
	0.1024	
	0.1013	
	0.1009	
	0.1020	
	0.1005	
	0.0994	
Average =	0.1007	
$m_0 = \text{mass of PAH added from } 100\text{ }\mu\text{L stock}$		

Table B.7. Pipet calibration for anthracene experiments, $T = 40\text{ }^{\circ}\text{C}$.

Stock Solution (mg/L)	DI Water (mL)	m_0 (mg)
5090	0.1008	0.5098
	0.0993	
	0.1014	
	0.0995	
	0.0980	
	0.1014	
	0.1011	
	0.0993	
	0.1007	
	0.1001	
Average =	0.1002	
$m_0 = \text{mass of PAH added from } 100\text{ }\mu\text{L stock}$		

Appendix B.6: 100 μL pipet calibrations for benzo[a]pyrene experiments.

Table B.8. Pipet calibration for benzo[a]pyrene experiments, $T = 25\text{ }^{\circ}\text{C}$.

Stock Solution (mg/L)	DI Water (mL)	m_0 (mg)
4999	0.1004	0.5025
	0.1012	
	0.1001	
	0.1011	
	0.0992	
	0.1016	
	0.1008	
	0.0989	
	0.1011	
	0.1000	
	0.1010	
	0.1008	
	0.1010	
	0.1017	
	0.1007	
0.1004		
0.1000		
0.1000		
0.0990		
0.1010		
0.1008		
Average =		
$m_0 =$ mass of PAH added from 100 μL stock		

Table B.9. Pipet calibration for benzo[a]pyrene experiments, $T = 32\text{ }^{\circ}\text{C}$.

Stock Solution (mg/L)	DI Water (mL)	m_0 (mg)
5060	0.0999	0.5084
	0.0997	
	0.0995	
	0.1000	
	0.1005	
	0.1022	
	0.1012	
	0.1002	
	0.1008	
	0.1008	
	0.1005	
Average =		
$m_0 =$ mass of PAH added from 100 μL stock		

Table B.10. Pipet calibration for benzo[a]pyrene experiments, $T = 40\text{ }^{\circ}\text{C}$.

Stock Solution (mg/L)	DI Water (mL)	m_0 (mg)
5060	0.1008	0.5068
	0.0993	
	0.1014	
	0.0995	
	0.0980	
	0.1014	
	0.1011	
	0.0993	
	0.1007	
	0.1001	
	0.1002	
Average =		
$m_0 =$ mass of PAH added from 100 μL stock		

Appendix B.7: 100 μL pipet calibrations for phenanthrene experiments.

Table B.11. Pipet calibration for phenanthrene experiments, $T = 25\text{ }^{\circ}\text{C}$.

Stock Solution (mg/L)	DI Water (mL)	m_0 (mg)
5030	0.1007	0.5064
	0.1013	
	0.1006	
	0.0995	
	0.1012	
	0.1000	
	0.1014	
	0.1009	
	0.1008	
	0.1003	
	Average = 0.1007	
$m_0 = \text{mass of PAH added from } 100\text{ }\mu\text{L stock}$		

Table B.12. Pipet calibration for phenanthrene experiments, $T = 32\text{ }^{\circ}\text{C}$.

Stock Solution (mg/L)	DI Water (mL)	m_0 (mg)
5080	0.1002	0.5108
	0.1025	
	0.1004	
	0.0992	
	0.1005	
	0.1010	
	0.1033	
	0.1005	
	0.0990	
	0.0989	
	Average = 0.1006	
$m_0 = \text{mass of PAH added from } 100\text{ }\mu\text{L stock}$		

Table B.13. Pipet calibration for phenanthrene experiments, $T = 40\text{ }^{\circ}\text{C}$.

Stock Solution (mg/L)	DI Water (mL)	m_0 (mg)		
5080	0.0992	0.5097		
	0.0996			
	0.1007			
	0.1007			
	0.1000			
	0.1012			
	0.1006			
	0.1006			
	Average = 0.1003			
	$m_0 = \text{mass of PAH added from } 100\text{ }\mu\text{L stock}$			

Appendix B.8: 100 μL pipet calibrations for pyrene experiments.

Table B.14. Pipet calibration for pyrene experiments, $T = 25\text{ }^{\circ}\text{C}$.

Stock Solution (mg/L)	DI Water (mL)	m_0 (mg)
5040	0.0992	0.5060
	0.0995	
	0.1009	
	0.1002	
	0.1001	
	0.1012	
	0.0991	
	0.1010	
	0.1005	
	0.1023	
	0.1004	
Average ^a =		
Calibration for all exp. times, except $t = 2$ hr.		
5100	0.1031	0.5145
	0.1005	
	0.1003	
	0.1013	
	0.0992	
	0.1009	
Average ^b =		
Calibration for all controls and exp. $t = 2$ hr.		
$m_0 =$ mass of PAH added from 100 μL stock		

Table B.15. Pipet calibration for pyrene experiments, $T = 32\text{ }^{\circ}\text{C}$.

Stock Solution (mg/L)	DI Water (mL)	m_0 (mg)
5040	0.0996	0.5081
	0.1005	
	0.1010	
	0.1022	
	0.1018	
	0.1020	
	0.1001	
	0.0995	
	0.1005	
	0.1009	
	0.1008	
Average =		
$m_0 =$ mass of PAH added from 100 μL stock		

Table B.16. Pipet calibration for pyrene experiments, $T = 40\text{ }^{\circ}\text{C}$.

Stock Solution (mg/L)	DI Water (mL)	m_0 (mg)
5040	0.1008	0.5050
	0.0993	
	0.1014	
	0.0995	
	0.0980	
	0.1014	
	0.1014	
	0.0993	
	0.1007	
	0.1001	
	0.1002	
Average =		
$m_0 =$ mass of PAH added from 100 μL stock		

Appendix C: GAS CHROMATOGRAPHY OVEN METHODS

Appendix C.4: Gas chromatography method for pyrene.

GC-17A

Method: Pyrene-10-16-12.met

Over Parameters	
Max Temperature:	320 C
Equilibration Time:	1.0 min

Rate (C/min)	Temp (C)	Wait (min)
1 Initial	170	1.0
2	300	3.0
3		

Isothermal Zone Temperatures		
Zone	Set	Max
Injector:	317 C	350 C
Detector:	317 C	350 C
Aux 1:	280 C	350 C
Aux 2:		
Aux 3:		
Aux 4:		
Aux 5:		

Total Over Temperature Program Time: 10.5 min

Pyrene Retention Time: 6.36 min

Figure C.4. Sample pyrene gas chromatography oven method.

Appendix D: PAH DEGRADATION STUDIES

Table D.1.1. Anthracene degradation at T = 25 °C, experimental set-up.

				m ₀ = 0.5054 mg		Error Bar Calculations										
				Hexane Extraction		m/m ₀ avg					m/m ₀ avg					
Sample Id	Rep	Conc (mg/L)	Δ Time (hr)	m (mg)	m/m ₀	m/m ₀ avg	Std Dev	Std Error	In(m/m ₀)	m/m ₀ avg	Std Dev	Std Error	In(m/m ₀)	m/m ₀ avg	Std Dev	Std Error
Exp t=0 A	1	45.202	0.017	0.4520	0.8945	0.9022	0.0103	0.0051	-0.1115	-0.1030	0.0114	0.0057	-0.1138	-0.0960	0.0057	0.0057
Exp t=0 A	2	45.100		0.4510	0.8924				-0.1138							
Exp t=0 B	1	46.154		0.4615	0.9133				-0.0907							
Exp t=0 B	2	45.908		0.4591	0.9084				-0.0960							
Exp t=1 A	1	46.036	1.283	0.4604	0.9110	0.9137	0.0096	0.0048	-0.0933	-0.0903	0.0105	0.0053	-0.1034	-0.0787	0.0053	0.0053
Exp t=1 A	2	45.572		0.4557	0.9018				-0.1034							
Exp t=1 B	1	46.710		0.4671	0.9243				-0.0787							
Exp t=1 B	2	46.373		0.4637	0.9176				-0.0860							
Exp t=2 A	1	45.864	2.117	0.4586	0.9076	0.9069	0.0011	0.0006	-0.0970	-0.0977	0.0012	0.0006	-0.0994	-0.0978	0.0006	0.0006
Exp t=2 A	2	45.753		0.4575	0.9054				-0.0994							
Exp t=2 B	1	45.828		0.4583	0.9068				-0.0978							
Exp t=2 B	2	45.879		0.4588	0.9079				-0.0967							
Exp t=4 A	1	45.120	4.000	0.4512	0.8928	0.8959	0.0055	0.0028	-0.1134	-0.1100	0.0062	0.0031	-0.1164	-0.1024	0.0031	0.0031
Exp t=4 A	2	44.982		0.4498	0.8901				-0.1164							
Exp t=4 B	1	45.615		0.4562	0.9026				-0.1024							
Exp t=4 B	2	45.375		0.4538	0.8979				-0.1077							
Exp t=6 A	1	43.519	6.000	0.4352	0.8612	0.8567	0.0037	0.0018	-0.1495	-0.1547	0.0043	0.0021	-0.1578	-0.1528	0.0021	0.0021
Exp t=6 A	2	43.159		0.4316	0.8540				-0.1578							
Exp t=6 B	1	43.374		0.4337	0.8583				-0.1528							
Exp t=6 B	2	43.128		0.4313	0.8534				-0.1585							
Exp t=12 A	1	44.004	12.000	0.4400	0.8707	0.8659	0.0120	0.0060	-0.1384	-0.1440	0.0139	0.0069	-0.1271	-0.1535	0.0069	0.0069
Exp t=12 A	2	44.506		0.4451	0.8807				-0.1271							
Exp t=12 B	1	43.344		0.4334	0.8577				-0.1535							
Exp t=12 B	2	43.192		0.4319	0.8547				-0.1570							
Exp t=18 A	1	38.804	18.000	0.3880	0.7679	0.7680	0.0053	0.0027	-0.2642	-0.2639	0.0069	0.0035	-0.2736	-0.2600	0.0035	0.0035
Exp t=18 A	2	38.439		0.3844	0.7606				-0.2736							
Exp t=18 B	1	39.044		0.3904	0.7726				-0.2580							
Exp t=18 B	2	38.967		0.3897	0.7711				-0.2600							
Exp t=24 A	1	35.486	24.000	0.3549	0.7022	0.6951	0.0090	0.0045	-0.3535	-0.3637	0.0130	0.0065	-0.3529	-0.3798	0.0065	0.0065
Exp t=24 A	2	35.508		0.3551	0.7026				-0.3529							
Exp t=24 B	1	34.565		0.3457	0.6840				-0.3798							
Exp t=24 B	2	34.955		0.3496	0.6917				-0.3686							

Table D.2. Anthracene degradation at T = 25 °C, all control set-ups.

Sample Id	Rep	Conc (ng/L)	Δ Time (hr)	$m_0 = 0.5054 \text{ mg}$			Error Bar Calculations					
				Hexane Extraction			m/m ₀ a vg					
				m (mg)	m/m ₀	m/m ₀ avg	Std Dev	Std Error	In (m/m ₀)	m/m ₀ a vg	Std Dev	Std Error
DI t=0 A	1	46.961	0.050	0.4696	0.9293	0.8960	0.0409	0.0204	-0.0734	-0.1106	0.0456	0.0228
DI t=0 A	2	47.171		0.4717	0.9334		-0.0689					
DI t=0 B	1	43.425		0.4343	0.8593		-0.1516					
DI t=0 B	2	43.561	0.4356	0.8620	-0.1485							
DI t=6 A	1	51.584	6.000	0.5158	1.0207	0.9287	0.1049	0.0525	0.0205	-0.0788	0.1133	0.0567
DI t=6 A	2	51.486		0.5147	1.0184		0.0182					
DI t=6 B	1	42.368		0.4237	0.8384		-0.1763					
DI t=6 B	2	42.317	0.4232	0.8374	-0.1775							
DI t=24 A	1	43.088	24.000	0.4307	0.8522	0.8716	0.0163	0.0081	-0.1599	-0.1376	0.0187	0.0093
DI t=24 A	2	43.672		0.4367	0.8642		-0.1460					
DI t=24 B	1	44.656		0.4466	0.8836		-0.1237					
DI t=24 B	2	44.791	0.4479	0.8863	-0.1207							
AA t=0 A	1	48.584	0.017	0.4858	0.9614	0.9234	0.0407	0.0204	-0.0394	-0.0804	0.0448	0.0224
AA t=0 A	2	43.747		0.4375	0.8657		-0.1443					
AA t=0 B	1	47.140		0.4714	0.9328		-0.0696					
AA t=0 B	2	47.198	0.4720	0.9340	-0.0683							
AA t=6 A	1	44.632	6.000	0.4463	0.8832	0.8917	0.0107	0.0054	-0.1242	-0.1147	0.0120	0.0060
AA t=6 A	2	44.574		0.4457	0.8820		-0.1255					
AA t=6 B	1	45.396		0.4540	0.8983		-0.1073					
AA t=6 B	2	45.650	0.4565	0.9033	-0.1017							
AA t=24 A	1	46.441	24.000	0.4644	0.9190	0.9405	0.0155	0.0077	-0.0845	-0.0615	0.0165	0.0083
AA t=24 A	2	47.628		0.4763	0.9425		-0.0593					
AA t=24 B	1	48.303		0.4830	0.9558		-0.0452					
AA t=24 B	2	47.743	0.4774	0.9447	-0.0569							
H2O2 t=0 A	1	50.930	0.017	0.5093	1.0078	1.0014	0.0185	0.0092	0.0078	0.0013	0.0186	0.0093
H2O2 t=0 A	2	50.927		0.5093	1.0077		0.0077					
H2O2 t=0 B	1	51.336		0.5134	1.0158		0.0157					
H2O2 t=0 B	2	49.235	0.4924	0.9743	-0.0261							
H2O2 t=6 A	1	51.933	6.000	0.5193	1.0276	0.9903	0.0302	0.0151	0.0273	-0.0100	0.0303	0.0152
H2O2 t=6 A	2	48.597		0.4860	0.9616		-0.0391					
H2O2 t=6 B	1	49.050		0.4905	0.9706		-0.0298					
H2O2 t=6 B	2	50.612	0.5061	1.0015	0.0015							
H2O2 t=24 A	1	53.148	24.000	0.5315	1.0517	0.9945	0.0872	0.0436	0.0504	-0.0086	0.0917	0.0459
H2O2 t=24 A	2	43.721		0.4372	0.8651		-0.1449					
H2O2 t=24 B	1	51.534		0.5153	1.0198		0.0196					
H2O2 t=24 B	2	52.619	0.5262	1.0412	0.0404							

Table D.3. Anthracene degradation at T = 32 °C, experimental set-up.

				$m_0 = 0.5127$ mg								
				Hexane Extraction								
Sample Id	Rep	Conc (mg/L)	Δ Time (hr)	m (mg)	m/ m_0	m/ m_0 avg	Error Bar Calculations					
							Std Dev	Std Error	In(m/ m_0)	m/ m_0 avg	Std Dev	Std Error
Exp t=0 A	1	44.863	0.000	0.4486	0.8751	0.8943	0.0168	0.0084	-0.1334	-0.1118	0.0188	0.0094
Exp t=0 A	2	45.422		0.4542	0.8860				-0.1210			
Exp t=0 B	1	46.743		0.4674	0.9118				-0.0924			
Exp t=0 B	2	46.369		0.4637	0.9045				-0.1004			
Exp t=1 A	1	46.309	1.000	0.4631	0.9033	0.8872	0.0175	0.0087	-0.1017	-0.1199	0.0198	0.0099
Exp t=1 A	2	44.261		0.4426	0.8634				-0.1469			
Exp t=1 B	1	45.402		0.4540	0.8856				-0.1215			
Exp t=1 B	2	45.956		0.4596	0.8964				-0.1094			
Exp t=2 A	1	44.270	2.000	0.4427	0.8635	0.8415	0.0379	0.0189	-0.1467	-0.1734	0.0449	0.0225
Exp t=2 A	2	45.293		0.4529	0.8835				-0.1239			
Exp t=2 B	1	41.436		0.4144	0.8082				-0.2129			
Exp t=2 B	2	41.560		0.4156	0.8107				-0.2099			
Exp t=4 A	1	43.973	4.033	0.4397	0.8577	0.8591	0.0065	0.0032	-0.1535	-0.1519	0.0075	0.0038
Exp t=4 A	2	43.637		0.4364	0.8512				-0.1611			
Exp t=4 B	1	44.436		0.4444	0.8668				-0.1430			
Exp t=4 B	2	44.119		0.4412	0.8606				-0.1501			
Exp t=6 A	1	43.165	6.000	0.4317	0.8420	0.8360	0.0092	0.0046	-0.1720	-0.1792	0.0111	0.0056
Exp t=6 A	2	42.157		0.4216	0.8223				-0.1956			
Exp t=6 B	1	42.976		0.4298	0.8383				-0.1764			
Exp t=6 B	2	43.128		0.4313	0.8413				-0.1729			
Exp t=12 A	1	38.829	11.983	0.3883	0.7574	0.7483	0.0101	0.0051	-0.2779	-0.2901	0.0135	0.0068
Exp t=12 A	2	37.690		0.3769	0.7352				-0.3076			
Exp t=12 B	1	38.223		0.3822	0.7456				-0.2936			
Exp t=12 B	2	38.704		0.3870	0.7550				-0.2811			
Exp t=18 A	1	35.829	18.017	0.3583	0.6989	0.6920	0.0075	0.0037	-0.3583	-0.3682	0.0108	0.0054
Exp t=18 A	2	35.107		0.3511	0.6848				-0.3786			
Exp t=18 B	1	35.783		0.3578	0.6980				-0.3596			
Exp t=18 B	2	35.183		0.3518	0.6863				-0.3765			
Exp t=24 A	1	28.919	24.000	0.2892	0.5641	0.5543	0.0123	0.0061	-0.5725	-0.5902	0.0222	0.0111
Exp t=24 A	2	28.962		0.2896	0.5649				-0.5711			
Exp t=24 B	1	27.678		0.2768	0.5399				-0.6164			
Exp t=24 B	2	28.118		0.2812	0.5485				-0.6006			

Table D.4. Anthracene degradation at T = 32 °C, all control set-ups.

Sample Id	Rep	Conc (ng/L)	Δ Time (hr)	$m_0 = 0.5127$ mg			Error Bar Calculations								
				Hexane Extraction			m/m ₀ a vg								
				m (mg)	m/m ₀	m/m ₀ avg	Std Dev	Std Error	In (m/m ₀)	m/m ₀ a vg	Std Dev	Std Error			
DI t=0 A	1	46.961		0.4696	0.9160										
DI t=0 A	2	47.171	0.000	0.4717	0.9201	0.8832	0.0403	0.0201	-0.0877	-0.1250	0.0456	0.0228			
DI t=0 B	1	43.425		0.4343	0.8470				-0.0833						
DI t=0 B	2	43.561		0.4356	0.8497				-0.1660						
DI t=6 A	1	51.584		0.5158	1.0062				-0.1629						
DI t=6 A	2	51.486	6.017	0.5147	1.0039	0.9155	0.1034	0.0517	0.0062	-0.0931	0.1133	0.0567			
DI t=6 B	1	42.368		0.4237	0.8264				0.0039						
DI t=6 B	2	42.317		0.4232	0.8254				-0.1906						
DI t=24 A	1	43.088		0.4307	0.8401				-0.1918						
DI t=24 A	2	43.672	24.000	0.4367	0.8519	0.8592	0.0160	0.0080	-0.1743	-0.1519	0.0187	0.0093			
DI t=24 B	1	44.656		0.4466	0.8711				-0.1603						
DI t=24 B	2	44.791		0.4479	0.8737				-0.1380						
AA t=0 A	1	48.584		0.4858	0.9477				-0.1350						
AA t=0 A	2	43.747	0.000	0.4375	0.8533	0.9103	0.0401	0.0201	-0.0537	-0.0947	0.0448	0.0224			
AA t=0 B	1	47.140		0.4714	0.9195				-0.1586						
AA t=0 B	2	47.198		0.4720	0.9206				-0.0839						
AA t=6 A	1	44.632		0.4463	0.8706				-0.0827						
AA t=6 A	2	44.574	6.017	0.4457	0.8695	0.8790	0.0106	0.0053	-0.1386	-0.1290	0.0120	0.0060			
AA t=6 B	1	45.396		0.4540	0.8855				-0.1399						
AA t=6 B	2	45.650		0.4565	0.8904				-0.1216						
AA t=24 A	1	46.441		0.4644	0.9059				-0.1160						
AA t=24 A	2	47.628	24.017	0.4763	0.9290	0.9271	0.0153	0.0076	-0.0989	-0.0758	0.0165	0.0083			
AA t=24 B	1	48.303		0.4830	0.9422				-0.0736						
AA t=24 B	2	47.743		0.4774	0.9313				-0.0595						
H2O2 t=0 A	1	50.930		0.5093	0.9934				-0.0712						
H2O2 t=0 A	2	50.927	0.000	0.5093	0.9934	0.9871	0.0182	0.0091	-0.0066	-0.0131	0.0186	0.0093			
H2O2 t=0 B	1	51.336		0.5134	1.0014				-0.0066						
H2O2 t=0 B	2	49.235		0.4924	0.9604				0.0014						
H2O2 t=6 A	1	51.933		0.5193	1.0130				-0.0404						
H2O2 t=6 A	2	48.597	6.033	0.4860	0.9479	0.9762	0.0297	0.0149	0.0129	-0.0244	0.0303	0.0152			
H2O2 t=6 B	1	49.050		0.4905	0.9668				-0.0535						
H2O2 t=6 B	2	50.612		0.5061	0.9872				-0.0442						
H2O2 t=24 A	1	53.148		0.5315	1.0367				-0.0128						
H2O2 t=24 A	2	43.721	24.000	0.4372	0.8528	0.9803	0.0860	0.0430	0.0360	-0.0230	0.0917	0.0459			
H2O2 t=24 B	1	51.534		0.5153	1.0052				-0.1592						
H2O2 t=24 B	2	52.619		0.5262	1.0264				0.0052						

Table D.5. Anthracene degradation at T = 40 °C, experimental set-up.

				m ₀ = 0.5098 mg		Error Bar Calculations							
				Hexane Extraction		Std Error		m/m ₀ avg		Std Dev		Std Error	
Sample Id	Rep	Conc (mg/L)	Δ Time (hr)	m (mg)	m/m ₀	Std Error	m/m ₀ avg	Std Error	m/m ₀ avg	Std Dev	Std Error	Std Error	Std Error
Exp t=0 A	1	46.300	0.017	0.4630	0.9082	0.0090	0.9243	0.0179	-0.0789	0.0194	0.0097	-0.0963	
Exp t=0 A	2	46.368		0.4637	0.9095							-0.0949	
Exp t=0 B	1	47.799		0.4780	0.9376							-0.0645	
Exp t=0 B	2	48.018		0.4802	0.9419							-0.0599	
Exp t=1 A	1	47.261	1.050	0.4726	0.9270	0.0067	0.9390	0.0133	-0.0630	0.0141	0.0071	-0.0758	
Exp t=1 A	2	47.413		0.4741	0.9300							-0.0726	
Exp t=1 B	1	48.078		0.4808	0.9430							-0.0586	
Exp t=1 B	2	48.740		0.4874	0.9560							-0.0450	
Exp t=2 A	1	44.106	2.017	0.4411	0.8651	0.0082	0.8658	0.0164	-0.1443	0.0191	0.0095	-0.1449	
Exp t=2 A	2	42.972		0.4297	0.8429							-0.1709	
Exp t=2 B	1	44.831		0.4483	0.8794							-0.1286	
Exp t=2 B	2	44.645		0.4465	0.8757							-0.1327	
Exp t=4 A	1	42.220	4.017	0.4222	0.8281	0.0046	0.8219	0.0092	-0.1962	0.0112	0.0056	-0.1886	
Exp t=4 A	2	42.234		0.4223	0.8284							-0.1882	
Exp t=4 B	1	41.920		0.4192	0.8223							-0.1957	
Exp t=4 B	2	41.234		0.4123	0.8088							-0.2122	
Exp t=6 A	1	35.727	6.017	0.3573	0.7008	0.0167	0.7332	0.0334	-0.3111	0.0455	0.0227	-0.3556	
Exp t=6 A	2	36.205		0.3621	0.7102							-0.3423	
Exp t=6 B	1	39.338		0.3934	0.7716							-0.2593	
Exp t=6 B	2	38.249		0.3825	0.7503							-0.2873	
Exp t=12 A	1	23.095	12.000	0.2310	0.4530	0.0170	0.4314	0.0339	-0.8430	0.0786	0.0393	-0.7918	
Exp t=12 A	2	23.837		0.2384	0.4676							-0.7602	
Exp t=12 B	1	20.375		0.2038	0.3997							-0.9172	
Exp t=12 B	2	20.673		0.2067	0.4055							-0.9026	
Exp t=18 A	1	4.113	18.083	0.0411	0.0807	0.0242	0.1209	0.0485	-2.1766	0.4184	0.2092	-2.5173	
Exp t=18 A	2	3.941		0.0394	0.0773							-2.5600	
Exp t=18 B	1	8.309		0.0831	0.1630							-1.8141	
Exp t=18 B	2	8.301		0.0830	0.1628							-1.8151	
Exp t=24 A	1	1.085	24.000	0.0109	0.0213	0.0022	0.0186	0.0044	-4.0048	0.2370	0.1185	-3.8499	
Exp t=24 A	2	1.192		0.0119	0.0234							-3.7558	
Exp t=24 B	1	0.743		0.0074	0.0146							-4.2285	
Exp t=24 B	2	0.776		0.0078	0.0152							-4.1851	

Table D.6. Anthracene degradation at T = 40 °C, all control set-ups.

Sample Id	Rep	Conc (mg/L)	Δ Time (hr)	m ₀ = 0.5098 mg		Error Bar Calculations					
				Hexane Extraction		m/m ₀ avg			m/m ₀ avg		
				m (mg)	m/m ₀	Std Dev	Std Error	In(m/m ₀)	Std Dev	Std Error	Std Error
DI t=0 A	1	42.119		0.4212	0.8282	0.8835	0.0822	0.0411	-0.1910	0.0912	0.0456
DI t=0 A	2	41.597	0.000	0.4160	0.8159				-0.2034		
DI t=0 B	1	45.780		0.4578	0.8980				-0.1076	-0.1270	
DI t=0 B	2	50.674		0.5067	0.9940				-0.0060		
DI t=6 A	1	48.725		0.4873	0.9557				-0.0453		
DI t=6 A	2	42.297	6.167	0.4230	0.8297	0.8679	0.0589	0.0294	-0.1867	-0.1433	0.0329
DI t=6 B	1	42.990		0.4299	0.8432				-0.1705		
DI t=6 B	2	42.979		0.4298	0.8430				-0.1708		
DI t=24 A	1	72.423		0.7242	1.4206				0.3511		
DI t=24 A	2	43.840	24.017	0.4384	0.8599	1.0287	0.2672	0.1336	-0.1509	0.0057	0.1191
DI t=24 B	1	49.838		0.4984	0.9776				-0.0227		
DI t=24 B	2	43.679		0.4368	0.8568				-0.1546		
AA t=0 A	1	39.194		0.3919	0.7688				-0.2629		
AA t=0 A	2	38.888	0.000	0.3889	0.7628	0.7674	0.0050	0.0025	-0.2708	-0.2648	0.0032
AA t=0 B	1	39.963		0.3896	0.7643				-0.2688		
AA t=0 B	2	39.448		0.3945	0.7738				-0.2565		
AA t=6 A	1	42.607		0.4261	0.8357				-0.1794		
AA t=6 A	2	43.328	6.167	0.4333	0.8499	0.8537	0.0138	0.0069	-0.1627	-0.1583	0.0081
AA t=6 B	1	44.102		0.4410	0.8651				-0.1450		
AA t=6 B	2	44.045		0.4405	0.8639				-0.1462		
AA t=24 A	1	41.747		0.4175	0.8189				-0.1998		
AA t=24 A	2	41.803	24.000	0.4180	0.8200	0.8341	0.0170	0.0085	-0.1985	-0.1816	0.0102
AA t=24 B	1	43.247		0.4325	0.8483				-0.1645		
AA t=24 B	2	43.298		0.4330	0.8493				-0.1634		
H2O2 t=0 A	1	44.558		0.4456	0.8740				-0.1347		
H2O2 t=0 A	2	44.754	0.000	0.4475	0.8778	0.8652	0.0125	0.0063	-0.1303	-0.1449	0.0072
H2O2 t=0 B	1	43.553		0.4355	0.8543				-0.1575		
H2O2 t=0 B	2	43.564		0.4356	0.8545				-0.1572		
H2O2 t=6 A	1	40.797		0.4080	0.8002				-0.2229		
H2O2 t=6 A	2	40.028	6.000	0.4003	0.7851	0.7933	0.0071	0.0036	-0.2419	-0.2316	0.0045
H2O2 t=6 B	1	40.696		0.4070	0.7983				-0.2253		
H2O2 t=6 B	2	40.252		0.4025	0.7895				-0.2363		
H2O2 t=24 A	1	40.853		0.4085	0.8013				-0.2215		
H2O2 t=24 A	2	39.496	24.017	0.3950	0.7747	0.8309	0.0508	0.0254	-0.2553	-0.1866	0.0307
H2O2 t=24 B	1	44.751		0.4475	0.8778				-0.1303		
H2O2 t=24 B	2	44.346		0.4435	0.8698				-0.1394		

Table D.7. Benzo[a]pyrene degradation at T = 25 °C, experimental set-up.

Sample Id		Rep		Conc (mg/L)		Δ Time (hr)		m ₀ = 0.5025 mg				Error Bar Calculations							
								Hexane Extraction				m/m ₀ avg				m/m ₀ avg			
								m (mg)	m/m ₀	m/m ₀ avg	Std Dev	Std Error	In (m/m ₀)	m/m ₀ avg	Std Dev	Std Error			
Exp t=0 A	1	47.001	0.4700	0.9354	0.9628	0.0365	0.0182	-0.0668	-0.0384	0.0379	0.0190								
Exp t=0 A	2	49.912	0.4991	0.9933				-0.0067											
Exp t=0 B	1	50.010	0.5001	0.9953				-0.0047											
Exp t=0 B	2	46.597	0.4660	0.9274				-0.0754											
Exp t=1 A	1	47.271	0.4727	0.9408				-0.0611											
Exp t=1 A	2	47.706	0.4771	0.9494	0.9713	0.0315	0.0157	-0.0519	-0.0295	0.0324	0.0162								
Exp t=1 B	1	50.619	0.5062	1.0074				0.0074											
Exp t=1 B	2	49.618	0.4962	0.9875				-0.0126											
Exp t=2 A	1	48.157	0.4816	0.9584				-0.0425											
Exp t=2 A	2	49.595	0.4960	0.9870	0.9596	0.0315	0.0158	-0.0131	-0.0416	0.0332	0.0166								
Exp t=2 B	1	46.017	0.4602	0.9158				-0.0879											
Exp t=2 B	2	49.103	0.4910	0.9772				-0.0230											
Exp t=4 A	1	46.355	0.4636	0.9225				-0.0806											
Exp t=4 A	2	48.006	0.4801	0.9554	0.9391	0.0138	0.0069	-0.0456	-0.0629	0.0147	0.0074								
Exp t=4 B	1	47.401	0.4740	0.9434				-0.0583											
Exp t=4 B	2	46.985	0.4699	0.9351				-0.0671											
Exp t=6 A	1	46.870	0.4687	0.9328				-0.0696											
Exp t=6 A	2	47.101	0.4710	0.9374	0.9211	0.0280	0.0140	-0.0647	-0.0825	0.0309	0.0154								
Exp t=6 B	1	46.986	0.4699	0.9351				-0.0671											
Exp t=6 B	2	44.179	0.4418	0.8792				-0.1287											
Exp t=12 A	1	44.472	0.4447	0.8851				-0.1221											
Exp t=12 A	2	43.684	0.4368	0.8694	0.8773	0.0064	0.0032	-0.1400	-0.1309	0.0073	0.0037								
Exp t=12 B	1	44.092	0.4409	0.8775				-0.1307											
Exp t=12 B	2	44.084	0.4408	0.8773				-0.1309											
Exp t=18 A	1	42.468	0.4247	0.8452				-0.1682											
Exp t=18 A	2	42.459	0.4246	0.8450	0.8401	0.0152	0.0076	-0.1684	-0.1744	0.0183	0.0091								
Exp t=18 B	1	42.824	0.4282	0.8523				-0.1599											
Exp t=18 B	2	41.091	0.4109	0.8178				-0.2012											
Exp t=24 A	1	39.903	0.3990	0.7941				-0.2305											
Exp t=24 A	2	41.377	0.4138	0.8235	0.7998	0.0344	0.0172	-0.1942	-0.2241	0.0436	0.0218								
Exp t=24 B	1	37.852	0.3785	0.7533				-0.2833											
Exp t=24 B	2	41.615	0.4162	0.8282				-0.1885											

Table D.8. Benzo[a]pyrene degradation at T = 25 °C, all control set-ups.

				m ₀ = 0.5025 mg								
				Hexane Extraction				Error Bar Calculations				
Sample Id	Rep	Conc (mg/L)	Δ Time (hr)	m (mg)	m/m ₀	m/m ₀ avg	Std Dev	Std Error	ln(m/m ₀)	m/m ₀ avg	Std Dev	Std Error
DI t=0 A	1	48.750	0.033	0.4875	0.9702	0.9899	0.0195	0.0098	-0.0302	-0.0103	0.0197	0.0099
DI t=0 A	2	50.336		0.5034	1.0018				0.0018			
DI t=0 B	1	50.793		0.5079	1.0109				0.0108			
DI t=0 B	2	49.070		0.4907	0.9766				-0.0237			
DI t=6 A	1	46.547	6.000	0.4655	0.9264	0.9419	0.0156	0.0078	-0.0765	-0.0599	0.0165	0.0083
DI t=6 A	2	46.780		0.4678	0.9310				-0.0715			
DI t=6 B	1	48.125		0.4813	0.9578				-0.0432			
DI t=6 B	2	47.863		0.4786	0.9526				-0.0486			
DI t=24 A	1	49.055	24.000	0.4906	0.9763	0.9517	0.0391	0.0195	-0.0240	-0.0501	0.0412	0.0206
DI t=24 A	2	49.826		0.4983	0.9916				-0.0084			
DI t=24 B	1	46.825		0.4683	0.9319				-0.0705			
DI t=24 B	2	45.575		0.4558	0.9070				-0.0976			
AA t=0 A	1	48.712	0.0167	0.4871	0.9694	0.9910	0.0368	0.0184	-0.0310	-0.0096	0.0371	0.0185
AA t=0 A	2	50.559		0.5056	1.0062				0.0062			
AA t=0 B	1	47.892		0.4789	0.9531				-0.0480			
AA t=0 B	2	52.009		0.5201	1.0351				0.0345			
AA t=6 A	1	51.795	6.0000	0.5180	1.0308	1.0329	0.0074	0.0037	0.0303	0.0323	0.0071	0.0036
AA t=6 A	2	51.463		0.5146	1.0242				0.0239			
AA t=6 B	1	51.992		0.5199	1.0347				0.0341			
AA t=6 B	2	52.350		0.5235	1.0419				0.0410			
AA t=24 A	1	52.291	24.0000	0.5229	1.0407	1.0406	0.0157	0.0078	0.0399	0.0397	0.0150	0.0075
AA t=24 A	2	53.272		0.5327	1.0602				0.0585			
AA t=24 B	1	52.244		0.5224	1.0397				0.0390			
AA t=24 B	2	51.345		0.5135	1.0219				0.0216			
H2O2 t=0 A	1	48.366	0.0167	0.4837	0.9626	0.9628	0.0198	0.0099	-0.0382	-0.0381	0.0204	0.0102
H2O2 t=0 A	2	47.603		0.4760	0.9474				-0.0541			
H2O2 t=0 B	1	49.785		0.4979	0.9908				-0.0092			
H2O2 t=0 B	2	47.759		0.4776	0.9505				-0.0508			
H2O2 t=6 A	1	46.402	6.0000	0.4640	0.9235	0.9016	0.0256	0.0128	-0.0796	-0.1039	0.0285	0.0143
H2O2 t=6 A	2	46.251		0.4625	0.9205				-0.0829			
H2O2 t=6 B	1	43.668		0.4367	0.8691				-0.1403			
H2O2 t=6 B	2	44.891		0.4489	0.8934				-0.1127			
H2O2 t=24 A	1	46.815	24.0000	0.4682	0.9317	0.9499	0.0297	0.0149	-0.0707	-0.0518	0.0314	0.0157
H2O2 t=24 A	2	48.987		0.4899	0.9749				-0.0254			
H2O2 t=24 B	1	49.007		0.4901	0.9753				-0.0250			
H2O2 t=24 B	2	46.101		0.4610	0.9175				-0.0861			

Table D.9. Benzo[a]pyrene degradation at T = 32 °C, experimental set-up.

		m ₀ = 0.5084 mg				Error Bar Calculations						
		Hexane Extraction										
Sample Id	Rep	Conc (mg/L)	Δ Time (hr)	m (mg)	m/m ₀	m/m ₀ avg	Std Dev	Std Error	In(m/m ₀)	m/m ₀ avg	Std Dev	Std Error
Exp t=0 A	1	43.427		0.4343	0.8541				-0.1577			
Exp t=0 A	2	42.889	0.000	0.4289	0.8436	0.8613	0.0188	0.0094	-0.1701	-0.1495	0.0217	0.0108
Exp t=0 B	1	45.130		0.4513	0.8876				-0.1192			
Exp t=0 B	2	43.723		0.4372	0.8600				-0.1509			
Exp t=1 A	1	44.220		0.4422	0.8697				-0.1396			
Exp t=1 A	2	43.533	1.017	0.4353	0.8562	0.8668	0.0075	0.0038	-0.1552	-0.1429	0.0087	0.0043
Exp t=1 B	1	44.424		0.4442	0.8738				-0.1350			
Exp t=1 B	2	44.111		0.4411	0.8676				-0.1420			
Exp t=2 A	1	43.568		0.4357	0.8569				-0.1544			
Exp t=2 A	2	41.574	2.000	0.4157	0.8177	0.8384	0.0167	0.0084	-0.2013	-0.1764	0.0200	0.0100
Exp t=2 B	1	42.399		0.4240	0.8339				-0.1816			
Exp t=2 B	2	42.971		0.4297	0.8452				-0.1682			
Exp t=4 A	1	41.584		0.4158	0.8179				-0.2010			
Exp t=4 A	2	41.174	4.067	0.4117	0.8098	0.8162	0.0164	0.0082	-0.2109	-0.2033	0.0200	0.0100
Exp t=4 B	1	40.628		0.4063	0.7991				-0.2243			
Exp t=4 B	2	42.600		0.4260	0.8379				-0.1769			
Exp t=6 A	1	40.452		0.4045	0.7956				-0.2286			
Exp t=6 A	2	40.297	6.000	0.4030	0.7926	0.7953	0.0022	0.0011	-0.2325	-0.2291	0.0028	0.0014
Exp t=6 B	1	40.413		0.4041	0.7949				-0.2296			
Exp t=6 B	2	40.572		0.4057	0.7980				-0.2257			
Exp t=12 A	1	38.250		0.3825	0.7523				-0.2846			
Exp t=12 A	2	38.651	12.267	0.3865	0.7602	0.7528	0.0081	0.0041	-0.2742	-0.2840	0.0108	0.0054
Exp t=12 B	1	38.491		0.3849	0.7571				-0.2783			
Exp t=12 B	2	37.705		0.3771	0.7416				-0.2989			
Exp t=18 A	1	35.397		0.3540	0.6962				-0.3621			
Exp t=18 A	2	37.561	18.017	0.3756	0.7388	0.6941	0.0326	0.0163	-0.3028	-0.3659	0.0464	0.0232
Exp t=18 B	1	34.451		0.3445	0.6776				-0.3892			
Exp t=18 B	2	33.754		0.3375	0.6639				-0.4096			
Exp t=24 A	1	31.845		0.3185	0.6263				-0.4679			
Exp t=24 A	2	31.623	24.017	0.3162	0.6220	0.6185	0.0079	0.0040	-0.4749	-0.4805	0.0129	0.0064
Exp t=24 B	1	30.900		0.3090	0.6078				-0.4980			
Exp t=24 B	2	31.421		0.3142	0.6180				-0.4813			

Table D.10. Benzo[a]pyrene degradation at T = 32 °C, all control set-ups.

				m ₀ = 0.5084 mg		Error Bar Calculations									
				Hexane Extraction		m/m ₀ avg		Std Dev		Std Error		Std Dev		Std Error	
Sample Id	Rep	Conc (mg/L)	Δ Time (hr)	m (mg)	m/m ₀	m/m ₀ avg	Std Dev	Std Error	ln(m/m ₀)	m/m ₀ avg	Std Dev	Std Error	ln(m/m ₀)	m/m ₀ avg	Std Error
DI t=0 A	1	42.973		0.4297	0.8452				-0.1682				-0.1682		
DI t=0 A	2	46.770		0.4677	0.9199				-0.0835				-0.0835		
DI t=0 B	1	42.551	0.000	0.4255	0.8369	0.8515	0.0489	0.0245	-0.1780	0.8515	0.0489	0.0245	-0.1780	-0.1620	0.0566
DI t=0 B	2	40.879		0.4088	0.8040				-0.2181				-0.2181		
DI t=6 A	1	42.552		0.4255	0.8369				-0.1780				-0.1780		
DI t=6 A	2	41.233		0.4123	0.8110	0.8344	0.0185	0.0092	-0.2095	0.8344	0.0185	0.0092	-0.2095	-0.1813	0.0222
DI t=6 B	1	42.377	5.983	0.4238	0.8335				-0.1821				-0.1821		
DI t=6 B	2	43.523		0.4352	0.8560				-0.1555				-0.1555		
DI t=24 A	1	37.961		0.3796	0.7466				-0.2922				-0.2922		
DI t=24 A	2	37.744		0.3774	0.7424	0.7472	0.0126	0.0063	-0.2979	0.7472	0.0126	0.0063	-0.2979	-0.2915	0.0168
DI t=24 B	1	37.378	24.017	0.3738	0.7352				-0.3077				-0.3077		
DI t=24 B	2	38.886		0.3889	0.7648				-0.2681				-0.2681		
AA t=0 A	1	42.379		0.4238	0.8335				-0.1821				-0.1821		
AA t=0 A	2	47.141		0.4714	0.9272	0.8706	0.0547	0.0273	-0.0756	0.8706	0.0547	0.0273	-0.0756	-0.1401	0.0628
AA t=0 B	1	46.096	0.017	0.4610	0.9066				-0.0980				-0.0980		
AA t=0 B	2	41.438		0.4144	0.8150				-0.2045				-0.2045		
AA t=6 A	1	43.166		0.4317	0.8490				-0.1637				-0.1637		
AA t=6 A	2	41.142		0.4114	0.8092	0.8377	0.0205	0.0103	-0.2117	0.8377	0.0205	0.0103	-0.2117	-0.1773	0.0247
AA t=6 B	1	43.506	6.000	0.4351	0.8557				-0.1558				-0.1558		
AA t=6 B	2	42.547		0.4255	0.8368				-0.1781				-0.1781		
AA t=24 A	1	41.508		0.4151	0.8164				-0.2029				-0.2029		
AA t=24 A	2	42.082		0.4208	0.8277				-0.1891				-0.1891		
AA t=24 B	1	45.248	24.017	0.4525	0.8900	0.8336	0.0392	0.0196	-0.1166	0.8336	0.0392	0.0196	-0.1166	-0.1828	0.0462
AA t=24 B	2	40.696		0.4070	0.8004				-0.2226				-0.2226		
H2O2 t=0 A	1	42.277		0.4228	0.8315				-0.1845				-0.1845		
H2O2 t=0 A	2	40.817		0.4082	0.8028	0.8380	0.0274	0.0137	-0.2196	0.8380	0.0274	0.0137	-0.2196	-0.1771	0.0328
H2O2 t=0 B	1	44.013	0.000	0.4401	0.8657				-0.1443				-0.1443		
H2O2 t=0 B	2	43.325		0.4333	0.8521				-0.1600				-0.1600		
H2O2 t=6 A	1	42.348		0.4235	0.8329				-0.1828				-0.1828		
H2O2 t=6 A	2	41.529		0.4153	0.8168	0.8212	0.0130	0.0065	-0.2023	0.8212	0.0130	0.0065	-0.2023	-0.1970	0.0158
H2O2 t=6 B	1	42.216	5.983	0.4222	0.8303				-0.1859				-0.1859		
H2O2 t=6 B	2	40.924		0.4092	0.8049				-0.2170				-0.2170		
H2O2 t=24 A	1	39.154		0.3915	0.7701				-0.2612				-0.2612		
H2O2 t=24 A	2	39.609	24.000	0.3961	0.7790	0.7743	0.0038	0.0019	-0.2497	0.7743	0.0038	0.0019	-0.2497	-0.2557	0.0049
H2O2 t=24 B	1	39.303		0.3930	0.7730				-0.2574				-0.2574		
H2O2 t=24 B	2	39.414		0.3941	0.7752				-0.2546				-0.2546		

Table D.11. Benzo[a]pyrene degradation at T = 40 °C, experimental set-up.

				m ₀ = 0.5068 mg				Error Bar Calculations				
				Hexane Extraction								
Sample Id	Rep	Conc (mg/L)	Δ Time (hr)	m (mg)	m/m ₀	m/m ₀ avg	Std Dev	Std Error	ln(m/m ₀)	m/m ₀ avg	Std Dev	Std Error
Exp t=0 A	1	45.017	0.000	0.4502	0.8882	0.8786	0.0129	0.0064	-0.1185	-0.1295	0.0147	0.0073
Exp t=0 A	2	44.101		0.4410	0.8702				-0.1391			
Exp t=0 B	1	43.839		0.4384	0.8650				-0.1450			
Exp t=0 B	2	45.149		0.4515	0.8908				-0.1156			
Exp t=1 A	1	45.317	1.083	0.4532	0.8942	0.8929	0.0236	0.0118	-0.1119	-0.1135	0.0265	0.0133
Exp t=1 A	2	46.679		0.4668	0.9210				-0.0823			
Exp t=1 B	1	45.270		0.4527	0.8932				-0.1129			
Exp t=1 B	2	43.747		0.4375	0.8632				-0.1471			
Exp t=2 A	1	42.612	2.000	0.4261	0.8408	0.8601	0.0297	0.0149	-0.1734	-0.1512	0.0346	0.0173
Exp t=2 A	2	41.994		0.4199	0.8286				-0.1880			
Exp t=2 B	1	44.841		0.4484	0.8848				-0.1224			
Exp t=2 B	2	44.912		0.4491	0.8862				-0.1208			
Exp t=4 A	1	36.418	4.000	0.3642	0.7186	0.7729	0.0413	0.0206	-0.3305	-0.2587	0.0541	0.0271
Exp t=4 A	2	38.668		0.3867	0.7630				-0.2705			
Exp t=4 B	1	40.868		0.4087	0.8064				-0.2152			
Exp t=4 B	2	40.724		0.4072	0.8035				-0.2187			
Exp t=6 A	1	37.099	6.017	0.3710	0.7320	0.7217	0.0099	0.0050	-0.3120	-0.3262	0.0138	0.0069
Exp t=6 A	2	36.723		0.3672	0.7246				-0.3221			
Exp t=6 B	1	36.594		0.3659	0.7220				-0.3257			
Exp t=6 B	2	35.893		0.3589	0.7082				-0.3450			
Exp t=12 A	1	29.663	12.083	0.2966	0.5853	0.6053	0.0216	0.0108	-0.5356	-0.5025	0.0354	0.0177
Exp t=12 A	2	30.047		0.3005	0.5929				-0.5228			
Exp t=12 B	1	30.857		0.3086	0.6088				-0.4982			
Exp t=12 B	2	32.137		0.3214	0.6341				-0.4555			
Exp t=18 A	1	7.656	17.817	0.0766	0.1511	0.1582	0.0198	0.0099	-1.8901	-1.8497	0.1194	0.0597
Exp t=18 A	2	7.218		0.0722	0.1424				-1.9490			
Exp t=18 B	1	7.705		0.0771	0.1520				-1.8837			
Exp t=18 B	2	9.482		0.0948	0.1871				-1.6762			
Exp t=24 A	1	3.474	23.967	0.0347	0.0685	0.0761	0.0138	0.0069	-2.6802	-2.5876	0.1786	0.0893
Exp t=24 A	2	4.021		0.0402	0.0793				-2.5340			
Exp t=24 B	1	3.168		0.0317	0.0625				-2.7724			
Exp t=24 B	2	4.767		0.0477	0.0941				-2.3638			

Table D.12. Benzo[a]pyrene degradation at T = 40 °C, all control set-ups.

				m ₀ = 0.5068 mg				Error Bar Calculations				
				Hexane Extraction								
Sample Id	Rep	Conc (mg/L)	Δ Time (hr)	m (mg)	m/m ₀	m/m ₀ avg	Std Dev	Std Error	ln(m/m ₀)	m/m ₀ avg	Std Dev	Std Error
DI t=0 A	1	46.961		0.4696	0.9266				-0.0762			
DI t=0 A	2	47.171		0.4717	0.9307				-0.0718			
DI t=0 B	1	43.425	0.050	0.4343	0.8568	0.8934	0.0408	0.0204	-0.1545	-0.1135	0.0456	0.0228
DI t=0 B	2	43.561		0.4356	0.8595				-0.1514			
DI t=6 A	1	51.584		0.5158	1.0178				0.0177			
DI t=6 A	2	51.466	6.000	0.5147	1.0155	0.9261	0.1046	0.0523	0.0154	-0.0816	0.1133	0.0567
DI t=6 B	1	42.368		0.4237	0.8360				-0.1792			
DI t=6 B	2	42.317		0.4232	0.8350				-0.1804			
DI t=24 A	1	43.068		0.4307	0.8498				-0.1628			
DI t=24 A	2	43.672	24.000	0.4367	0.8617	0.8691	0.0162	0.0081	-0.1488	-0.1404	0.0187	0.0093
DI t=24 B	1	44.656		0.4466	0.8811				-0.1266			
DI t=24 B	2	44.791		0.4479	0.8838				-0.1235			
AA t=0 A	1	48.584		0.4858	0.9586				-0.0423			
AA t=0 A	2	43.747	0.017	0.4375	0.8632	0.9208	0.0406	0.0203	-0.1471	-0.0833	0.0448	0.0224
AA t=0 B	1	47.140		0.4714	0.9301				-0.0724			
AA t=0 B	2	47.198		0.4720	0.9313				-0.0712			
AA t=6 A	1	44.632		0.4463	0.8806				-0.1271			
AA t=6 A	2	44.574	6.000	0.4457	0.8795	0.8892	0.0107	0.0053	-0.1284	-0.1175	0.0120	0.0060
AA t=6 B	1	45.396		0.4540	0.8957				-0.1101			
AA t=6 B	2	45.650		0.4565	0.9007				-0.1045			
AA t=24 A	1	46.441		0.4644	0.9163				-0.0874			
AA t=24 A	2	47.628	24.000	0.4763	0.9398	0.9378	0.0154	0.0077	-0.0621	-0.0643	0.0165	0.0083
AA t=24 B	1	48.303		0.4830	0.9531				-0.0481			
AA t=24 B	2	47.743		0.4774	0.9420				-0.0697			
H2O2 t=0 A	1	50.930		0.5093	1.0049				0.0049			
H2O2 t=0 A	2	50.927	0.017	0.5093	1.0049	0.9985	0.0184	0.0092	0.0048	-0.0016	0.0186	0.0093
H2O2 t=0 B	1	51.336		0.5134	1.0129				0.0128			
H2O2 t=0 B	2	49.235		0.4924	0.9715				-0.0289			
H2O2 t=6 A	1	51.933		0.5193	1.0247				0.0244			
H2O2 t=6 A	2	48.597	6.000	0.4860	0.9589	0.9875	0.0301	0.0150	-0.0420	-0.0129	0.0303	0.0152
H2O2 t=6 B	1	49.050		0.4905	0.9678				-0.0327			
H2O2 t=6 B	2	50.612		0.5061	0.9986				-0.0014			
H2O2 t=24 A	1	53.148		0.5315	1.0487				0.0475			
H2O2 t=24 A	2	43.721	24.000	0.4372	0.8627	0.9916	0.0870	0.0435	-0.1477	-0.0115	0.0917	0.0459
H2O2 t=24 B	1	51.534		0.5153	1.0168				0.0167			
H2O2 t=24 B	2	52.619		0.5262	1.0382				0.0375			

Table D.13. Phenanthrene degradation at T = 25 °C, experimental set-up.

				m ₀ = 0.5064 mg				Error Bar Calculations				
				Hexane Extraction								
Sample Id	Rep	Conc (mg/L)	Δ Time (hr)	m (mg)	m/m ₀	m/m ₀ avg	Std Dev	Std Error	In(m/m ₀)	m/m ₀ avg	Std Dev	Std Error
Exp t=0 A	1	49.080	0.000	0.4908	0.9693	0.9731	0.0066	0.0033	-0.0312	-0.0273	0.0068	0.0034
Exp t=0 A	2	48.908		0.4891	0.9659				-0.0347			
Exp t=0 B	1	49.584		0.4958	0.9792				-0.0210			
Exp t=0 B	2	49.534		0.4953	0.9782				-0.0220			
Exp t=1 A	1	47.924	1.000	0.4792	0.9464	0.9751	0.0293	0.0146	-0.0551	-0.0255	0.0301	0.0150
Exp t=1 A	2	48.289		0.4829	0.9536				-0.0475			
Exp t=1 B	1	50.440		0.5044	0.9961				-0.0039			
Exp t=1 B	2	50.853		0.5085	1.0043				0.0043			
Exp t=2 A	1	49.693	2.000	0.4969	0.9814	0.9660	0.0158	0.0079	-0.0188	-0.0347	0.0164	0.0082
Exp t=2 A	2	49.342		0.4934	0.9744				-0.0259			
Exp t=2 B	1	47.869		0.4787	0.9453				-0.0562			
Exp t=2 B	2	48.748		0.4875	0.9627				-0.0380			
Exp t=4 A	1	50.079	4.000	0.5008	0.9890	0.9837	0.0059	0.0029	-0.0111	-0.0164	0.0060	0.0030
Exp t=4 A	2	49.987		0.4999	0.9872				-0.0129			
Exp t=4 B	1	49.773		0.4977	0.9829				-0.0172			
Exp t=4 B	2	49.410		0.4941	0.9758				-0.0245			
Exp t=6 A	1	48.802	6.000	0.4880	0.9638	0.9637	0.0030	0.0015	-0.0369	-0.0370	0.0031	0.0015
Exp t=6 A	2	48.642		0.4864	0.9606				-0.0402			
Exp t=6 B	1	49.002		0.4900	0.9677				-0.0328			
Exp t=6 B	2	48.747		0.4875	0.9627				-0.0380			
Exp t=12 A	1	46.378	12.000	0.4638	0.9159	0.9118	0.0039	0.0020	-0.0879	-0.0924	0.0043	0.0021
Exp t=12 A	2	46.189		0.4619	0.9122				-0.0919			
Exp t=12 B	1	46.207		0.4621	0.9125				-0.0916			
Exp t=12 B	2	45.900		0.4590	0.9065				-0.0982			
Exp t=18 A	1	45.194	18.033	0.4519	0.8925	0.8944	0.0053	0.0027	-0.1137	-0.1116	0.0060	0.0030
Exp t=18 A	2	45.527		0.4553	0.8991				-0.1064			
Exp t=18 B	1	45.486		0.4549	0.8983				-0.1073			
Exp t=18 B	2	44.950		0.4495	0.8877				-0.1191			
Exp t=24 A	1	41.885	24.000	0.4189	0.8272	0.8210	0.0111	0.0056	-0.1898	-0.1973	0.0136	0.0068
Exp t=24 A	2	42.174		0.4217	0.8329				-0.1829			
Exp t=24 B	1	41.315		0.4132	0.8159				-0.2035			
Exp t=24 B	2	40.919		0.4092	0.8081				-0.2131			

Table D.14. Phenanthrene degradation at T = 25 °C, all control set-ups.

				$m_0 = 0.5064 \text{ mg}$								
				Hexane Extraction				Error Bar Calculations				
Sample Id	Rep	Conc (mg/L)	Δ Time (hr)	m (mg)	m/m ₀	m/m ₀ avg	Std Dev	Std Error	ln(m/m ₀)	m/m ₀ avg	Std Dev	Std Error
DI t=0 A	1	52.176		0.5218	1.0304				0.0299			
DI t=0 A	2	52.083		0.5208	1.0286				0.0282			
DI t=0 B	1	57.222	0.000	0.5722	1.1300	1.0834	0.0626	0.0313	0.1223	0.0789	0.0578	0.0289
DI t=0 B	2	57.961		0.5796	1.1446				0.1351			
DI t=6 A	1	50.806		0.5081	1.0033				0.0033			
DI t=6 A	2	50.796	6.000	0.5080	1.0031	1.0045	0.0047	0.0023	0.0031	0.0045	0.0047	0.0023
DI t=6 B	1	51.207		0.5121	1.0113				0.0112			
DI t=6 B	2	50.655		0.5066	1.0004				0.0004			
DI t=24 A	1	50.815		0.5082	1.0035				0.0035			
DI t=24 A	2	50.773	24.000	0.5077	1.0027	0.9872	0.0188	0.0094	0.0027	-0.0130	0.0190	0.0095
DI t=24 B	1	49.437		0.4944	0.9763				-0.0240			
DI t=24 B	2	48.935		0.4894	0.9664				-0.0342			
AA t=0 A	1	50.253		0.5025	0.9924				-0.0076			
AA t=0 A	2	50.464	0.000	0.5046	0.9966	1.0039	0.0117	0.0059	-0.0034	0.0039	0.0117	0.0058
AA t=0 B	1	51.059		0.5106	1.0083				0.0083			
AA t=0 B	2	51.566		0.5157	1.0183				0.0182			
AA t=6 A	1	49.981		0.4998	0.9870				-0.0130			
AA t=6 A	2	49.493	6.000	0.4949	0.9774	0.9896	0.0098	0.0049	-0.0229	-0.0105	0.0099	0.0049
AA t=6 B	1	50.654		0.5065	1.0003				0.0003			
AA t=6 B	2	50.316		0.5032	0.9937				-0.0064			
AA t=24 A	1	50.258		0.5026	0.9925				-0.0075			
AA t=24 A	2	50.589	24.000	0.5059	0.9991	0.9869	0.0106	0.0053	-0.0009	-0.0132	0.0107	0.0054
AA t=24 B	1	49.546		0.4955	0.9785				-0.0218			
AA t=24 B	2	49.508		0.4951	0.9777				-0.0225			
H2O2 t=0 A	1	50.313		0.5031	0.9936				-0.0064			
H2O2 t=0 A	2	51.198	0.000	0.5120	1.0111	0.9780	0.0290	0.0145	0.0110	-0.0226	0.0296	0.0148
H2O2 t=0 B	1	48.277		0.4828	0.9534				-0.0477			
H2O2 t=0 B	2	48.295		0.4830	0.9537				-0.0474			
H2O2 t=6 A	1	49.780		0.4978	0.9831				-0.0171			
H2O2 t=6 A	2	49.707	6.000	0.4971	0.9816	0.9840	0.0024	0.0012	-0.0185	-0.0161	0.0025	0.0012
H2O2 t=6 B	1	49.996		0.5000	0.9873				-0.0127			
H2O2 t=6 B	2	49.822		0.4982	0.9839				-0.0162			
H2O2 t=24 A	1	49.525		0.4953	0.9780				-0.0222			
H2O2 t=24 A	2	49.146	24.000	0.4915	0.9706	0.9857	0.0138	0.0069	-0.0299	-0.0145	0.0140	0.0070
H2O2 t=24 B	1	50.672		0.5067	1.0007				0.0007			
H2O2 t=24 B	2	50.301		0.5030	0.9934				-0.0067			

Table D.15. Phenanthrene degradation at T = 32 °C, experiment set-up.

Sample Id		Rep		Conc (mg/L)		Δ Time (hr)		$m_0 = 0.5108$ mg				Error Bar Calculations							
								Hexane Extraction				m/m ₀ avg				m/m ₀ avg			
								m (mg)	m/m ₀	m/m ₀ avg	Std Dev	Std Error	In(m/m ₀)	m/m ₀ avg	Std Dev	Std Error	In(m/m ₀)	m/m ₀ avg	Std Dev
Exp t=0 A	1	48.134	0.4813	0.9423	0.9507	0.0136	0.0068	-0.0594	-0.0506	0.0142	0.0071								
Exp t=0 A	2	48.148	0.4815	0.9426	0.9507	0.0136	0.0068	-0.0591	-0.0506	0.0142	0.0071								
Exp t=0 B	1	49.588	0.4959	0.9708	0.9507	0.0136	0.0068	-0.0296	-0.0506	0.0142	0.0071								
Exp t=0 B	2	48.377	0.4838	0.9471	0.9507	0.0136	0.0068	-0.0544	-0.0506	0.0142	0.0071								
Exp t=1 A	1	48.771	0.4877	0.9548	0.9347	0.0156	0.0078	-0.0462	-0.0676	0.0167	0.0083								
Exp t=1 A	2	47.517	0.4752	0.9303	0.9347	0.0156	0.0078	-0.0723	-0.0676	0.0167	0.0083								
Exp t=1 B	1	47.839	0.4784	0.9366	0.9347	0.0156	0.0078	-0.0655	-0.0676	0.0167	0.0083								
Exp t=1 B	2	46.855	0.4686	0.9173	0.9347	0.0156	0.0078	-0.0863	-0.0676	0.0167	0.0083								
Exp t=2 A	1	51.432	0.5143	1.0069	0.9524	0.0376	0.0188	0.0069	-0.0493	0.0389	0.0194								
Exp t=2 A	2	47.771	0.4777	0.9552	0.9524	0.0376	0.0188	-0.0670	-0.0493	0.0389	0.0194								
Exp t=2 B	1	48.299	0.4830	0.9456	0.9524	0.0376	0.0188	-0.0560	-0.0493	0.0389	0.0194								
Exp t=2 B	2	47.094	0.4709	0.9220	0.9524	0.0376	0.0188	-0.0812	-0.0493	0.0389	0.0194								
Exp t=4 A	1	46.697	0.4670	0.9142	0.9185	0.0098	0.0049	-0.0897	-0.0851	0.0106	0.0053								
Exp t=4 A	2	46.386	0.4639	0.9081	0.9185	0.0098	0.0049	-0.0964	-0.0851	0.0106	0.0053								
Exp t=4 B	1	47.021	0.4702	0.9205	0.9185	0.0098	0.0049	-0.0828	-0.0851	0.0106	0.0053								
Exp t=4 B	2	47.557	0.4756	0.9310	0.9185	0.0098	0.0049	-0.0715	-0.0851	0.0106	0.0053								
Exp t=6 A	1	44.755	0.4476	0.8762	0.8830	0.0201	0.0100	-0.1322	-0.1247	0.0228	0.0114								
Exp t=6 A	2	46.088	0.4609	0.9023	0.8830	0.0201	0.0100	-0.1028	-0.1247	0.0228	0.0114								
Exp t=6 B	1	43.816	0.4382	0.8578	0.8830	0.0201	0.0100	-0.1534	-0.1247	0.0228	0.0114								
Exp t=6 B	2	45.745	0.4575	0.8956	0.8830	0.0201	0.0100	-0.1103	-0.1247	0.0228	0.0114								
Exp t=12 A	1	44.676	0.4468	0.8746	0.8543	0.0178	0.0089	-0.1339	-0.1576	0.0208	0.0104								
Exp t=12 A	2	44.119	0.4412	0.8637	0.8543	0.0178	0.0089	-0.1465	-0.1576	0.0208	0.0104								
Exp t=12 B	1	42.916	0.4292	0.8402	0.8543	0.0178	0.0089	-0.1741	-0.1576	0.0208	0.0104								
Exp t=12 B	2	42.838	0.4284	0.8387	0.8543	0.0178	0.0089	-0.1760	-0.1576	0.0208	0.0104								
Exp t=18 A	1	39.715	0.3972	0.7775	0.7874	0.0075	0.0038	-0.2517	-0.2391	0.0096	0.0048								
Exp t=18 A	2	40.647	0.4065	0.7958	0.7874	0.0075	0.0038	-0.2285	-0.2391	0.0096	0.0048								
Exp t=18 B	1	40.219	0.4022	0.7874	0.7874	0.0075	0.0038	-0.2390	-0.2391	0.0096	0.0048								
Exp t=18 B	2	40.295	0.4030	0.7889	0.7874	0.0075	0.0038	-0.2372	-0.2391	0.0096	0.0048								
Exp t=24 A	1	37.752	0.3775	0.7391	0.7233	0.0113	0.0056	-0.3023	-0.3240	0.0155	0.0078								
Exp t=24 A	2	36.791	0.3679	0.7203	0.7233	0.0113	0.0056	-0.3281	-0.3240	0.0155	0.0078								
Exp t=24 B	1	36.853	0.3685	0.7215	0.7233	0.0113	0.0056	-0.3264	-0.3240	0.0155	0.0078								
Exp t=24 B	2	36.384	0.3638	0.7123	0.7233	0.0113	0.0056	-0.3393	-0.3240	0.0155	0.0078								

Table D.16. Phenanthrene degradation at T = 32 °C, all control set-ups.

				m ₀ = 0.5108 mg				Error Bar Calculations				
				Hexane Extraction								
Sample Id	Rep	Conc (mg/L)	Δ Time (hr)	m (mg)	m/m ₀	m/m ₀ avg	Std Dev	Std Error	ln(m/m ₀)	m/m ₀ avg	Std Dev	Std Error
DI t=0 A	1	48.168		0.4817	0.9430				-0.0587			
DI t=0 A	2	47.998		0.4800	0.9397				-0.0622			
DI t=0 B	1	45.237	0.000	0.4524	0.8856	0.9162	0.0294	0.0147	-0.1215	-0.0879	0.0322	0.0161
DI t=0 B	2	45.786		0.4579	0.8964				-0.1094			
DI t=6 A	1	50.359		0.5036	0.9859				-0.0142			
DI t=6 A	2	49.829	6.117	0.4983	0.9755	0.9683	0.0167	0.0084	-0.0248	-0.0323	0.0173	0.0087
DI t=6 B	1	48.358		0.4836	0.9467				-0.0547			
DI t=6 B	2	49.298		0.4930	0.9651				-0.0355			
DI t=24 A	1	52.773		0.5277	1.0332				0.0326			
DI t=24 A	2	50.921	24.000	0.5092	0.9989	0.9979	0.0326	0.0163	-0.0031	-0.0025	0.0329	0.0164
DI t=24 B	1	48.767		0.4877	0.9547				-0.0463			
DI t=24 B	2	51.427		0.5143	1.0068				0.0068			
AA t=0 A	1	47.127		0.4713	0.9226				-0.0805			
AA t=0 A	2	46.427	0.000	0.4643	0.9089	0.9151	0.0091	0.0045	-0.0955	-0.0887	0.0099	0.0050
AA t=0 B	1	47.157		0.4716	0.9232				-0.0799			
AA t=0 B	2	46.270		0.4627	0.9058				-0.0989			
AA t=6 A	1	48.860		0.4886	0.9174				-0.0862			
AA t=6 A	2	48.390	6.117	0.4839	0.9473	0.9443	0.0190	0.0095	-0.0541	-0.0575	0.0202	0.0101
AA t=6 B	1	48.546		0.4855	0.9504				-0.0509			
AA t=6 B	2	49.134		0.4913	0.9619				-0.0388			
AA t=24 A	1	51.532		0.5153	1.0089				0.0088			
AA t=24 A	2	51.186	24.000	0.5119	1.0021	1.0103	0.0072	0.0036	0.0021	0.0102	0.0071	0.0036
AA t=24 B	1	52.082		0.5208	1.0196				0.0194			
AA t=24 B	2	51.623		0.5162	1.0106				0.0106			
H2O2 t=0 A	1	48.101		0.4810	0.9417				-0.0601			
H2O2 t=0 A	2	48.448	0.000	0.4845	0.9485	0.9503	0.0084	0.0042	-0.0529	-0.0510	0.0088	0.0044
H2O2 t=0 B	1	49.131		0.4913	0.9619				-0.0389			
H2O2 t=0 B	2	48.482		0.4848	0.9491				-0.0522			
H2O2 t=6 A	1	49.551		0.4955	0.9701				-0.0304			
H2O2 t=6 A	2	49.514	6.117	0.4951	0.9694	0.9558	0.0162	0.0081	-0.0311	-0.0454	0.0169	0.0085
H2O2 t=6 B	1	48.038		0.4804	0.9405				-0.0614			
H2O2 t=6 B	2	48.176		0.4818	0.9432				-0.0585			
H2O2 t=24 A	1	48.589		0.4859	0.9512				-0.0500			
H2O2 t=24 A	2	48.897	24.000	0.4890	0.9573	0.9732	0.0277	0.0139	-0.0437	-0.0275	0.0282	0.0141
H2O2 t=24 B	1	51.734		0.5173	1.0128				0.0127			
H2O2 t=24 B	2	49.621		0.4962	0.9714				-0.0290			

Table D.17. Phenanthrene degradation at T = 40 °C, experimental set-up.

				m ₀ = 0.5097 mg				Error Bar Calculations				
				Hexane Extraction								
Sample Id	Rep	Conc (mg/L)	Δ Time (hr)	m (mg)	m/m ₀	m/m ₀ avg	Std Dev	Std Error	In(m/m ₀)	m/m ₀ avg	Std Dev	Std Error
Exp t=0 A	1	49.573	0.000	0.4957	0.9727	0.9420	0.0241	0.0121	-0.0277	-0.0600	0.0255	0.0128
Exp t=0 A	2	48.412		0.4841	0.9499							
Exp t=0 B	1	47.063		0.4706	0.9234							
Exp t=0 B	2	46.993		0.4699	0.9221							
Exp t=1 A	1	49.489	1.000	0.4949	0.9710	0.9774	0.0168	0.0084	-0.0294	-0.0229	0.0171	0.0086
Exp t=1 A	2	49.068		0.4907	0.9628							
Exp t=1 B	1	51.047		0.5105	1.0016							
Exp t=1 B	2	49.658		0.4966	0.9744							
Exp t=2 A	1	46.369	2.000	0.4637	0.9098	0.9280	0.0173	0.0087	-0.0260	-0.0749	0.0186	0.0093
Exp t=2 A	2	46.795		0.4680	0.9182							
Exp t=2 B	1	47.682		0.4768	0.9356							
Exp t=2 B	2	48.333		0.4833	0.9484							
Exp t=4 A	1	46.056	4.000	0.4606	0.9037	0.8944	0.0131	0.0066	-0.1013	-0.1117	0.0147	0.0073
Exp t=4 A	2	44.738		0.4474	0.8778							
Exp t=4 B	1	46.174		0.4617	0.9060							
Exp t=4 B	2	45.358		0.4536	0.8900							
Exp t=6 A	1	33.933	6.050	0.3393	0.6658	0.7227	0.0598	0.0299	-0.4068	-0.3273	0.0829	0.0414
Exp t=6 A	2	34.477		0.3448	0.6765							
Exp t=6 B	1	39.536		0.3954	0.7757							
Exp t=6 B	2	39.393		0.3939	0.7729							
Exp t=12 A	1	33.439	12.017	0.3344	0.6561	0.7074	0.0588	0.0294	-0.4214	-0.3487	0.0833	0.0416
Exp t=12 A	2	33.483		0.3348	0.6570							
Exp t=12 B	1	38.832		0.3883	0.7619							
Exp t=12 B	2	38.463		0.3846	0.7547							
Exp t=18 A	1	33.057	18.000	0.3306	0.6486	0.6328	0.0264	0.0132	-0.4329	-0.4582	0.0417	0.0208
Exp t=18 A	2	33.725		0.3373	0.6617							
Exp t=18 B	1	31.234		0.3123	0.6129							
Exp t=18 B	2	30.997		0.3100	0.6082							
Exp t=24 A	1	18.538	24.017	0.1854	0.3637	0.3869	0.0375	0.0188	-1.0113	-0.9532	0.0975	0.0487
Exp t=24 A	2	17.667		0.1767	0.3466							
Exp t=24 B	1	21.600		0.2160	0.4238							
Exp t=24 B	2	21.066		0.2107	0.4133							

Table D.18. Phenanthrene degradation at T = 40 °C, all control set-ups.

				m ₀ = 0.5097 mg				Hexane Extraction				Error Bar Calculations				
Sample Id	Rep	Conc (mg/L)	Δ Time (hr)	m (mg)	m/m ₀	m/m ₀ avg	Std Dev	Std Error	ln(m/m ₀)	m/m ₀ avg	Std Dev	Std Error	ln(m/m ₀)	m/m ₀ avg	Std Dev	Std Error
DI t=0 A	1	49.261		0.4926	0.9666				-0.0340							
DI t=0 A	2	47.362		0.4736	0.9293				-0.0733							
DI t=0 B	1	45.464	0.000	0.4546	0.8921	0.9220	0.0337	0.0169	-0.1142					-0.0817	0.0363	0.0181
DI t=0 B	2	45.878		0.4588	0.9002				-0.1052							
DI t=6 A	1	51.014		0.5101	1.0010				0.0010							
DI t=6 A	2	50.993	6.000	0.5099	1.0005	1.0124	0.0140	0.0070	0.0005					0.0123	0.0138	0.0069
DI t=6 B	1	52.431		0.5243	1.0288				0.0284							
DI t=6 B	2	51.959		0.5196	1.0195				0.0193							
DI t=24 A	1	50.619		0.5062	0.9932				-0.0068							
DI t=24 A	2	50.030	24.100	0.5003	0.9817	0.9981	0.0135	0.0068	-0.0185					-0.0020	0.0136	0.0068
DI t=24 B	1	51.226		0.5123	1.0051				0.0051							
DI t=24 B	2	51.600		0.5160	1.0125				0.0124							
AA t=0 A	1	46.624		0.4662	0.9148				-0.0890							
AA t=0 A	2	46.025	0.000	0.4603	0.9031	0.9481	0.0455	0.0228	-0.1020					-0.0542	0.0480	0.0240
AA t=0 B	1	50.127		0.5013	0.9836				-0.0166							
AA t=0 B	2	50.494		0.5049	0.9908				-0.0093							
AA t=6 A	1	49.367		0.4937	0.9686				-0.0319							
AA t=6 A	2	49.767	6.000	0.4977	0.9765	0.9936	0.0252	0.0126	-0.0238					-0.0067	0.0253	0.0127
AA t=6 B	1	51.337		0.5134	1.0073				0.0073							
AA t=6 B	2	52.081		0.5208	1.0219				0.0217							
AA t=24 A	1	50.337		0.5034	0.9877				-0.0124							
AA t=24 A	2	49.290	24.000	0.4929	0.9671	0.9606	0.0226	0.0113	-0.0334					-0.0404	0.0235	0.0118
AA t=24 B	1	47.605		0.4761	0.9341				-0.0682							
AA t=24 B	2	48.593		0.4859	0.9535				-0.0477							
H2O2 t=0 A	1	48.308		0.4831	0.9479				-0.0635							
H2O2 t=0 A	2	46.766	0.000	0.4677	0.9176	0.9202	0.0208	0.0104	-0.0860					-0.0834	0.0225	0.0112
H2O2 t=0 B	1	46.775		0.4678	0.9178				-0.0858							
H2O2 t=0 B	2	45.740		0.4574	0.8975				-0.1082							
H2O2 t=6 A	1	49.788		0.4979	0.9769				-0.0234							
H2O2 t=6 A	2	53.414	6.000	0.5341	1.0481	0.9673	0.0599	0.0300	0.0469					-0.0347	0.0611	0.0305
H2O2 t=6 B	1	46.684		0.4668	0.9160				-0.0877							
H2O2 t=6 B	2	47.301		0.4730	0.9281				-0.0746							
H2O2 t=24 A	1	48.273		0.4827	0.9472				-0.0543							
H2O2 t=24 A	2	49.208	24.083	0.4921	0.9655	0.8495	0.1237	0.0618	-0.0351					-0.1712	0.1463	0.0731
H2O2 t=24 B	1	37.824		0.3782	0.7422				-0.2982							
H2O2 t=24 B	2	37.866		0.3787	0.7430				-0.2971							

Table D.19. Pyrene degradation at T = 25 °C, experimental set-up.

				m ₀ = 0.5060 mg		m ₀ = 0.5145 mg					
				Hexane Extraction		Error Bar Calculations					
Sample Id	Rep	Conc (mg/L)	Δ Time (hr)	m (mg)	m/m ₀	Std Dev	Std Error	ln(m/m ₀)	m/m ₀ avg	Std Dev	Std Error
Exp t=0 A	1	49.287		0.4929	0.9740			-0.0263			
Exp t=0 A	2	49.900	0.000	0.4990	0.9861	0.0167	0.0084	-0.0140	-0.0196	0.0170	0.0085
Exp t=0 B	1	48.663		0.4866	0.9617			-0.0391			
Exp t=0 B	2	50.642		0.5064	1.0008			0.0008			
Exp t=1 A	1	48.136		0.4814	0.9513			-0.0500			
Exp t=1 A	2	47.934	1.000	0.4793	0.9473	0.0092	0.0046	-0.0542	-0.0582	0.0098	0.0049
Exp t=1 B	1	47.827		0.4783	0.9452			-0.0564			
Exp t=1 B	2	47.068		0.4707	0.9302			-0.0724			
Exp t=2 A	1	50.914		0.5091	0.9896			-0.0104			
Exp t=2 A	2	50.946	2.083	0.5095	0.9902	0.0797	0.0399	-0.0098	-0.0852	0.0867	0.0434
Exp t=2 B	1	43.729		0.4373	0.8500			-0.1626			
Exp t=2 B	2	43.926		0.4393	0.8538			-0.1581			
Exp t=4 A	1	45.301		0.4530	0.8952			-0.1107			
Exp t=4 A	2	45.289	4.000	0.4529	0.8950	0.0155	0.0078	-0.1109	-0.1057	0.0172	0.0086
Exp t=4 B	1	44.865		0.4487	0.8866			-0.1203			
Exp t=4 B	2	46.671		0.4667	0.9223			-0.0809			
Exp t=6 A	1	45.211		0.4521	0.8935			-0.1126			
Exp t=6 A	2	44.437	6.050	0.4444	0.8782	0.0114	0.0057	-0.1299	-0.1271	0.0129	0.0065
Exp t=6 B	1	44.769		0.4477	0.8847			-0.1225			
Exp t=6 B	2	43.843		0.4384	0.8664			-0.1434			
Exp t=12 A	1	41.465		0.4147	0.8194			-0.1991			
Exp t=12 A	2	42.815	12.000	0.4282	0.8461	0.0142	0.0071	-0.1671	-0.1740	0.0170	0.0085
Exp t=12 B	1	42.783		0.4278	0.8455			-0.1678			
Exp t=12 B	2	43.041		0.4304	0.8506			-0.1618			
Exp t=18 A	1	41.475		0.4148	0.8196			-0.1989			
Exp t=18 A	2	42.347	18.033	0.4235	0.8369	0.0076	0.0038	-0.1781	-0.1896	0.0092	0.0046
Exp t=18 B	1	41.647		0.4165	0.8230			-0.1948			
Exp t=18 B	2	41.978		0.4198	0.8296			-0.1868			
Exp t=24 A	1	38.566		0.3857	0.7621			-0.2716			
Exp t=24 A	2	40.775	23.967	0.4078	0.8058	0.0273	0.0137	-0.2159	-0.2213	0.0346	0.0173
Exp t=24 B	1	41.594		0.4159	0.8220			-0.1960			
Exp t=24 B	2	41.360		0.4136	0.8174			-0.2017			

Table D.20. Pyrene degradation at T = 25 °C, all control set-ups.

Sample Id	Rep	Conc (mg/L)	Δ Time (hr)	m ₀ = 0.5145 mg			Error Bar Calculations								
				Hexane Extraction			m/m ₀ avg			m/m ₀ avg			m/m ₀ avg		
				m (mg)	m/m ₀	m/m ₀ avg	Std Dev	Std Error	In(m/m ₀)	Std Dev	Std Error	In(m/m ₀)	Std Dev	Std Error	
DI t=0 A	1	45.031		0.4503	0.8753	0.8401	0.0428	0.0214	-0.1332	-0.1291	-0.1752	0.0510	0.0255		
DI t=0 A	2	45.217	0.017	0.4522	0.8789				-0.1291	-0.2232					
DI t=0 B	1	41.158		0.4116	0.8000				-0.2232	-0.153					
DI t=0 B	2	41.482		0.4148	0.8063				-0.2153	-0.1525					
DI t=2 A	1	44.174		0.4417	0.8586				-0.1525	-0.2062					
DI t=2 A	2	41.863	1.983	0.4186	0.8137	0.8623	0.0482	0.0241	-0.2062	-0.1644	-0.1493	0.0551	0.0276		
DI t=2 B	1	43.650		0.4365	0.8484				-0.1644	-0.0741					
DI t=2 B	2	47.772		0.4777	0.9285				-0.0741	-0.1086					
DI t=4 A	1	46.155		0.4616	0.8971				-0.1086	-0.0917					
DI t=4 A	2	46.943		0.4694	0.9124	0.9170	0.0220	0.0110	-0.0917	-0.0941	-0.0868	0.0237	0.0119		
DI t=4 B	1	46.828	4.000	0.4683	0.9102				-0.0941	-0.0530					
DI t=4 B	2	48.791		0.4879	0.9483				-0.0530	-0.1103					
DI t=24 A	1	46.078		0.4608	0.8956				-0.1103	-0.0582					
DI t=24 A	2	48.541		0.4854	0.9435	0.8663	0.0678	0.0339	-0.0582	-0.1761	-0.1459	0.0786	0.0393		
DI t=24 B	1	43.143	24.000	0.4314	0.8386				-0.1761	-0.2390					
DI t=24 B	2	40.511		0.4051	0.7874				-0.2390	-0.1475					
AA t=0 A	1	44.394		0.4439	0.8629				-0.1475	-0.1466					
AA t=0 A	2	44.432		0.4443	0.8636	0.8780	0.0205	0.0103	-0.1466	-0.0978	-0.1304	0.0232	0.0116		
AA t=0 B	1	46.655	0.017	0.4666	0.9068				-0.0978	-0.1295					
AA t=0 B	2	45.199		0.4520	0.8785				-0.1295	-0.1148					
AA t=3 A	1	45.871		0.4587	0.8916				-0.1148	-0.0651					
AA t=3 A	2	48.204		0.4820	0.9369	0.9302	0.0312	0.0156	-0.0651	-0.0336	-0.0728	0.0336	0.0168		
AA t=3 B	1	49.749	3.000	0.4975	0.9670				-0.0336	-0.1444					
AA t=3 B	2	47.609		0.4761	0.9254				-0.1444	-0.0776					
AA t=24 A	1	45.110		0.4511	0.8768				-0.0776	-0.1315					
AA t=24 A	2	44.530		0.4453	0.8655	0.8824	0.0137	0.0069	-0.1315	-0.1124	-0.1253	0.0156	0.0078		
AA t=24 B	1	45.980	24.017	0.4598	0.8937				-0.1124	-0.1810					
AA t=24 B	2	45.964		0.4596	0.8934				-0.1810	-0.1699					
H2O2 t=0 A	1	42.930		0.4293	0.8344				-0.1699	-0.0911					
H2O2 t=0 A	2	43.408		0.4341	0.8437	0.8632	0.0350	0.0175	-0.0911	-0.1489	-0.1477	0.0401	0.0200		
H2O2 t=0 B	1	46.970	0.017	0.4697	0.9129				-0.1489	-0.2660					
H2O2 t=0 B	2	44.331		0.4433	0.8617				-0.2660	-0.2213					
H2O2 t=3 A	1	39.432		0.3943	0.7664				-0.2213	-0.2488					
H2O2 t=3 A	2	41.236	3.000	0.4124	0.8015	0.8097	0.0562	0.0281	-0.2488	-0.1152	-0.2128	0.0676	0.0338		
H2O2 t=3 B	1	40.118		0.4012	0.7798				-0.1152	-0.1135					
H2O2 t=3 B	2	45.850		0.4585	0.8912				-0.1135	-0.1528					
H2O2 t=24 A	1	45.928		0.4593	0.8927				-0.1528	-0.0873					
H2O2 t=24 A	2	44.157	24.017	0.4416	0.8583	0.8903	0.0240	0.0120	-0.0873	-0.1123	-0.1165	0.0271	0.0135		
H2O2 t=24 B	1	47.148		0.4715	0.9164				-0.1123						
H2O2 t=24 B	2	45.984		0.4598	0.8938										

Table D.21. Pyrene degradation at T = 32 °C, experimental set-up.

				m ₀ = 0.5081 mg				Error Bar Calculations				
				Hexane Extraction								
Sample Id	Rep	Conc (mg/L)	Δ Time (hr)	m (mg)	m/m ₀	m/m ₀ avg	Std Dev	Std Error	ln(m/m ₀)	m/m ₀ avg	Std Dev	Std Error
Exp t=0 A	1	50.152	0.000	0.5015	0.9871	0.9738	0.0128	0.0064	-0.0130	-0.0266	0.0132	0.0066
Exp t=0 A	2	49.754		0.4975	0.9793				-0.0210			
Exp t=0 B	1	48.625		0.4863	0.9570				-0.0439			
Exp t=0 B	2	49.375		0.4938	0.9718				-0.0286			
Exp t=1 A	1	43.762	1.017	0.4376	0.8613	0.9444	0.0556	0.0278	-0.1493	-0.0585	0.0607	0.0304
Exp t=1 A	2	49.377		0.4938	0.9718				-0.0286			
Exp t=1 B	1	49.116		0.4912	0.9667				-0.0339			
Exp t=1 B	2	49.687		0.4969	0.9779				-0.0223			
Exp t=2 A	1	46.093	2.000	0.4609	0.9072	0.9165	0.0123	0.0061	-0.0974	-0.0873	0.0134	0.0067
Exp t=2 A	2	47.355		0.4736	0.9320				-0.0704			
Exp t=2 B	1	46.768		0.4677	0.9205				-0.0829			
Exp t=2 B	2	46.038		0.4604	0.9061				-0.0986			
Exp t=4 A	1	48.091	4.050	0.4809	0.9465	0.8504	0.0940	0.0470	-0.0550	-0.1667	0.1108	0.0654
Exp t=4 A	2	46.451		0.4645	0.9142				-0.0897			
Exp t=4 B	1	38.458		0.3846	0.7569				-0.2785			
Exp t=4 B	2	39.823		0.3982	0.7838				-0.2436			
Exp t=6 A	1	45.052	6.000	0.4505	0.8867	0.8367	0.0618	0.0309	-0.1202	-0.1803	0.0740	0.0370
Exp t=6 A	2	45.406		0.4541	0.8937				-0.1124			
Exp t=6 B	1	39.785		0.3979	0.7830				-0.2446			
Exp t=6 B	2	39.806		0.3981	0.7835				-0.2440			
Exp t=12 A	1	36.861	11.550	0.3686	0.7255	0.7309	0.0074	0.0037	-0.3209	-0.3135	0.0102	0.0051
Exp t=12 A	2	36.800		0.3680	0.7243				-0.3226			
Exp t=12 B	1	37.288		0.3729	0.7339				-0.3094			
Exp t=12 B	2	37.602		0.3760	0.7401				-0.3010			
Exp t=18 A	1	34.944	18.000	0.3494	0.6878	0.6746	0.0106	0.0053	-0.3743	-0.3938	0.0157	0.0078
Exp t=18 A	2	33.764		0.3376	0.6645				-0.4087			
Exp t=18 B	1	33.921		0.3392	0.6676				-0.4040			
Exp t=18 B	2	34.462		0.3446	0.6783				-0.3882			
Exp t=24 A	1	31.035	24.000	0.3104	0.6108	0.6032	0.0060	0.0030	-0.4929	-0.5056	0.0099	0.0050
Exp t=24 A	2	30.498		0.3050	0.6003				-0.5104			
Exp t=24 B	1	30.330		0.3033	0.5970				-0.5159			
Exp t=24 B	2	30.717		0.3072	0.6046				-0.5032			

Table D.22. Pyrene degradation at T = 32 °C, all control set-ups.

				m ₀ = 0.5081 mg				Hexane Extraction				Error Bar Calculations					
Sample Id	Rep	Conc (mg/L)	Δ Time (hr)	m (mg)	m/m ₀	m/m ₀ avg	Std Dev	Std Error	ln(m/m ₀)	m/m ₀ avg	Std Dev	Std Error	ln(m/m ₀)	m/m ₀ avg	Std Dev	Std Error	
DI t=0 A	1	37.450		0.3745	0.7371	0.7303	0.0114	0.0057	-0.3051								
DI t=0 A	2	36.328	0.000	0.3633	0.7150				-0.3355					-0.3143	0.0157	0.0079	
DI t=0 B	1	37.016		0.3702	0.7285				-0.3167								
DI t=0 B	2	37.636		0.3764	0.7407				-0.3001								
DI t=6 A	1	35.288		0.3529	0.6945				-0.3645								
DI t=6 A	2	34.392	6.017	0.3439	0.6769	0.7872	0.1176	0.0588	-0.3902					-0.2478	0.1502	0.0751	
DI t=6 B	1	44.718		0.4472	0.8801				-0.1277								
DI t=6 B	2	45.577		0.4558	0.8970				-0.1087								
DI t=24 A	1	42.400		0.4240	0.8345				-0.1809								
DI t=24 A	2	42.094	24.000	0.4209	0.8285	0.7647	0.0773	0.0386	-0.1882					-0.2722	0.1013	0.0507	
DI t=24 B	1	35.646		0.3565	0.7016				-0.3544								
DI t=24 B	2	35.264		0.3526	0.6941				-0.3652								
AA t=0 A	1	44.679		0.4468	0.8794				-0.1286								
AA t=0 A	2	45.715	0.000	0.4572	0.8998	0.8522	0.0439	0.0220	-0.1056					-0.1609	0.0515	0.0257	
AA t=0 B	1	41.445		0.4145	0.8157				-0.2037								
AA t=0 B	2	41.355		0.4136	0.8139				-0.2059								
AA t=6 A	1	45.194		0.4519	0.8895				-0.1171								
AA t=6 A	2	44.830	6.000	0.4483	0.8823	0.8540	0.0383	0.0191	-0.1252					-0.1585	0.0450	0.0225	
AA t=6 B	1	42.396		0.4240	0.8344				-0.1810								
AA t=6 B	2	41.150		0.4115	0.8099				-0.2108								
AA t=24 A	1	42.811		0.4281	0.8426				-0.1713								
AA t=24 A	2	42.440	24.000	0.4244	0.8353	0.8526	0.0180	0.0090	-0.1800					-0.1597	0.0210	0.0105	
AA t=24 B	1	43.501		0.4350	0.8562				-0.1553								
AA t=24 B	2	44.517		0.4452	0.8762				-0.1322								
H2O2 t=0 A	1	37.792		0.3779	0.7438				-0.2960								
H2O2 t=0 A	2	37.436	0.000	0.3744	0.7368	0.7699	0.0343	0.0172	-0.3054					-0.2622	0.0446	0.0223	
H2O2 t=0 B	1	40.712		0.4071	0.8013				-0.2215								
H2O2 t=0 B	2	40.532		0.4053	0.7977				-0.2260								
H2O2 t=6 A	1	36.897		0.3690	0.7262				-0.3199								
H2O2 t=6 A	2	39.715	6.000	0.3972	0.7817	0.7611	0.0267	0.0133	-0.2463					-0.2735	0.0353	0.0177	
H2O2 t=6 B	1	39.743		0.3974	0.7822				-0.2456								
H2O2 t=6 B	2	38.322		0.3832	0.7542				-0.2820								
H2O2 t=24 A	1	36.430		0.3643	0.7170				-0.3327								
H2O2 t=24 A	2	36.749	24.000	0.3675	0.7233	0.7261	0.0122	0.0061	-0.3239					-0.3201	0.0167	0.0084	
H2O2 t=24 B	1	36.590		0.3659	0.7202				-0.3283								
H2O2 t=24 B	2	37.804		0.3780	0.7441				-0.2956								

Table D.23. Pyrene degradation at T = 40 °C, experimental set-up.

				m ₀ = 0.5050 mg				Error Bar Calculations				
				Hexane Extraction								
Sample Id	Rep	Conc (mg/L)	Δ Time (hr)	m (mg)	m/m ₀	m/m ₀ avg	Std Dev	Std Error	ln(m/m ₀)	m/m ₀ avg	Std Dev	Std Error
Exp t=0 A	1	50.646	0.000	0.5065	1.0030	0.9724	0.0373	0.0187	0.0030	-0.0285	0.0388	0.0194
Exp t=0 A	2	50.438		-0.0011								
Exp t=0 B	1	48.757		-0.0350								
Exp t=0 B	2	46.577		-0.0808								
Exp t=1 A	1	48.168	1.017	0.4817	0.9539	0.9514	0.0128	0.0064	-0.0472	-0.0499	0.0135	0.0067
Exp t=1 A	2	48.308		-0.0443								
Exp t=1 B	1	48.579		-0.0387								
Exp t=1 B	2	47.109		-0.0694								
Exp t=2 A	1	48.221	2.000	0.4822	0.9550	0.9609	0.0040	0.0020	-0.0461	-0.0399	0.0042	0.0021
Exp t=2 A	2	48.601		-0.0382								
Exp t=2 B	1	48.609		-0.0381								
Exp t=2 B	2	48.660		-0.0370								
Exp t=4 A	1	45.953	4.000	0.4595	0.9100	0.9208	0.0123	0.0062	-0.0943	-0.0826	0.0133	0.0067
Exp t=4 A	2	46.170		-0.0896								
Exp t=4 B	1	46.498		-0.0825								
Exp t=4 B	2	47.366		-0.0640								
Exp t=6 A	1	41.616	6.033	0.4162	0.8241	0.8370	0.0236	0.0118	-0.1934	-0.1782	0.0278	0.0139
Exp t=6 A	2	41.724		-0.1908								
Exp t=6 B	1	44.051		-0.1365								
Exp t=6 B	2	41.678		-0.1919								
Exp t=12 A	1	29.808	14.233	0.2981	0.5903	0.5612	0.0334	0.0167	-0.5271	-0.5790	0.0595	0.0298
Exp t=12 A	2	29.780		-0.5281								
Exp t=12 B	1	26.771		-0.6346								
Exp t=12 B	2	26.991		-0.6264								
Exp t=18 A	1	17.991	18.000	0.1799	0.3563	0.3147	0.0503	0.0251	-1.0320	-1.1657	0.1608	0.0804
Exp t=18 A	2	18.187		-1.0212								
Exp t=18 B	1	13.594		-1.3123								
Exp t=18 B	2	13.800		-1.2972								
Exp t=24 A	1	3.830	23.917	0.0383	0.0758	0.1038	0.0309	0.0154	-2.5790	-2.2999	0.3046	0.1523
Exp t=24 A	2	3.951		-2.5479								
Exp t=24 B	1	6.572		-2.0391								
Exp t=24 B	2	6.607		-2.0338								

Table D.24. Pyrene degradation at T = 40 °C, all control set-ups.

				m ₀ = 0.5050 mg				Hexane Extraction				Error Bar Calculations				
Sample Id	Rep	Conc (mg/L)	Δ Time (hr)	m (mg)	m/m ₀	m/m ₀ avg	Std Dev	Std Error	ln(m/m ₀)	m/m ₀ avg	Std Dev	Std Error	ln(m/m ₀)	m/m ₀ avg	Std Dev	Std Error
DI t=0 A	1	40.733		0.4073	0.8067				-0.2149							
DI t=0 A	2	41.571	0.000	0.4157	0.8233	0.8358	0.0250	0.0125	-0.1945					-0.1798	0.0300	0.0150
DI t=0 B	1	43.139		0.4314	0.8543				-0.1575							
DI t=0 B	2	43.365		0.4337	0.8588				-0.1522							
DI t=6 A	1	40.321		0.4032	0.7985				-0.2250							
DI t=6 A	2	40.833	6.167	0.4083	0.8086	0.8123	0.0112	0.0056	-0.2124					-0.2080	0.0138	0.0069
DI t=6 B	1	41.619		0.4162	0.8242				-0.1933							
DI t=6 B	2	41.298		0.4130	0.8179				-0.2011							
DI t=24 A	1	44.097		0.4410	0.8733				-0.1355							
DI t=24 A	2	44.995	23.983	0.4500	0.8911	0.9005	0.0229	0.0114	-0.1153					-0.1051	0.0255	0.0127
DI t=24 B	1	46.699		0.4670	0.9248				-0.0782							
DI t=24 B	2	46.091		0.4609	0.9128				-0.0913							
AA t=0 A	1	44.488		0.4449	0.8810				-0.1267							
AA t=0 A	2	45.457	0.000	0.4546	0.9002	0.8931	0.0107	0.0054	-0.1051					-0.1131	0.0120	0.0060
AA t=0 B	1	44.804		0.4480	0.8873				-0.1196							
AA t=0 B	2	45.639		0.4564	0.9038				-0.1011							
AA t=6 A	1	45.727		0.4573	0.9056				-0.0992							
AA t=6 A	2	46.491	6.117	0.4649	0.9207	0.9139	0.0064	0.0032	-0.0826					-0.0901	0.0071	0.0035
AA t=6 B	1	46.083		0.4608	0.9126				-0.0914							
AA t=6 B	2	46.286		0.4629	0.9166				-0.0870							
AA t=24 A	1	47.601		0.4760	0.9427				-0.0590							
AA t=24 A	2	47.188	23.933	0.4719	0.9345	0.9517	0.0165	0.0083	-0.0677					-0.0497	0.0173	0.0087
AA t=24 B	1	49.073		0.4907	0.9718				-0.0286							
AA t=24 B	2	48.356		0.4836	0.9576				-0.0433							
H2O2 t=0 A	1	40.003		0.4000	0.7922				-0.2329							
H2O2 t=0 A	2	39.698	0.000	0.3970	0.7862	0.8109	0.0253	0.0126	-0.2406					-0.2100	0.0312	0.0156
H2O2 t=0 B	1	41.907		0.4191	0.8299				-0.1864							
H2O2 t=0 B	2	42.174		0.4217	0.8382				-0.1801							
H2O2 t=6 A	1	42.035		0.4204	0.8324				-0.1834							
H2O2 t=6 A	2	40.574	6.083	0.4057	0.8035	0.8564	0.0483	0.0241	-0.2188					-0.1563	0.0563	0.0282
H2O2 t=6 B	1	46.115		0.4612	0.9132				-0.0908							
H2O2 t=6 B	2	44.245		0.4425	0.8762				-0.1321							
H2O2 t=24 A	1	43.195		0.4320	0.8554				-0.1562							
H2O2 t=24 A	2	41.716	23.900	0.4172	0.8261	0.8260	0.0421	0.0210	-0.1910					-0.1921	0.0519	0.0260
H2O2 t=24 B	1	38.706		0.3871	0.7665				-0.2659							
H2O2 t=24 B	2	43.228		0.4323	0.8561				-0.1554							

Table D.25. Mass % of PAH after 24 hours, T = 25, 32, and 40 °C.

Temperature (°C)	Mass % PAH After 24 Hour Degradation Time			
	Anthracene	Benzo[a]pyrene	Phenanthrene	Pyrene
25	69.5	79.9	82.1	80.1
32	55.4	61.8	72.3	60.3
40	1.86	7.61	38.7	10.3

Appendix E: PERACETIC ACID GENERATION STUDY

Appendix E.1: Initial H₂O₂ and PAA Determination Study.

Table E.1. Initial H₂O₂ and PAA determination study set-up. **Table E.2.** Values of used titrant solutions.

Sample	DI Water (mL)	Acetic Acid (mL)	H ₂ O ₂ (mL)	Sulfuric Acid (mL)	Total Volume (mL)
T1	9	3	3	-	15
T2	8	3	3	1	15
T3	5	5	5	-	15
T4	4	5	5	1	15

Normality (N)	
Sodium Thiosulfate (mL)	Potassium Permanganate (mL)
Reported as 0.0995-0.1005,	0.09536 ^a
Used as: 0.1000	0.09854 ^b

^a Used for all Initial Study titrations, and PAH degradation titrations except t = 0.5, 1, 2, 3, 4, 5 hrs.

^b Used for PAH degradation titrations at t = 0.5, 1, 2, 3, 4, 5 hrs.

Table E.3. Initial H₂O₂ and PAA determination study titration results.

Sample Id	Rep	Mass (g)	Δ Time (hr)	Sodium Thiosulfate (mL)	Potassium Permanganate (mL)	% H ₂ O ₂	% PAA	% H ₂ O ₂ Avg	% PAA Avg
T1	1	1.058	0.000	0.16	14.72	11.206	0.198	11.356	0.240
	2			0.22	15.05	11.459	0.305		
	3			0.17	14.98	11.405	0.216		
T2	1	1.229	0.000	2.07	11.69	7.647	3.125	7.610	3.130
	2			2.06	11.79	7.713	3.109		
	3			2.09	11.42	7.469	3.156		
T3	1	1.099	0.000	0.10	24.95	16.396	0.086	16.396	0.086
	1	1.162	0.000	6.34	18.10	12.561	10.292	12.561	10.292

Appendix E.2: Behavior of H₂O₂ and PAA in PAH Degradation.

Table E.4. 100 µL pipet calibration for H₂O₂ and PAA study.

Anthracene Stock Solution (mg/L)	DI Water (mL)	m ₀ (mg)
5010	0.0980	0.5045
	0.1045	
	0.1000	
	0.1012	
	0.1010	
	0.1010	
	0.1022	
	0.1008	
	0.0993	
	0.1007	
	0.1001	
	0.1007	
	0.0995	
	Average = 0.1007	

m₀ = mass of PAH added from 100 µL stock

Table E.5. Solution pH values for all set-ups, T = 25 and 40 °C, time = 0 and 24 hrs.

Temperature (°C)	Time (hrs)	pH Value		
		Experimental	DI Water	Acetic
25	0	1.81	5.12	2.09
	24	1.89	5.02	2.11
40	0	1.78	4.99	2.11
	25	1.77	4.96	2.09

Table E.6. Values of % H₂O₂ and % PAA for the PAH degradation study.

Sample Id	Rep	Mass (g)	Δ Time (hr)	Sodium Thiosulfate (mL)	Potassium Permanganate (mL)	% H ₂ O ₂	% PAA	H ₂ O ₂ Avg	Std Dev	Std Error	PAA Avg	Std Dev	Std Error
DI Blank	1	0.988	0.058	0.05	0.10	0.082	0.096	0.0822	0.0002	0.0002	0.1254	0.0413	0.0292
	2	0.984		0.08	0.10	0.082	0.155						
Acetic Blank	1	1.044	0.067	0.09	0.10	0.078	0.164	0.0776	0.0002	0.0001	0.2000	0.0510	0.0361
	2	1.047		0.13	0.10	0.077	0.236						
H ₂ O ₂ Blank 0	1	1.050	0.071	0.10	12.77	9.785	0.091	9.2353	0.7774	0.5497	0.0808	0.0137	0.0097
	2	1.069		0.09	11.55	8.686	0.071						
H ₂ O ₂ Blank 3	1	1.048	2.100	0.13	11.49	8.813	0.145	8.7683	0.0635	0.0449	0.1365	0.0122	0.0086
	2	1.040		0.12	11.29	8.723	0.128						
H ₂ O ₂ Blank 24	1	1.034	24.017	0.11	11.49	8.933	0.110	9.1725	0.3394	0.2400	0.1101	0.0004	0.0003
	2	1.039		0.11	12.16	9.412	0.110						
Exp 0	1	1.092	0.075	0.17	12.09	8.904	0.209	8.8870	0.0236	0.0167	0.1840	0.0353	0.0250
	2	1.076		0.14	11.87	8.870	0.159						
Exp 0.5	1	1.064	0.500	0.13	11.63	9.083	0.143	8.7897	0.4142	0.2929	0.0982	0.0633	0.0448
	2	1.068		0.08	10.93	8.497	0.053						
Exp 1	1	1.067	1.000	0.17	11.16	8.683	0.214	8.7534	0.0996	0.0704	0.1956	0.0258	0.0182
	2	1.072		0.15	11.39	8.824	0.177						
Exp 2	1	1.071	2.000	0.13	11.43	8.863	0.142	8.7845	0.1115	0.0788	0.1506	0.0121	0.0086
	2	1.075		0.14	11.27	8.706	0.159						
Exp 3	1	1.066	3.017	0.20	10.49	8.165	0.267	8.3621	0.2793	0.1975	0.2138	0.0758	0.0536
	2	1.068		0.14	11.01	8.560	0.160						
Exp 4	1	1.063	4.000	0.17	10.96	8.560	0.215	8.5953	0.0494	0.0349	0.2405	0.0365	0.0258
	2	1.071		0.20	11.13	8.630	0.266						
Exp 5	1	1.064	5.000	0.24	11.15	8.700	0.339	8.5622	0.1953	0.1381	0.3635	0.0340	0.0241
	2	1.079		0.27	10.95	8.424	0.388						
Exp 24	1	1.040	24.083	0.34	9.74	7.517	0.530	7.4693	0.0668	0.0472	0.4333	0.1370	0.0969
	2	1.074		0.24	9.93	7.422	0.336						

**Appendix F: REACTION RATES & ACTIVATION
ENERGIES**

Table F.1. Peroxy-acid process reaction rates and E_a of anthracene.

T (°C)	T (K)	1/T (K)	k (hr ⁻¹)	ln(k)	k (s ⁻¹)	ln(k)	A (s ⁻¹)	E _a (kJ mol ⁻¹)
25	298.15	0.00335	0.0107	-4.538	2.972E-06	-12.73	5.07E+18	138.96
32	305.15	0.00328	0.0182	-4.006	5.056E-06	-12.20		
40	313.15	0.00319	0.1536	-1.873	4.267E-05	-10.06		

Table F.2. Peroxy-acid process reaction rates and E_a of benzo[a]pyrene.

T (°C)	T (K)	1/T (K)	k (hr ⁻¹)	ln(k)	k (s ⁻¹)	ln(k)	A (s ⁻¹)	E _a (kJ mol ⁻¹)
25	298.15	0.00335	0.0080	-4.828	2.222E-06	-13.02	3.65E+17	133.13
32	305.15	0.00328	0.0133	-4.320	3.694E-06	-12.51		
40	313.15	0.00319	0.1027	-2.276	2.853E-05	-10.46		

Table F.3. Peroxy-acid process reaction rates and E_a of phenanthrene.

T (°C)	T (K)	1/T (K)	k (hr ⁻¹)	ln(k)	k (s ⁻¹)	ln(k)	A (s ⁻¹)	E _a (kJ mol ⁻¹)
25	298.15	0.00335	0.0068	-4.991	1.889E-06	-13.18	6.17E+08	83.07
32	305.15	0.00328	0.0112	-4.492	3.111E-06	-12.68		
40	313.15	0.00319	0.0336	-3.393	9.333E-06	-11.58		

Table F.4. Peroxy-acid process reaction rates and E_a of pyrene.

T (°C)	T (K)	1/T (K)	k (hr ⁻¹)	ln(k)	k (s ⁻¹)	ln(k)	A (s ⁻¹)	E _a (kJ mol ⁻¹)
25	298.15	0.00335	0.0074	-4.906	2.056E-06	-13.09	3.09E+16	126.76
32	305.15	0.00328	0.0194	-3.942	5.389E-06	-12.13		
40	313.15	0.00319	0.0852	-2.463	2.367E-05	-10.65		

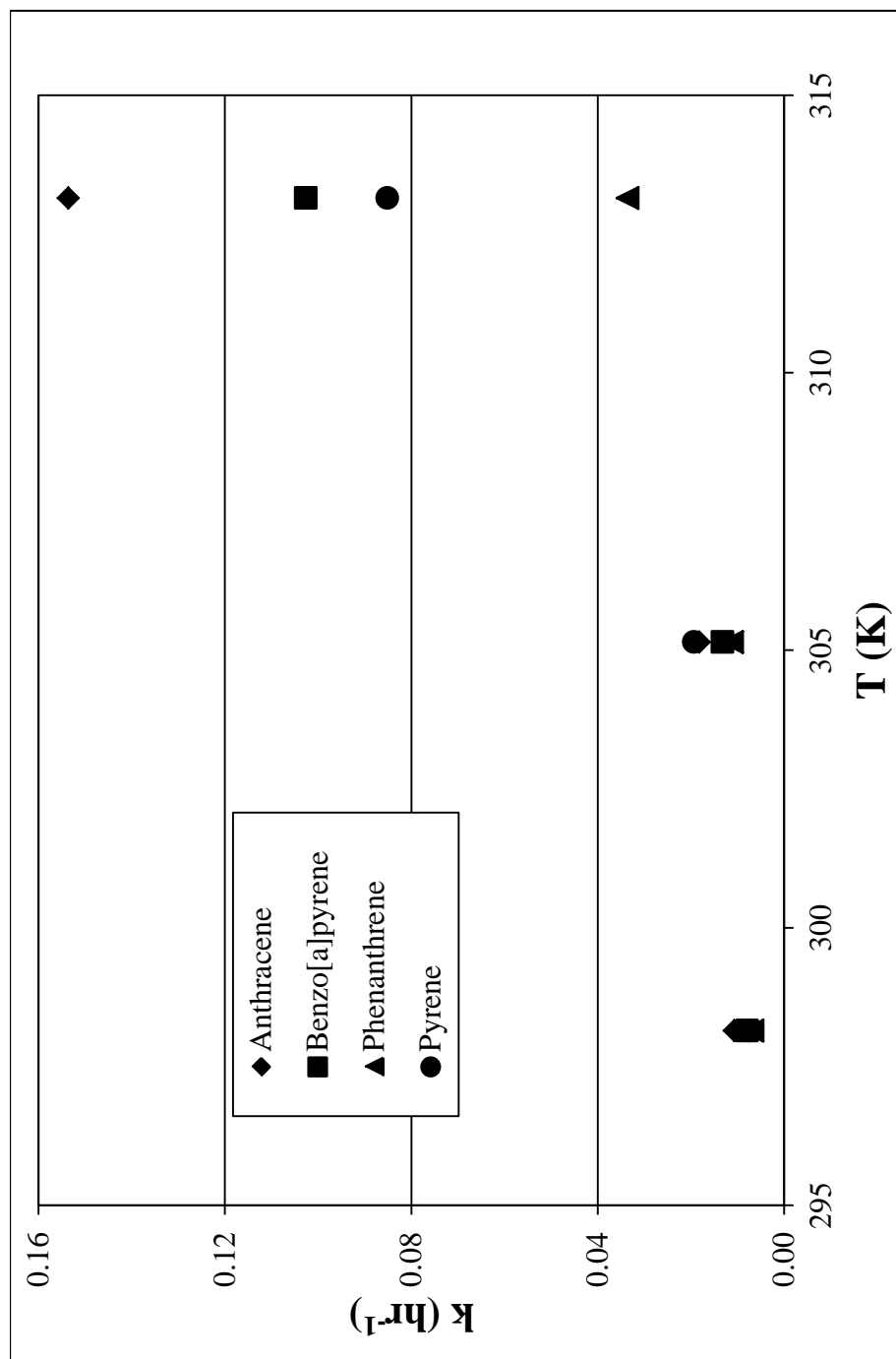


Figure F.1. All reaction rates (hr^{-1}) for all PAHs vs. T (K).